McKelvey School of Engineering Theses & Dissertations

McKelvey School of Engineering

Spring 5-15-2016

Learning with Scalability and Compactness

Wenlin Chen
Washington University in St. Louis

Recommended Citation

WASHINGTON UNIVERSITY IN ST. LOUIS

School of Engineering and Applied Science
Department of Computer Science and Engineering

Dissertation Examination Committee:
Yixin Chen, Chair
Sanmay Das
Yasutaka Furukawa
Roman Garnett
Nan Lin
Kilian Q. Weinberger

Learning with Scalability and Compactness
by
Wenlin Chen

Contents

List of Tables

List of Figures

Acknowledgments

First and foremost, I would like to express my special appreciation and sincerest gratitude to my advisor Yixin Chen. None of the work described in this dissertation would have been possible without his guidance and support. I very much enjoy discussing ideas with him as I always get valuable advice and inspiration from him. I especially thank him for giving me much academic freedom during my entire course of PhD study, which allows me to work on any research topic I like and collaborate with people inside or outside the lab. I could not have imagined having a better advisor and mentor for my Ph.D study.

I would like to thank Kilian Q. Weinberger for co-supervising me and introducing me into the field of machine learning. The joy and enthusiasm he has for machine learning was always contagious and motivational for me. I am also thankful for the excellent example he has provided as a successful researcher.

I would also like to thank the rest of my dissertation committee, Sanmay Das, Roman Garnett, Yasutaka Furukawa and Nan Lin for their valuable comments and suggestions to this dissertation. I also thank them for hosting seminars and talks which keep me up-to-date about the state-of-the-art research.

I would like to thank David Grangier, Michael Auli, Nicolas Mayoraz and Sally A. Goldman for providing me with great internship opportunities at Facebook AI Research and Google

Research. Their great supervision not only gives me two wonderful summers, but also helps shape my long-term career path after graduation.

I would like to thank my friends and colleagues Minmin Chen, Zheng Chen, Zhicheng Cui, Jake Gardener, Yujie He, Gao Huang, Matt Kusner, Qiang Lu, Gustavo Malkomes, Yi Mao, Yu Sun, Paras Tiwari, Stephen Tyree, Wenlin Wang, Yuan Wang, James Wilson, Eddie Xu, Muhan Zhang and Quan Zhou for bouncing off ideas, discussing papers, collaborating on projects, hanging out together and all the time we have shared.

I would like to thank my parents. Words cannot express how grateful I am to my father Wenzhang Chen and my mother Guihua Hong for their unconditional love and support during my life time. I would also like to thank my uncle Wenming Chen for buying me a computer when I was a child, which brought me into the world of computer science.

Last but not the least, I would like to thank my beloved fiancée Ming Zou for her love, support and encouragement. I could not have completed this journey without Ming by my side. Because of her company, my PhD study is full of joys and happiness.

<div align="right">Wenlin Chen</div>

Washington University in Saint Louis
May 2016

Dedicated to my parents.

ABSTRACT OF THE DISSERTATION

Learning with Scalability and Compactness

by

Wenlin Chen

Doctor of Philosophy in Computer Science

Washington University in St. Louis, 2016

Professor Yixin Chen, Chair

Artificial Intelligence has been thriving for decades since its birth. Traditional AI features heuristic search and planning, providing good strategy for tasks that are inherently search-based problems, such as games and GPS searching. In the meantime, machine learning, arguably the hottest subfield of AI, embraces data-driven methodology with great success in a wide range of applications such as computer vision and speech recognition. As a new trend, the applications of both learning and search have shifted toward mobile and embedded devices which entails not only scalability but also compactness of the models. Under this general paradigm, we propose a series of work to address the issues of scalability and compactness within machine learning and its applications on heuristic search.

We first focus on the scalability issue of memory-based heuristic search which is recently ameliorated by Maximum Variance Unfolding (MVU), a manifold learning algorithm capable of learning state embeddings as effective heuristics to speed up A^* search. Though achieving unprecedented online search performance with constraints on memory footprint, MVU is notoriously slow on offline training. To address this problem, we introduce Maximum Variance

Correction (MVC), which finds large-scale feasible solutions to MVU by post-processing embeddings from any manifold learning algorithm. It increases the scale of MVU embeddings by several orders of magnitude and is naturally parallel. We further propose Goal-oriented Euclidean Heuristic (GOEH), a variant to MVU embeddings, which preferably optimizes the heuristics associated with goals in the embedding while maintaining their admissibility. We demonstrate unmatched reductions in search time across several non-trivial A^* benchmark search problems. Through these work, we bridge the gap between the manifold learning literature and heuristic search which have been regarded as fundamentally different, leading to cross-fertilization for both fields.

Deep learning has made a big splash in the machine learning community with its superior accuracy performance. However, it comes at a price of huge model size that might involves billions of parameters, which poses great challenges for its use on mobile and embedded devices. To achieve the compactness, we propose HashedNets, a general approach to compressing neural network models leveraging feature hashing. At its core, HashedNets randomly group parameters using a low-cost hash function, and share parameter value within the group. According to our empirical results, a neural network could be 32x smaller with little drop in accuracy performance. We further introduce Frequency-Sensitive Hashed Nets (FreshNets) to extend this hashing technique to convolutional neural network by compressing parameters in the frequency domain.

Compared with many AI applications, neural networks seem not graining as much popularity as it should be in traditional data mining tasks. For these tasks, categorical features need to be first converted to numerical representation in advance in order for neural networks to process them. We show that a naïve use of the classic one-hot encoding may result in gigantic weight matrices and therefore lead to prohibitively expensive memory cost in neural

networks. Inspired by word embedding, we advocate a compellingly simple, yet effective neural network architecture with category embedding. It is capable of directly handling both numerical and categorical features as well as providing visual insights on feature similarities. At the end, we conduct comprehensive empirical evaluation which showcases the efficacy and practicality of our approach, and provides surprisingly good visualization and clustering for categorical features.

Chapter 1

Introduction

Artificial intelligence (AI) is a long-standing field and has been thriving for decades. Generally speaking, AI studies and designs intelligent agents that is capable of perceiving its environment and taking actions to maximize its chances of success [119]. Traditional AI features deduction, reasoning, planning and problem solving, which try to mimic the human reasoning and thinking process when they are solving puzzles and logical problems. Therefore, the developed method involves a huge amount of logic and domain knowledge. Different than traditional AI, machine learning, arguably the hottest subfield of AI, develops the intelligent agents through learning from past experience and has been central to AI research since the field's inception[1].

In this chapter, we first introduce supervised learning and unsupervised learning, which serve as preliminaries for the following chapters of this dissertation. Then we point out the issues of scalability and compactness that widely exists within machine learning, and motivate this dissertation.

---

[1]https://en.wikipedia.org/wiki/Artificial_intelligence

1.1 Supervised learning

Depending on the type of problems, machine learning is further divided into several subfields. As a brief introduction, we describe *supervised learning* in this section.

For supervised learning, the label of each training instance is given. Suppose $\mathcal{D} = \{\mathbf{x}_i, y_i\}_{i=1}^N$ is our training data that consists of N training samples, where $\mathbf{x}_i \in \mathcal{X}$ is a feature vector that represents the ith training instance and $y_i \in \mathcal{Y}$ stands for the label of this instance. Here $\mathcal{X}$ and $\mathcal{Y}$ are the input space and output space, respectively. The goal of supervised learning is to find a mapping function $f \in \mathcal{H} : \mathcal{X} \to \mathcal{Y}$ to minimize the "difference" between the predicted label $f(\mathbf{x}_i)$ and its true label y_i, where $\mathcal{H}$ is called hyperthesis that includes all possible feasible functions. Mathematically, a loss function L is introduced to measure this difference. Therefore, supervised learning aims to solve the following *empirical risk minimization* problem:

$$\underset{f \in \mathcal{H}}{\text{minimize}} \quad \frac{1}{N} \sum_{i=1}^{N} L(f(\mathbf{x}_i), y_i) \tag{1.1}$$

Depending on the type of labels, supervised learning is further be divided into two categories: *classification* when the label is a discrete/categorical value and *regression* when the label is a real value. In this dissertation, we focus on classification problems when it comes to supervised learning.

1.1.1 Data for supervised learning problems

For readers to get a better picture of what kind of data will be studied and tested in this dissertation, we introduce several examples of supervised learning problems and visualize the corresponding data set and feature vectors.
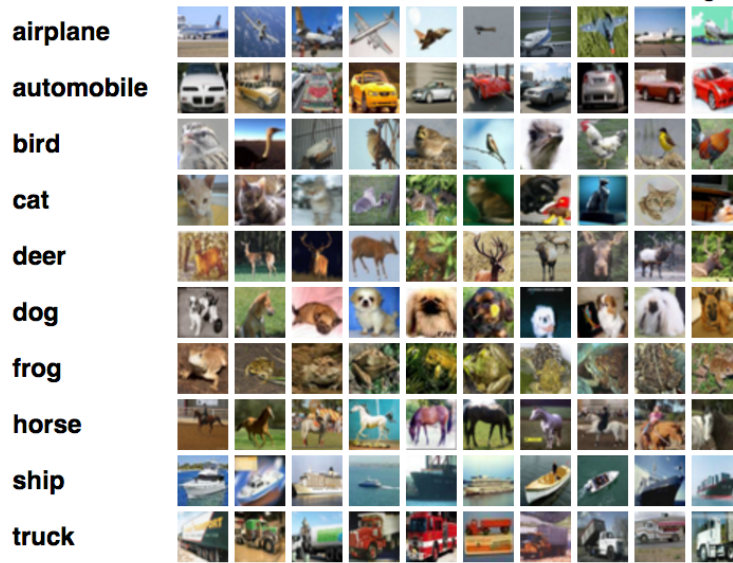
Figure 1.1: Examples from CIFAR-10 dataset

Image data One of the most high-impact application of machine learning is dealing with image classification, which classifies a given image to a particular category. For example, Figure 1.1 shows a number of examples of training instances from CIFAR-10 dataset [71]. An image contains three color channels R, G, B each of which is of size 32×32, and belongs to a category. There are 10 labels in total. In this dataset, the feature vector of each image could be represented by a $3 \times 32 \times 32 = 3072$ dimensional vector where each element in the feature vector is the pixel intensity for the corresponding pixel in a channel. The label set $\mathcal{Y} = \{\text{airplane, automobile, bird, cat, deer, dog, frog, horse, ship, truck}\}$.

Hand-crafted data For traditional data mining, the feature vector in the data is often hand-crafted or generated from feature engineering. This type of data widely exists in various data mining problems, such as clinical prediction [90, 22, 143] and ads prediction [60, 92]. Figure 1.2 shows a cooked up example where the feature vector is a description of a person and the task is to predict whether the annual salary of this person is greater than $10,000$

age, height, gender, degree, Country

$$x_i = (24,\ 1.8,\ \text{male},\ \text{master},\ \text{USA})$$
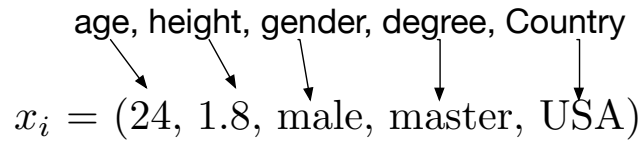
Figure 1.2: An example feature vector

dollars or not. The specialness about this type of data is that the feature vector contains both numerical and categorical inputs. In this example, age and height are both numerical, while gender, degree and country are categorical. For numerical classifiers, categorical input should be first converted to a numerical representation. The most popular way to handle categorical input is the so-called *one-hot encoding*, which will be discussed in Chapter 4.

1.1.2 Linear classification models

There are various classification models in the literature [58]. In this section, we only describe several linear classifiers for introduction purpose. Specifically, we focus on binary classification where $\mathcal{Y} = \{-1, +1\}$, and assume the feature vector $\mathbf{x} \in \mathcal{R}^d$ is a numerical representation.

Linear classifiers take the following general form:

$$f(\mathbf{x}) = \mathbf{w}^\top \mathbf{x} + b \tag{1.2}$$

where $\mathbf{w} \in \mathcal{R}^d$ is the weight vector and $b \in \mathcal{R}$ is a bias term. Both are parameters in the linear model and the learning process is to adjust the values of $\mathbf{w}$ and b such that the loss function is minimized. Typically, a $\ell 2$ regularization of the weight vector is added to the

4

objective function to alleviate the overfitting problem. Following Eq 1.1, we have that

$$\underset{\mathbf{w}\in\mathcal{R}^d, b\in\mathcal{R}}{\text{minimize}} \ \frac{1}{N}\sum_{i=1}^{N} L(\mathbf{w}^\top\mathbf{x}_i + b, y_i) + \lambda\|\mathbf{w}\|_2 \tag{1.3}$$

where λ is a factor for $\ell 2$ regularization and controls the tradeoff between loss function and regularization. Different choices of the loss function L leads to different classifiers.

Logistic Regression. If we adopt the *logistic loss* as the loss function, Eq. 1.3 ends up with a *logistic regression*. For logistic loss, $L(u, v) = \log(1 + \exp(-uv))$. Therefore, Eq. 1.3 can be rewritten as

$$\underset{\mathbf{w}\in\mathcal{R}^d, b\in\mathcal{R}}{\text{minimize}} \ \frac{1}{N}\sum_{i=1}^{N} \log\left(1 + \exp\left(-y_i(\mathbf{w}^\top\mathbf{x}_i + b)\right)\right) + \lambda\|\mathbf{w}\|_2 \tag{1.4}$$

Logistic regression not only predicts the label for the testing instances, but also providing the probability of its prediction. Eq. 1.4 is also equivalent to maximizing the likelihood of the dataset when the probability of y_i being 1 is a sigmoid function of the linear score $f(\mathbf{x}_i)$ as follows:

$$p(y = 1|\mathbf{x}) = \frac{1}{1 + e^{-(\mathbf{w}^\top\mathbf{x}+b)}} \tag{1.5}$$

Logistic regression could be easily extended to handle multinomial classification by having multi-dimensional score functions. The probability of each class could be computed via a softmax function which will be discussed in the later section.

Support vector machines (SVM). If the loss function is *hinge loss*, then Eq. 1.3 becomes a SVM solver. In particular, hinge loss $L(u, v) = [1 - uv]_+$ is a piece-wise linear function where $[\cdot]_+ = \max(0, \cdot)$. Combing with $\ell 2$ regularization, Eq. 1.3 can be converted
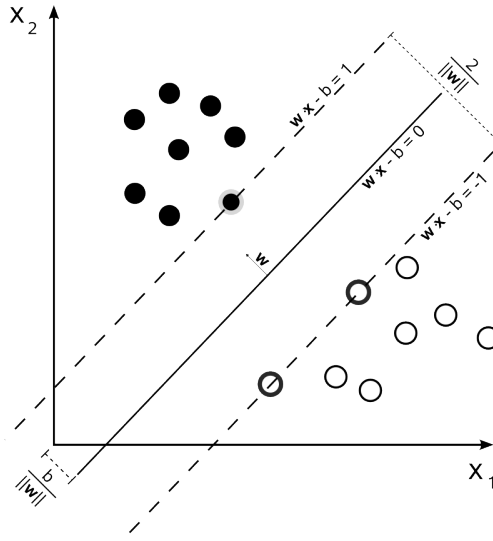
Figure 1.3: SVM classification in 2-dimensional space.

to the following:

$$\underset{\mathbf{w}\in\mathcal{R}^d, b\in\mathcal{R}}{\text{minimize}} \quad \frac{1}{N}\sum_{i=1}^{N}\left[1 - y_i(\mathbf{w}^\top\mathbf{x}_i + b)\right]_+ + \lambda\|\mathbf{w}\|_2 \qquad (1.6)$$

As shown in Figure 1.3[2], SVM has a clear geometry interpretation that its decision hyperplane has the largest distance to the nearest training data instances of any class, leading to better *generalization* ability. The true power of SVM is its combination with the kernel trick [122] which enables itself to handle nonlinear classification. It can also be used to efficiently solve elastic nets [160].

More on loss functions. Both hinge loss and logistic loss can be regarded as a proxy for 0-1 loss which is the training error of the dataset. Specifically, they are both upper bounds of the 0-1 loss as shown in Figure 1.4. Therefore, minimizing these loss is approximately reducing the training error of the dataset. Eq 1.4 and Eq 1.6 are both convex and could be efficiently optimized with (subgradient) gradient descent [11] during training to finalize

---

[2]This figure is from `https://en.wikipedia.org/wiki/Support_vector_machine`
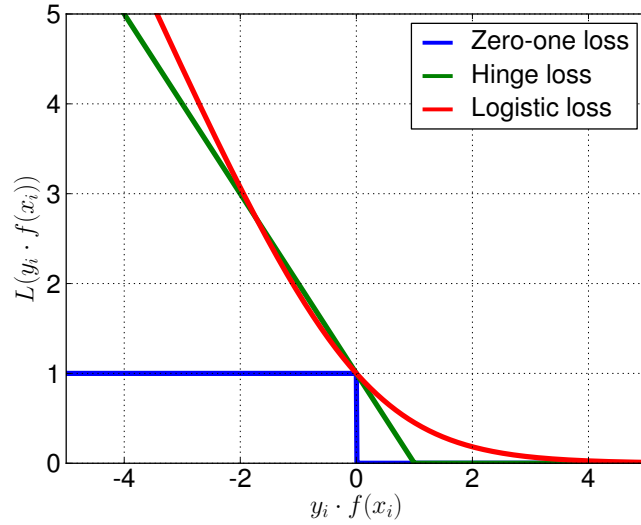
Figure 1.4: Loss functions

the parameter values. In terms of testing, the prediction of a new input is given by Eq. 1.2 where the parameter values of **w** and b are fixed. Recent studies [151, 152, 154, 74] show that the testing efficiency could be greatly improved by only extracting important features.

1.2   Neural networks

We introduce neural networks that a number of methods presented in this dissertation are based on.

1.2.1   From single layer to multiple layers

We have describe linear models such as logistic regression and SVM in Section 1.1. A neural network can be regarded as a composition of multiple such linear classifiers. Figure 1.5 shows
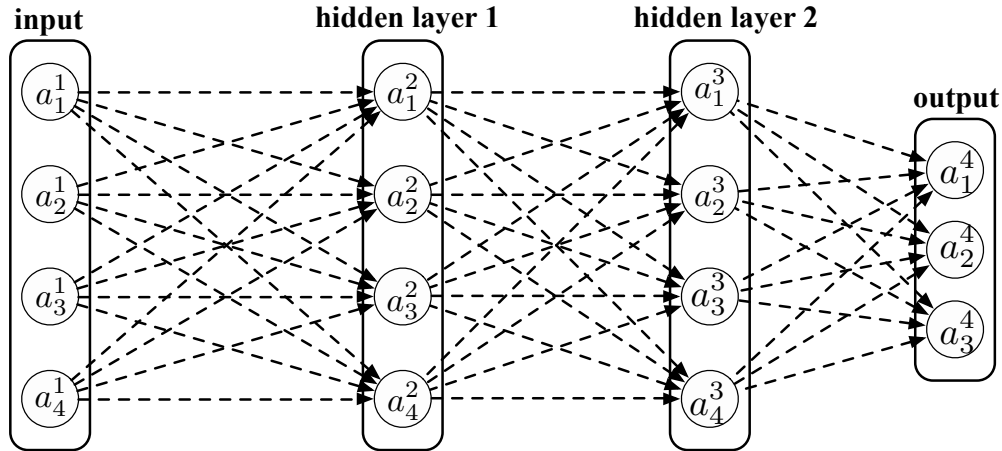
Figure 1.5: Architecture of neural networks

a small neural network for illustration. A vanilla neural network contains an input layer, an output layer and multiple hidden layers in between. Each layer contains a number of neurons which is a function of neurons in the previous layer. Each neuron has a value associated with it.

Suppose there are L layers and there are n^ℓ neurons in the ℓth layer. Let a_i^ℓ be the value of ith neuron in the ℓth layer where $1 \le i \le n^\ell$ and $1 \le \ell \le L$. We use $\mathbf{a}^\ell$ to denote the vector of neurons in the ℓth layer, $i.e.$ $\mathbf{a}^\ell = \{a_1^\ell, a_2^\ell, \cdots, a_{n^\ell}^\ell\}$. The input layer is simply the feature vector of the data. Suppose the input to the neural network is $\mathbf{x}$ and its label is y. We have $\mathbf{a}^1 = \mathbf{x}$. Each neuron in the hidden layers is a linear transformation of neurons in its previous layer followed by an $activation$ $function$. Specifically, we have that

$$\mathbf{a}^{\ell+1} = g(\mathbf{z}^{\ell+1}) \text{ where } \mathbf{z}^{\ell+1} = \mathbb{W}^\ell \mathbf{a}^\ell + \mathbf{b}^\ell \text{ for } \ell = 1, \cdots, L-2 \qquad (1.7)$$

Here, $\mathbb{W}^\ell \in \mathcal{R}^{n^{\ell+1} \times n^\ell}$ and $\mathbf{b}^\ell \in \mathcal{R}^{n^\ell}$ are the weight matrix and bias vector in the ℓth layer. The activation function g performs element-wise operation on each neuron, and there are three popular choices for this function: rectifier linear unit (ReLU), sigmoid and tanh, as
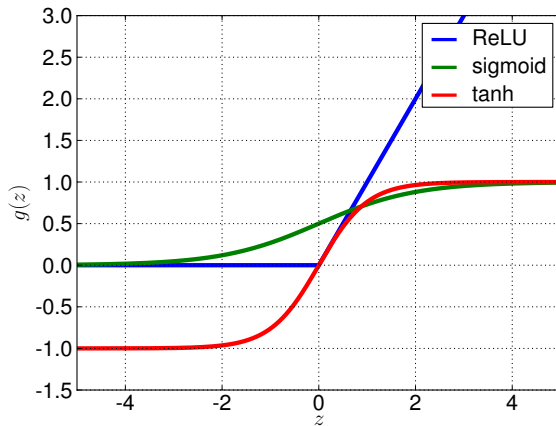
Figure 1.6: Activation functions.

follows (also shown in Figure 1.6):

$$
\begin{aligned}
\text{ReLU}: \quad & g(z) = \max(z, 0) \\
\text{sigmoid}: \quad & g(z) = \frac{1}{1 + e^z} \\
\text{tanh}: \quad & g(z) = \frac{e^z - e^{-z}}{e^z + e^{-z}}
\end{aligned}
\tag{1.8}
$$

Each activation function has its pros and cons. For example, ReLU promotes sparsity for hidden layers, but it is not differentiable at 0. Though tanh and sigmoid are differentiable everywhere, their gradient magnitudes are extremely small when the linear score is not close to 0, leading to the vanishing gradient problem [105], a big hassle for back propagation (described latter). There are many other options for activation functions [59] which is out of the scope of this dissertation.

Neural networks have a lot of flexibility in choosing its output. For classification purpose, the number of output neurons is equal to the number of possible labels, $i.e.$ $n^L = |\mathcal{Y}|$. After computing the linear score z_i^L for each output neuron, a $softmax$ function is used to normalize the output values so that the sum of output values is 1. Therefore, the final output of neural

9

networks can be considered a multinomial distribution over possible labels. In particular, a softmax function is a generalization of logistic regression described in Section 1.1 as follows:

$$a_i^L = \frac{e^{z_i^L}}{\sum_{k=1}^{n^L} e^{z_k^L}} \tag{1.9}$$

Why neural nets memory-consuming. The weight matrix of a neural network could easily take up a huge amount of memory. For example, a neural net for mnist dataset [79], a small image dataset about digits, usually has 784 input neurons, several layers of 1000 hidden units and an output layer of 10 neurons. In this case, a single hidden layer has a weight matrix of size 1000×1000, which consists of 1 million parameters in total. For larger network, the memory consumption would be much larger.

1.2.2 Backpropagation

A softmax output is usually combined with a *cross-entropy* loss as the objective function for parameter learning. For K-way multinomial classification, assume the output space of labels $\mathcal{Y} = \{1, 2, \cdots, K\}$. For the ease of presentation, suppose there is only one training instance in a batch. Let E be the negative log likelihood of an input, we have $E = -\log a_y^L = -z_y^L + \log(\sum_{k=1}^{n^L} e^{z_k^L})$. And the goal is to minimize E for every input:

$$\underset{\mathbb{W}^\ell, \mathbf{b}^\ell}{.\text{minimize}} \ -\log a_y^L \tag{1.10}$$

The parameters including the weight matrix and bias vector in each layer are learned via gradient descent. However, computing the gradient of each parameter independently result in a lot of redundant computation, which is why *backpropagation* [118] comes into play.

Backpropagation leverages the fact that the gradients of shallow layers can be expressed as the gradients of higher layers. Let δ_i^ℓ denote the gradient of the objective function in Eq (1.10) over activation i in the ℓth layer. This gradient is usually referred as the *error term* and play the role of propagating the gradient to shallow layers. When doing gradient descent, we compute the following two types of gradients: the error term and the gradient over parameters.

Error term. We compute the gradient of the objective function in Eq 1.9 over neurons. At the top layer, we have

$$\delta_j^L = \frac{\partial E}{\partial z_j^L} = I(j, y) - a_j^L \tag{1.11}$$

where $I(j, y) = 1$ when $j = y$ and $I(j, y) = 0$ otherwise. For layers $\ell = 1, \cdots, L - 1$, we have that

$$\delta_j^\ell = \frac{\partial E}{\partial z_j^\ell} = (\sum_{i=1}^{n^{\ell+1}} W_{ij} \delta_i^{\ell+1}) g'(z_j^\ell) \tag{1.12}$$

where W_{ij}^ℓ is the element in the weight matrix indexed by (i, j).

Gradient over parameters. For parameter learning, our goal is to compute the gradient over parameters $W_{i,j}^\ell$ and b_i^ℓ, which can be expressed by the error term as follows:

$$\frac{\partial E}{\partial W_{i,j}^\ell} = a_j^\ell \delta_i^{\ell+1} \text{ and } \frac{\partial E}{\partial b_i^\ell} = \delta_i^{\ell+1} \tag{1.13}$$

Once we have the gradients over parameters, we can do stochastic gradient descent on the parameters of the neural net until it converges. Usually, the training is coupled with other techniques such as dropout, momentum and $\ell 2$ regularization for preventing overfitting and better convergence.

1.3 Unsupervised learning - maximum variance unfolding (MVU)

Unsupervised learning is a machine learning task of exploring hidden patterns in the data. Just as its name implies, unsupervised learning does not harness the supervision information such as the label of the data. Unsupervised learning could be further divided into several fields such as manifold learning/ graph embedding, clustering and statistical density estimation. In this dissertation, we mainly focus on the graph embedding which aims to embed a graph into a Euclidean space so that each node in a graph has a coordinate. There are various graph embedding algorithms that are different in what properties are preserved during the embedding. For example, *Isomap* [137] embeds the graph that most faithfully preserves the shortest distance between any two nodes in the graph, while *Laplacian eigenmaps* [4] preserves proximity relations, mapping nearby input nodes to nearby outputs. For a more detailed survey we recommend [121]. The obtained embeddings can be used in a wide range of down-stream applications such as visualization, classification or even heuristic search which will be discussed in detail in Chapter 2.

In this section, we briefly review another graph embedding algorithm, **Maximum Variance Unfolding** (MVU), which a big part of this dissertation is based on. MVU stems from nonlinear dimensionality reduction [121] which maps high dimensional data points to low dimensional embeddings while preserving certain properties about the manifold during the embedding. Figure 1.7 illustrates a 3-dimensional Swiss roll graph being embedded into a 2-dimensional embeddings using MVU. We mainly introduce MVU from the perspective of graph embedding in which a graph to embed is given in advance.

Maximum Variance Unfolding
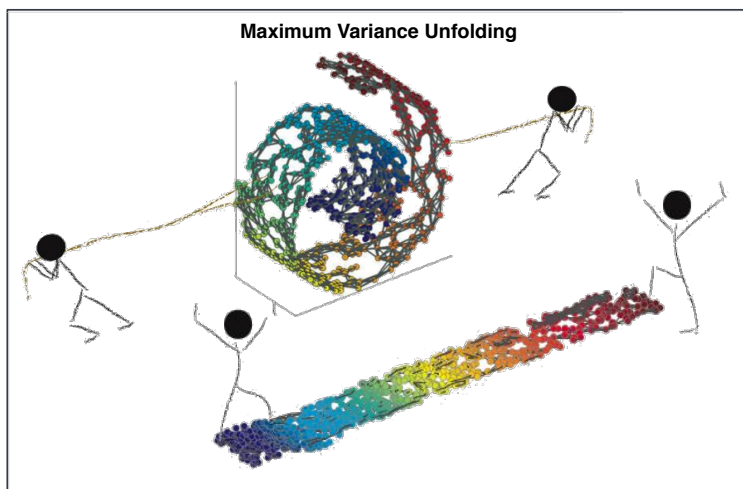
Figure 1.7: Maximum variance unfolding illustrated on a Swiss roll graph, embedded into a 2-dimensional Euclidean space.

Let $G = (V, E)$ denote the graph with undirected edges E and nodes V, with $|V| = n$. Edges $(i, j) \in E$ are weighted by some $d_{ij} \geq 0$. MVU embeds the nodes in V into a d-dimensional Euclidean space, $\mathbf{x}_1, \ldots, \mathbf{x}_n \in \mathcal{R}^d$, such that the embeddings most faithfully preserve the edge length between adjacent nodes, *i.e.* $\|\mathbf{x}_i - \mathbf{x}_j\|_2 \approx d_{ij}$ for $(i, j) \in E$.

MVU formulates this task as an optimization problem that maximizes the variance of the embedding, while enforcing strict constraints on the local edge distances:

$$\begin{aligned}
\underset{\mathbf{x}_1, \ldots, \mathbf{x}_n \in \mathcal{R}^d}{\text{maximize}} \quad & \sum_{i=1}^{n} \mathbf{x}_i^2 \\
\text{subject to} \quad & \|\mathbf{x}_i - \mathbf{x}_j\|_2 \leq d_{ij} \quad \forall (i, j) \in E \\
& \sum_{i=1}^{n} \mathbf{x}_i = 0
\end{aligned} \tag{1.14}$$

The last constraint centers the embedding at the origin, to remove translation as a degree of freedom in the optimization. Because the data is centered, the objective is identical to maximizing the variance, as $\sum_i \mathbf{x}_i^2 = 0.5 \sum_{i,j} \|\mathbf{x}_i - \mathbf{x}_j\|^2$. Although (1.14) is non-convex,

13

Weinberger and Saul [146] show that with a rank relaxation, $\mathbf{x} \in \mathcal{R}^n$, this problem can be rephrased as a convex semi-definite program by optimizing over the inner-product matrix $\mathbf{K}$, with $k_{ij} = \mathbf{x}_i^\top \mathbf{x}_j$:

$$
\begin{aligned}
\underset{\mathbf{K}}{\text{maximize}} \quad & \text{trace}(\mathbf{K}) \\
\text{subject to} \quad & k_{ii} - 2k_{ij} + k_{jj} \le d_{ij}^2 \quad \forall(i,j) \in E \\
& \sum_{i,j} k_{ij} = 0 \\
& \mathbf{K} \succeq 0.
\end{aligned}
\tag{1.15}
$$

The final constraint $\mathbf{K} \succeq 0$ ensures positive semi-definiteness and guarantees that $\mathbf{K}$ can be decomposed into vectors $\mathbf{x}_1, \ldots, \mathbf{x}_n$ with a straight-forward eigenvector decomposition. To ensure strictly $r-$dimensional output, the final embedding is projected into $\mathcal{R}^d$ with principal component analysis (PCA). (This is identical to composing the vectors $\mathbf{x}_i$ out of the r leading eigenvectors of $\mathbf{K}$.) The time-complexity of MVU is $O(n^3 + c^3)$ (where c is the number of constraints in the optimization problem), which makes it prohibitive for larger data sets.

1.4   Motivations

Over the past few decades, huge efforts have been made towards making machine learning models more efficient and accurate. However, people have not been aware of the growing memory and storage consumption by machine learning until recently when a salient shift toward mobile and embedded devices requires not only superior accuracy but also compactness of the models. Among many subfields of machine learning and artificial intelligence, we

observe that techniques leading to large model size often come from the following two areas: memory-based learning (*a.k.a* instance-based learning) and deep learning.

1. **memory-based Learning**. Many models using memory-based learning are essentially *lazy learning* in which the prediction of a model is based on pre-stored instances in the training set. The most commonly seen example is Support Vector Machines (SVM) with kernels. SVM requires storing the support vectors in the model file as they are needed for out-of-sample prediction. For datasets with large training instances, the number of support vectors could be many, which poses a great challenge for memory saving. The issue of memory consumption doesn't solely exist for pure instance-based learning, but also in its recent application on A^* search. A good heuristic is key to the efficiency and optimality of a heuristic search. The "perfect" heuristic is no doubt the pair-wise distance between any two states, which is prohibitively expensive to store in memory when there are many states in the graph. A good marriage between traditional heuristic search and graph embedding addresses this problem by compressing this "perfect" heuristic with the MVU embedding described in Section 1.3. It maps an AI state graph to a Euclidean space where the heuristics between any two states is measured by their Euclidean distance [110].

2. **Deep Learning**. In the past decade deep neural networks have set new performance standards in many high-impact applications. These include object classification [72, 124], speech recognition [63], image caption generation [141, 68] and domain adaptation [52]. As data sets increase in size, so do the number of parameters in these neural networks in order to absorb the enormous amount of supervision [32]. Increasingly, these networks are trained on industrial-sized clusters [76] or high-performance graphics processing units (GPUs) [32]. Simultaneously, there has been a second trend

as applications of machine learning have shifted toward mobile and embedded devices. As examples, modern smart phones are increasingly operated through speech recognition [123], robots and self-driving cars perform object recognition in real time [98], and medical devices collect and analyze patient data [82]. In contrast to GPUs or computing clusters, these devices are designed for low power consumption and long battery life.Most importantly, they typically have small working memory. For example, even the top-of-the-line iPhone 6 only features a mere 1GB of RAM[3], let alone other current wearable devices.

As a matter of fact, mobile and embedded devices fall short of memory capacity. The growing size of machine learning models creates a dilemma when they are to be deployed on mobile devices. While it is possible to train models offline on industrial-sized clusters (server-side), the sheer size of the most effective models would exceed the available memory, making it prohibitive to perform testing on-device. In speech recognition, one common cure is to transmit processed voice recordings to a computation center, where the voice recognition is performed server-side [29]. This approach is problematic, as it only works when sufficient bandwidth is available and incurs artificial delays through network traffic [70]. One solution is to train small models for the on-device usage; however, these tend to significantly impact accuracy [29], leading to customer frustration.

With scalability and, most importantly, compactness in mind, this dissertation describes a series of work addressing two main problems: 1) Scalability issue of MVU which is key to the compactness of the memory-based heuristics. 2) Redundancy in neural networks which poses a great challenge for both compactness and efficiency of deep learning.

---

[3]http://en.wikipedia.org/wiki/IPhone_6

1.4.1 Scalability of MVU

Euclidean heuristic (EH) [110] has been proposed for A* search. EH exploits manifold learning methods, in particular MVU, to construct an embedding for each state in the state space graph, and derives an admissible heuristic distance between two states from the Euclidean distance between their respective embedded points. EH has shown good performance and memory efficiency in comparison to other existing heuristics such as differential heuristics. However, the training of MVU is slow, which greatly limits the scale of AI problems EH can be applied to.

To address the scalability issue of MVU, we introduce MVC (Maximum Variance Correction) [20], which finds large-scale feasible solutions to MVU by post-processing embeddings from *any* manifold learning algorithm. It increases the scale of MVU embeddings by several orders of magnitude and is naturally parallel. We demonstrate unprecedented scalability on MVU training and un-matched reductions in search time across several non-trivial A^* benchmark search problems. Moreover, this work bridges the gap between the manifold learning literature and the traditional heuristic search, which have been regarded as two fundamentally different fields, leading to cross-fertilization of both fields. It is worth mentioning that we have another work [25] that solves general submodular maximization leveraging heuristic search, which serves as a concrete example of heuristic search helping machine learning.

We further propose a number of techniques [23, 86] that can significantly improve the quality of EH. We propose a goal-oriented manifold learning scheme that optimizes the Euclidean distance to goals in the embedding while maintaining admissibility and consistency. We also propose a state heuristic enhancement technique to reduce the gap between heuristic and true distances. The enhanced heuristic is admissible but no longer consistent. We

then employ a modified search algorithm, known as B′ algorithm, that achieves optimality with inconsistent heuristics using consistency check and propagation. We demonstrate the effectiveness of the above techniques and report superior reduction in search costs across several non-trivial benchmark search problems.

1.4.2 Redundancy in neural networks

As deep nets are increasingly used in applications suited for mobile devices, a fundamental dilemma becomes apparent: the trend in deep learning is to grow models to "absorb" ever-increasing data set sizes; however mobile devices are designed with very little memory and cannot store such large models. In the meantime, accumulated evidence suggests [39, 3, 78, 34, 57] that much of the information stored within network weights may be redundant.

We present a novel network architecture, HashedNets [26], that exploits inherent redundancy in neural networks to achieve drastic reductions in model sizes. HashedNets use a low-cost hash function to randomly group connection weights into hash buckets, and all connections within the same hash bucket share a single parameter value. These parameters are tuned to adjust to the HashedNets weight sharing architecture with standard backpropagation during training. Our hashing procedure introduces no additional memory overhead, and we demonstrate on several benchmark data sets that HashedNets shrink the storage requirements of neural networks substantially while mostly preserving generalization performance.

We further extend the hashing technique to convolutional neural networks (CNN) [27], which are increasingly used in many areas of computer vision. We present a novel network architecture, Frequency-Sensitive Hashed Nets (FreshNets), which exploits inherent redundancy in both convolutional layers and fully-connected layers of a deep learning model, leading to

dramatic savings in storage consumption. Based on the key observation that the weights of learned convolutional filters are typically smooth and low-frequency, we first convert filter weights to the frequency domain with a discrete cosine transform (DCT) and use a low-cost hash function to randomly group frequency parameters into hash buckets. All parameters assigned the same hash bucket share a single value learned with standard back-propagation. To further reduce model size we allocate fewer hash buckets to high-frequency components, which are generally less important. We evaluate FreshNets on eight data sets, and show that it leads to drastically better compressed performance than several relevant baselines.

Compared to its success in AI applications such as computer vision and speech recognition, neural networks seem not graining as much popularity as it should be in traditional data mining tasks. For these tasks, neural networks fall short of the following aspects: 1) the presence of categorical features can pose problems because neural networks only take numerical features inherently. 2) the interpretability of neural networks leaves something to be desired because it is a big hassle to extract knowledge from neural networks. Inspired by word embedding, we advocate a compellingly simple, yet effective neural network architecture with category embedding to address these problems. It not only directly handles both numerical and categorical features, but also (and more importantly) provides visual insights on category similarities. At its core, the model learns a numerical embedding for each category of a categorical feature, based on which we can visualize all categories in the embedding space and extract knowledge of similarity between categories. With the embedding, similar categories are mapped to nearby regions. In addition, we show that the category embedding can be seen as a matrix factorization of the weight matrix associated with the one-hot encoding, leading to great savings in memory consumption. We conduct comprehensive empirical evaluation which showcases the efficacy and practicality of our approach, and provides surprisingly good visualization and clustering for categorical features.

19

Chapter 2

Compressing Heuristics with Graph Embedding

Graph embedding and manifold learning have become a strong sub-field of machine learning with many mature algorithms [121, 81], often accompanied by large scale extensions [108, 129, 147] and thorough theoretical analysis [42, 104]. Until recently, this success story was not matched by comparably strong applications [8]. Rayner et al. [110] propose **Euclidean Heuristic** (EH) which uses the Euclidean embedding of a search space graph as a heuristic for A^* search [119]. The graph-distance between two states is approximated by the Euclidean distance between their respective embedded points.

Exact A^* search with informed heuristics is an application of great importance in many areas of real life. For example, GPS navigation systems need to find the shortest path between two locations *efficiently* and *repeatedly* (*e.g.* each time a new traffic update has been received, or when the driver makes a wrong turn). As the processor capabilities of these devices and the patience of the users are both limited, the quality of the search heuristic is of great importance. This importance only increases as increasingly *low powered* embedded devices (*e.g.* smart-phones) are equipped with similar capabilities.

A perfect heuristic is no doubt the pair-wise shortest-path distance between any two states in the state graph, which is prohibitively expensive to store in memory. In this chapter, we study how to use graph embedding to compress this perfect heuristic and how to scale it up. In particular, we introduce EH in Section 2.1 which at its core is a MVU embedding described in Chapter 1. We then present a novel embedding algorithm, maximum variance correction (MVC) [20], to speed up MVU by several order of magnitude. We further extend the EH to Goal-Oriented Euclidean Heuristics (GOEH) [23] in Section 2.2 to improve the performance of heuristic search.

2.1 Maximum variance correction for speeding up MVU

2.1.1 Introduction

For an embedding to be a A^* heuristic, it must satisfy two properties: 1. *admissible* (distances are never *overestimated*), 2. *consistent* (a triangular inequality like property is preserved). To be maximally effective, a heuristic should have a minimal gap between its estimate and the true distance—*i.e.* all pair-wise distances should be maximized under the admissibility and consistency constraints. In the applications highlighted by Rayner et al. [110], a heuristic must require small space to be broadcasted to the end-users. The authors show that the constraints of Maximum Variance Unfolding (MVU) [146][4] guarantee admissibility and consistency, while the objective maximizes distances and reduces space requirement of heuristics from $O(n^2)$ to $O(dn)$. In other words, the MVU manifold learning algorithm is a perfect fit to learn Euclidean heuristics for A^* search.

---

[4]Throughout this dissertation we refer to MVU as the formulation with *inequality* constraints.

Unfortunately, it is fair to say that due to its semi-definite programming (SDP) formulation [11], MVU is amongst the least scalable manifold learning algorithms and cannot embed state spaces beyond 4000 states—severally limiting the usefulness of the proposed heuristic in practice. Although there have been efforts to increase the scalability of MVU [145, 147], these lead to approximate solutions which no longer guarantee admissibility or consistency of heuristics.

In this chapter we propose a novel algorithm, Maximum Variance Correction (MVC), which improves the scalability of MVU by several orders of magnitude. In a nutshell, MVC post-processes embeddings from any manifold learning algorithm, to strictly satisfy the MVU constraints by rearranging embedded points within local patches. Hereby MVC combines the strict finite-size guarantees of MVU with the large-scale capabilities of alternative algorithms. Further, it bridges the gap between the rich literature on manifold learning and what we consider its most promising and high-impact application to date—the use of Euclidean state-space embeddings as A^* heuristics.

Our contributions are summarized as follows: 1) We introduce MVC, a fully *parallelizable* algorithm that scales up and speeds up MVU by several orders of magnitudes. 2) We provide a formal proof that any solution of our relaxed problem formulation still satisfies all MVU constraints. 3) We demonstrate on several A^* search benchmark problems that the resulting heuristics lead to impressive reductions in search-time—even beating the competitive differential heuristic [102] by a large factor on all data sets.

2.1.2 Background and related work

There have been several recent publications that increase the scalability of manifold learning algorithms. Vasiloglou et al. [140], Weinberger et al. [147], Weinberger and Saul [146] directly scale up MVU by relaxing its constraints and restricting the solution to the space spanned by landmark points or the eigenvectors of the graph laplacian matrix. Silva and Tenenbaum [129], Talwalkar et al. [136] scale up Isomap [137] with Nyström approximations. Our work is complementary as we refine these embeddings to meet the MVU constraints while maximizing the variance of the embedding.

Shaw and Jebara [126] introduce structure preserving embedding, which learns embeddings that strictly preserve graph properties (such as nearest neighbors). Zhang et al. [159] also focus on local patches of manifolds, however preserves discriminative ability rather than the finite-size guarantees of MVU.

From a technical stand-point, the technique used by MVC is probably most similar to Biswas and Ye [7] which uses a semi-definite program for sensor network embedding. Due to the nature of their application, they deal with different constraints and objectives.

Graph Embeddings

We have introduced MVU in Chapter 1. In this section, we mainly introduce other graph embedding algorithms. Let $G = (V, E)$ denote the graph with undirected edges E and nodes V, with $|V| = n$. Edges $(i, j) \in E$ are weighted by some $d_{ij} \geq 0$. Let δ_{ij} denote the shortest path distance from node i to j. Manifold learning algorithms embed the nodes in V into a d-dimensional Euclidean space, $\mathbf{x}_1, \ldots, \mathbf{x}_n \in \mathcal{R}^d$, such that $\|\mathbf{x}_i - \mathbf{x}_j\|_2 \approx \delta_{ij}$.

Graph Laplacian MVU (gl-MVU), Weinberger and Saul [146], Wu et al. [150], is an extension of MVU that reduces the size of $\mathbf{K}$ by matrix factorization, $\mathbf{K} = \mathbf{Q}^\top \mathbf{L} \mathbf{Q}$. Here, $\mathbf{Q}$ are the bottom eigenvectors of the Graph Laplacian, also referred to as **Laplacian Eigenmaps** [4]. All local distance constraints are removed and instead added as a penalty term into the objective. The resulting algorithm scales to larger data sets but makes no exact guarantees about the distance preservations.

Isomap, Tenenbaum et al. [137], preserves the global structure of the graph by directly preserving the graph distances between *all* pair-wise nodes:

$$\min_{\mathbf{x}_1,\dots,\mathbf{x}_n \in \mathcal{R}^d} \sum_{i,j} ((\mathbf{x}_i - \mathbf{x}_j)^2 - \delta_{ij}^2)^2. \tag{2.1}$$

Tenenbaum et al. [137] show that (2.1) can be approximated as an eigenvector decomposition by applying multi-dimensional scaling (MDS) [73] on the shortest path distances $\delta(i,j)$[5]. The landmark extension [129] leads to significant speed-ups with Nyström approximations of the graph-distance matrix. For simplicity, we refer to it also as "Isomap" throughout this dissertation.

Euclidean Heuristic

The A^* search algorithm finds the shortest path between two nodes in a graph. In the worst case, the complexity of the algorithm is exponential in the length of the shortest path, but the search time can be drastically reduced with a good heuristic, which estimates the graph distance between two nodes. Rayner et al. [110] suggest to use the distance $h(i,j) = \|\mathbf{x}_i - \mathbf{x}_j\|_2$

---

[5]Recent studies [88, 89] give efficient implementation for computing all-pair shortest-path distance on GPUs.

of the MVU graph embedding as such a heuristic, which they refer to as *Euclidean Heuristic*. A^* with this heuristic provably converges to the exact solution, as the heuristic is admissible and consistent. More precisely, for all nodes i, j, k the following holds:

$$\text{Admissibility:} \qquad \|\mathbf{x}_i - \mathbf{x}_k\|_2 \le \delta_{ik} \qquad (2.2)$$

$$\text{Consistency:} \qquad \|\mathbf{x}_i - \mathbf{x}_j\|_2 \le \delta_{ik} + \|\mathbf{x}_k - \mathbf{x}_j\|_2 \qquad (2.3)$$

The proof is straight-forward. As the shortest-path between nodes i and j in the embedding consists of edges which are all underestimated, it must be underestimated itself and so is $\|\mathbf{x}_i - \mathbf{x}_j\|_2$ (which implies admissibility). Consistency follows from the triangular inequality in combination with(2.2).

The closer the gap in the admissibility inequality (2.2), the better is the search heuristic. The perfect heuristic would be the actual shortest path, $h(i, j) = \delta_{ij}$ (with which A^* could find the exact solution in linear time with respect to the length of the shortest path). The MVU objective maximizes all pairwise distances, and therefore minimizes exactly the gap in (2.2). Consequently, MVU is the perfect optimization problem to find a Euclidean Heuristic—however in its original formulation it can only scale to $n \approx 4000$. In the following we will scale up MVU to much larger data sets.

2.1.3   Method

In this section, we introduce our MVC algorithm. Intuitively, MVC combines the scalability of gl-MVU and Isomap with the strong guarantees of MVU: It uses the former to obtain an initial embedding of the data and then post-processes it into a local optimum of the MVU

optimization. The post-processing only involves re-optimizations of local patches, which is fast and can be decomposed into independent sub-problems.

Initialization. We obtain an initial embedding $\hat{\mathbf{x}}_1, \ldots, \hat{\mathbf{x}}_n$ of the graph with any (large-scale) manifold learning algorithm (*e.g.* Isomap, gl-MVU or Eigenmaps). The resulting embedding is typically not a feasible solution to the exact MVU problem, because it violates many distance inequality constraints in (1.14). To make it feasible, we first center it and then rescale the entire embedding such that all inequalities hold with at least one equality,

$$\mathbf{x}_i = \alpha(\hat{\mathbf{x}}_i - \frac{1}{n}\sum_{i=1}^{n}\hat{\mathbf{x}}_i), \text{ with } \alpha = \min_{(i,j)\in E}\frac{d_{ij}}{\|\hat{\mathbf{x}}_i - \hat{\mathbf{x}}_j\|}. \tag{2.4}$$

After the translation and rescaling in (2.4) we obtain a solution in the feasible set of MVU embeddings, and therefore also an admissible and consistent Euclidean Heuristic. In practice, this heuristic is of very limited use because it has a very large admissibility gap (2.2). In the following sections we explain how to transform the embedding to maximize the MVU objective, while remaining inside the MVU feasible region.

Local patching

The (convex) MVU optimization is an SDP, which in their general formulation scale cubic in the input size n. To scale-up the optimization we therefore utilize a *specific* property of the MVU constraints: All constraints are strictly *local* as they only involve directly connected nodes. This allows us to divide up the graph embedding into local patches and re-optimize the MVU optimization on each patch individually. This approach has two clear advantages: the local patches can be made small enough to be re-optimized very quickly and the individual patch optimizations are inherently parallelizable—leading to even further speed-ups

on modern multi-core computers. A challenge is to ensure that the local optimizations do not interfere with each other and remain globally feasible.

Graph partitioning. There are several ways to divide the graph $G = (V, E)$ into r mutually exclusive connected components. We use repeated breadth first search (BFS) [119] because of its simplicity, fast speed and guarantee that all partitions are connected components. Specifically, we pick a node i uniformly at random and apply BFS to identify the m closest nodes according to graph distance, that are not already assigned to patches. These nodes form a new patch $G_p = (V_p, E_p)$. The partitioning is continued until all nodes in V are assigned to exactly one partition, resulting in approximately $r = \lceil n/m \rceil$ patches.[6] The final partitioning satisfies $V = V_1 \cup \ldots \cup V_r$ and $V_p \cap V_q = \{\}$ for all p, q.

We distinguish between two types of nodes within a partition V_p (illustrated in figure 2.1). A node $i \in V_p$ is an *inner point* (blue circle) of V_p if all edges $(i, j) \in E$ connect it to other nodes $j \in V_p$; i is an *anchor point* (red circle) of V_p if there exists an edge $(i, j) \in E$ to some $j \notin V_p$. Let V_p^x denote the set of all inner nodes and V_p^a the set of all anchor points in V_p. By definition, these sets are mutually exclusive and together contain all points, *i.e.* $V_p^x \cap V_p^a = \{\}$ and $V_p = V_p^x \cup V_p^a$.

Similarly, all edges in E can be divided into three mutual exclusive subsets (see figure 2.1): edges between inner points (E^{xx}, blue); between anchor points (E^{aa}, red); between anchor and inner points (E^{ax}, purple).

Optimization. We first re-state the non-convex MVU optimization (1.14) presented in Chapter 1, slightly re-formulated to incorporate the graph partitioning. As each input is either an anchor point or an inner point of its respective patch, we can denote the set of

---

[6]The exact number of patches and number of nodes per patch vary slightly, depending on the connectivity of the graph, but all $|V_p| \le m$.
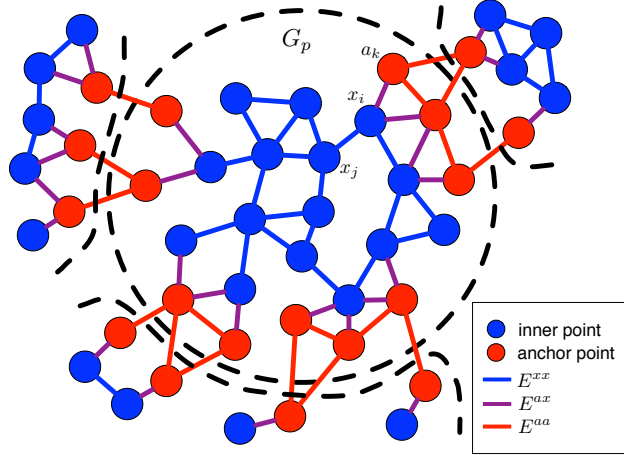
Figure 2.1: Drawing of a patch with inner and anchor points.

all inner points as $V^x = \bigcup_p V_p^x$ and the set of all anchor points as $V^a = \bigcup_p V_p^a$. If we re-order the summations and constraints by these sets, we can re-phrase the non-convex MVU optimization (1.14) as

$$
\begin{aligned}
\underset{\mathbf{x}_i, \mathbf{a}_k}{\text{maximize}} \quad & \sum_{i \in V^x} \mathbf{x}_i^2 + \sum_{k \in V^a} \mathbf{a}_k^2 \\
\text{subject to} \quad & ||\mathbf{x}_i - \mathbf{x}_j||_2 \le d_{ij} \quad \forall (i,j) \in E^{xx} \\
& ||\mathbf{x}_i - \mathbf{a}_k||_2 \le d_{ik} \quad \forall (i,k) \in E^{ax} \\
& ||\mathbf{a}_i - \mathbf{a}_j||_2 \le d_{ij} \quad \forall (i,j) \in E^{aa} \\
& \sum_{\mathbf{a}_i \in V^a} \mathbf{a}_i + \sum_{\mathbf{x}_i \in V^x} \mathbf{x}_i = \mathbf{0}.
\end{aligned}
\tag{2.5}
$$

For clarity, we denote all anchor points as $\mathbf{a}_i$'s and inner points as $\mathbf{x}_j$'s and with a slight abuse of notation write $\mathbf{a}_i \in V^a$.

Optimization by patches. The optimization (2.5) is identical to the non-convex MVU formulation (1.14) and just as hard to solve. To reduce the computational complexity we make two changes: we remove the centering constraint and fix the anchor points in place.

28

The removal of the centering constraint is a harmless relaxation because the fixed anchor points already remove translation as a degree of freedom and fixate the solution very close to zero-mean. (The objective changes slightly, but in practice this has minimal impact on the solution.) The fixing of the anchor points allows us to break down the optimization into r independent sub-problems. This can be seen from the fact that by definition all constraints in E^{xx} never cross patch boundaries, and constraints in E^{ax} only connect points within a patch with fixed points. Constraints over edges in E^{aa} can be dropped entirely, as edges between anchor points are necessarily fixed also. We obtain r independent optimization problems of the following type:

$$
\begin{aligned}
\underset{\mathbf{x}_i \in V_p^x}{\text{maximize}} \quad & \sum_{i \in V_p} \mathbf{x}_i^2 \\
\text{subject to} \quad & ||\mathbf{x}_i - \mathbf{x}_j||_2 \le d_{ij} \quad \forall (i,j) \in E_p^{xx} \\
& ||\mathbf{x}_i - \mathbf{a}_k||_2 \le d_{ik} \quad \forall (i,k) \in E_p^{ax}.
\end{aligned}
\tag{2.6}
$$

The solutions of the r sub-problems (2.6) can be combined and centered, to form a feasible solution to (2.5).

Convex patch re-optimization. Similar to the non-convex MVU formulation (1.14), optimization (2.6) is also non-convex and non-trivial to solve. However, with a change of variables and a slight relaxation we can transform it into a semi-definite program. Let $n_p = |V_p|$. Given a patch G_p, we define a matrix $X = [\mathbf{x}_1, \ldots, \mathbf{x}_{n_p}] \in \mathcal{R}^{d \times n_p}$, where each column corresponds to one embedded input of V_p^x—the variables we want to optimize. Further, let us define the matrix $K \in \mathcal{R}^{(d+n_p) \times (d+n_p)}$ as:

$$
\mathbf{K} = \begin{pmatrix} \mathbf{I} & \mathbf{X} \\ \mathbf{X}^\top & \mathbf{H} \end{pmatrix} \quad \text{where } \mathbf{H} = \mathbf{X}^\top \mathbf{X}.
\tag{2.7}
$$

The vector $\mathbf{e}_{i,j} \in \mathcal{R}^{n_p}$ is all-zero except the ith element is 1 and the jth element is -1. The vector $\mathbf{e}_i$ is all-zero except the ith element is -1. With this notation, we obtain

$$\begin{aligned}
(\mathbf{0}; \mathbf{e}_{ij})^\top \mathbf{K}(\mathbf{0}; \mathbf{e}_{ij}) &= \|\mathbf{x}_i - \mathbf{x}_j\|_2^2 \\
(\mathbf{a}_k; \mathbf{e}_i)^\top \mathbf{K}(\mathbf{a}_k; \mathbf{e}_i) &= \|\mathbf{x}_i - \mathbf{a}_k\|_2^2,
\end{aligned}$$
(2.8)

where $(\mathbf{0}; \mathbf{e}_{ij}) \in \mathcal{R}^{(d+n_p)}$ denotes the vector $\mathbf{e}_{ij}$ padded with zeros on top and $(\mathbf{a}_k; \mathbf{e}_i) \in \mathcal{R}^{(d+n_p)}$ the concatenation of $\mathbf{a}_k$ and $\mathbf{e}_i$.

Through (2.8), all constraints in (2.6) can be re-formulated as a linear form of $\mathbf{K}$ (after squaring). The objective reduces to $\text{trace}(\mathbf{H}) = \sum_{i=1}^{n_p} \mathbf{x}_i^2$. The resulting optimization problem becomes:

$$\begin{aligned}
\max_{\mathbf{X}, \mathbf{H}} \quad & \text{trace}(\mathbf{H}) \\
\text{s.t.} \quad & (\mathbf{0}; \mathbf{e}_{ij})^\top \mathbf{K}(\mathbf{0}; \mathbf{e}_{ij}) \leq d_{ij}^2 \qquad \forall (i,j) \in E_p^{xx} \\
& (\mathbf{a}_k; \mathbf{e}_i)^\top \mathbf{K}(\mathbf{a}_k; \mathbf{e}_i) \leq d_{ik}^2 \qquad \forall (i,k) \in E_p^{ax} \\
& \mathbf{H} = \mathbf{X}^\top \mathbf{X} \\
& \mathbf{K} = \begin{pmatrix} \mathbf{I} & \mathbf{X} \\ \mathbf{X}^\top & \mathbf{H} \end{pmatrix}.
\end{aligned}$$
(2.9)

The constraint $\mathbf{H} = \mathbf{X}^\top \mathbf{X}$ fixes the rank of $\mathbf{H}$ and is not convex. To mitigate, we relax it into $\mathbf{H} \succeq \mathbf{X}^\top \mathbf{X}$. In the following section we prove that this weaker constraint is sufficient to obtain MVU-feasible solutions. The Schur Complement Lemma [11] states that $\mathbf{H} \succeq \mathbf{X}^\top \mathbf{X}$

Algorithm 1 MVC (V,E)

1: compute initial solution $\mathbf{X}$ with gl-MVU or Isomap
2: center and rescale $\mathbf{X}$ according to (2.4)
3: **repeat**
4:   identify r random sub-graphs $(V_1, E_1), \ldots, (V_r, E_r)$
5:   **parfor** p=1 to r **do**
6:     solve (2.10) for (V_p, E_p) to obtain $\mathbf{X}_p$
7:   **end parfor**
8:   concatenate all $\mathbf{X}_p$ into $\mathbf{X}$ and center.
9: **until** variance of embedding $\mathbf{X}$ has converged.
10: **return X**

---

if and only if $\mathbf{K} \succeq 0$, which we enforce as an additional constraint:

$$
\begin{aligned}
\max_{\mathbf{X},\mathbf{H}} \quad & \text{trace}(\mathbf{H}) \\
\text{s.t.} \quad & (\mathbf{0}; \mathbf{e}_{ij})^\top \mathbf{K}(\mathbf{0}; \mathbf{e}_{ij}) \leq d_{ij}^2 \quad \forall (i,j) \in E_p^{xx} \\
& (\mathbf{a}_k; \mathbf{e}_i)^\top \mathbf{K}(\mathbf{a}_k; \mathbf{e}_i) \leq d_{ik}^2 \quad \forall (i,k) \in E_p^{ax} \\
& \mathbf{K} = \begin{pmatrix} \mathbf{I} & \mathbf{X} \\ \mathbf{X}^\top & \mathbf{H} \end{pmatrix} \succeq 0.
\end{aligned}
\tag{2.10}
$$

The optimization (2.10) is convex and scales $O((n_p + d)^3)$. It monotonically increases the objective in (2.5) and converges to a fixed point. For a maximum patch-size m, *i.e.* $n_p \leq m$ for all p, each iteration of MVC scales *linearly* with respect to n, with complexity $O(\lceil \frac{n}{m} \rceil (m + d)^3)$. As the choice of m is independent of n, it can be fixed to a medium-sized value *e.g.* $m \approx 500$ for maximum efficiency. The $r \approx \lceil \frac{n}{m} \rceil$ sub-problems are completely independent and can be solved *in parallel*, leading to almost perfect parallel speed-up on computing clusters. The same methodology also applies to 3D modeling [164, 163, 161, 162]. Algorithm 1 states MVC in pseudo-code.

MVU feasibility

We prove that the MVC algorithm returns a feasible MVU solution and consequently gives rise to a well defined Euclidean Heuristic. First we need to show that the relaxation from $\mathbf{H} = \mathbf{X}^\top\mathbf{X}$ to $\mathbf{H} \succeq \mathbf{X}^\top\mathbf{X}$ does not cause any constraint violations.

Lemma 1. The solution $\mathbf{X}$ of (2.10) satisfies all constraints in (2.6).

Proof. We first focus on constraints on $(i,j) \in E_p^{xx}$. The first constraint in (2.10) guarantees

$$\mathbf{H}_{ii} - 2\mathbf{H}_{ij} + \mathbf{H}_{jj} \leq d_{ij}^2. \tag{2.11}$$

The last constraint of (2.10) and the Schur Complement Lemma enforce that $\mathbf{H} - \mathbf{X}^\top\mathbf{X} \succeq 0$. Thus,

$$\mathbf{e}_{ij}^\top(\mathbf{H} - \mathbf{X}^\top\mathbf{X})\mathbf{e}_{ij} \geq 0$$

$$\Leftrightarrow \qquad \mathbf{e}_{ij}^\top(\mathbf{X}^\top\mathbf{X})\mathbf{e}_{ij} \leq \mathbf{e}_{ij}^\top\mathbf{H}\mathbf{e}_{ij} \tag{2.12}$$

$$\Leftrightarrow \quad \mathbf{x}_i^2 - 2\mathbf{x}_i^\top\mathbf{x}_j + \mathbf{x}_j^2 \leq \mathbf{H}_{ii} - 2\mathbf{H}_{ij} + \mathbf{H}_{jj}$$

$$\Leftrightarrow \qquad \|\mathbf{x}_i - \mathbf{x}_j\|_2^2 \leq \mathbf{H}_{ii} - 2\mathbf{H}_{ij} + \mathbf{H}_{jj}. \tag{2.13}$$

The first result follows from the combination of (2.11) and (2.13). Concerning constraints $(i,j) \in E_p^{ax}$, the second constraint in (2.10) guarantees that

$$\mathbf{a}_k^2 - 2\mathbf{a}_k^\top\mathbf{x}_i + \mathbf{H}_{ii} \leq d_{ik}^2. \tag{2.14}$$

With a similar reasoning as for (2.12) we obtain $\mathbf{e}_i^\top (\mathbf{X}^\top \mathbf{X}) \mathbf{e}_i \leq \mathbf{e}_i^\top \mathbf{H} \mathbf{e}_i$ and therefore $\mathbf{x}_i^2 \leq \mathbf{H}_{ii}$. Combining this inequality with (2.14) leads to the result:

$$\|\mathbf{a}_k - \mathbf{x}_i\|_2^2 \leq \mathbf{a}_k^2 - 2\mathbf{a}_k \mathbf{x}_i + \mathbf{H}_{ii} \leq d_{ik}^2. \ \blacksquare$$

Theorem 1. The embedding obtained with the MVC Algorithm 1 is in the feasible set of (1.14).

Proof. We apply an inductive argument. The initial solution after centering and re-scaling according to (2.4) is MVU feasible by construction. By **Lemma 1**, the solution of (2.10) for each patch satisfies all constraints in E_p^{xx} and E_p^{ax} in (2.6). As each distance constraint in (2.5) is associated with exactly one patch, all its constraints in E^{xx} and E^{ax} are satisfied. Constraints in E^{aa} are fixed and satisfied by the induction hypothesis. Centering $\mathbf{X}$ satisfies the last constraint in (2.5) and leaves all distance constraints unaffected. As (2.5) is equivalent to (1.14), we obtain an MVU feasible solution at the end of each iteration in Algorithm 1, which concludes the proof. $\blacksquare$

2.1.4 Experimental results

We evaluate our algorithm on a real world shortest path application data set and on two well-known benchmark AI problems.

Game Maps is a real world map dataset with 3,155 states from the international success multi-player game *Biowares Dragon Age: Origins*[TM].[7] A game map is a maze that consists of empty spaces (states) and obstacles. Cardinal moves take unit costs while diagonal moves

---

[7]http://en.wikipedia.org/wiki/Dragon_Age:_Origins
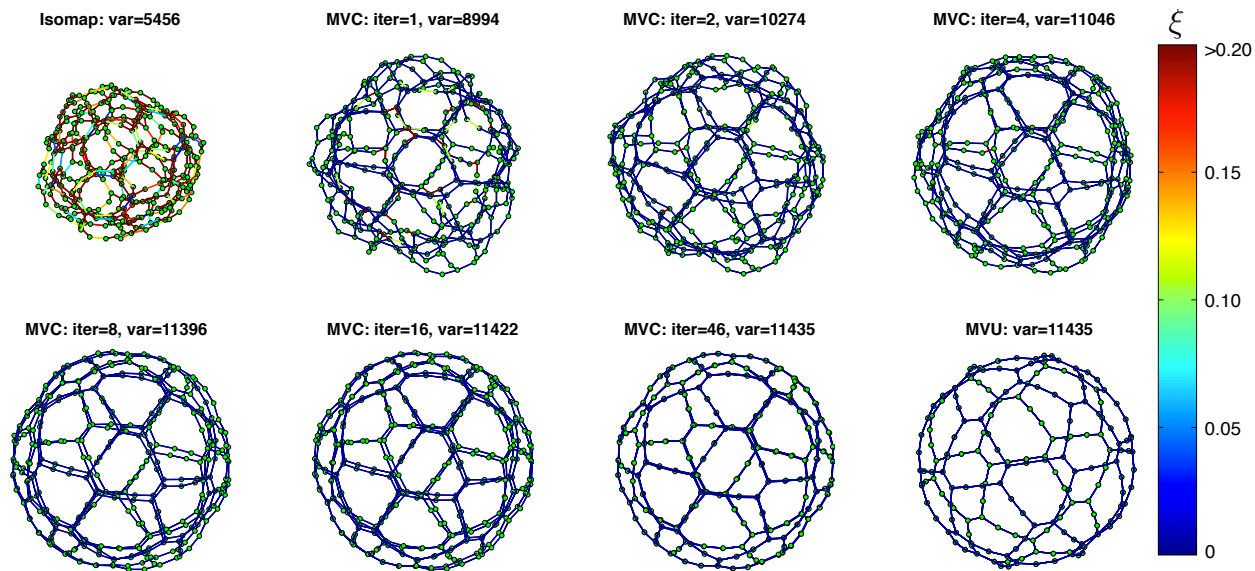
Figure 2.2: Visualization of several MVC iterations on the 5-puzzle data set ($m = 30$). The edges are colored proportional to their relative admissibility gap ξ, as defined in (2.15). The top left image shows the (rescaled) Isomap initialization. The successive graphs show that MVC decreases the edge admissibility gaps and increases the variance with each iteration (indicated in the title of each subplot) until it converges to the same variance as the MVU solution (bottom right).

cost 1.5. The search problem is to find an optimal path between a given start and goal state, while avoiding all obstacles. Although not large-scale, this data set is a great example for an application where the search heuristic is of extraordinary importance. Speedy solvers are essential to reduce upkeep costs and to ensure a positive user experience. In the game, many player and non-player characters interact and search problems have to be solved frequently as agents move. The shortest path solutions cannot be cached as the map changes dynamically with player actions.

M-**Puzzle Problem** [67] is a NP-hard sliding puzzle, often used as a benchmark problem for search algorithms/heuristics. It consists of a frame of M square tiles and one tile missing. All tiles are numbered and a state constitutes any order from which a path to the unique state with sorted (increasing) tiles exists. An action is to move a cardinal neighbor tile of

Table 2.1: Relative A^* search speedup over the differential heuristic (in expanded nodes) and embedding variance ($\times 10^5$).

	game map		6-blocksworld		7-puzzle		7-blocksworld		8-puzzle	
Method	speedup	var	speedup	var	speedup	var	speedup	var	speedup	var
Diff. Heuristic	1	N/A	1	N/A	1	N/A	1	N/A	1	N/A
Eigenmap	0.32	0.88	0.66	0.058	0.81	3.52	0.61	0.50	0.76	13.47
Isomap	0.50	12.13	0.61	0.046	0.84	3.73	0.65	0.46	0.67	10.62
MVU	**1.12**	**37.27**	1.23	0.154	N/A	N/A	N/A	N/A	N/A	N/A
gl-MVU	0.41	7.54	1.18	0.138	1.14	6.66	1.05	1.20	0.88	17.79
MVC-10 (eigenmap)	0.88	31.31	1.49	0.22	1.41	9.59	1.33	1.88	1.47	43.48
MVC-10 (isomap)	1.09	36.96	1.56	0.22	1.43	9.62	1.25	1.71	1.45	43.08
MVC-10 (gl-mvu)	0.90	32.98	1.96	0.27	1.45	9.82	1.67	2.27	1.52	45.75
MVC (eigenmap)	1.06	35.92	2.08	0.29	1.45	**9.86**	2.17	2.93	1.54	46.52
MVC (isomap)	**1.12**	37.22	2.22	0.30	**1.47**	9.85	**2.22**	**2.95**	1.54	46.58
MVC (gl-mvu)	1.11	36.47	**2.27**	**0.30**	1.45	**9.86**	**2.22**	**2.95**	**1.61**	**49.06**

the empty space into the empty space. The task is to find a shortest action sequence from a pre-defined start to a goal state. We evaluate our algorithm on the 5- (for visualization), 7- and 8-puzzle problem (3×2, 4×2 and 3×3 frames), which contain 360, 20160 and 181440 states respectively.

Blocks World [55] is a NP-hard problem with the goal to build several pre-defined stacks out of a set of numbered blocks. Blocks can be placed on the top of others or on the ground. Any block that is currently under another block cannot be moved. The goal is to find a minimum action sequence from a start state to a goal state. We evaluate our algorithm on block world problems with 6 blocks (4,051 states) and 7 blocks (37,633 states), respectively.

Problem characteristics. The three types of problems not only feature different sized state spaces but also have different state space characteristics. Game maps has random obstacles that prevents movement for some state pairs, and thus has an irregular state space. The puzzle problems have a more regular search space (which lie on the surface of a sphere, see figure 2.2) with stable out-degree for each state. The state space of the blocksworld problems

is also regular (it lies inside a sphere); however, the out-degree varies largely across states. For example, in 7-blocks, the state in which every block is placed on the ground has 42 edges, while the state in which all blocks are stacked in a single column has only 1 edge. We set $d_{ij} = 1$ for all edges in blocksworld and M-puzzle problems.

Experimental setting. Besides MVC, we evaluate four graph embedding algorithms: MVU [146], Isomap [137], (Laplacian) Eigenmap [4] and gl-MVU [150]. The last three are used as initializations for MVC. Following Rayner et al. 110, the embedding dimension is $d = 3$ for all experiments. For gl-MVU, we set the dimension of graph Laplacian to be 40. For datasets of size greater than 10K, we set 10K landmarks for Isomap. For MVC we use a patch-size of $m = 500$ throughout (for which problem (2.10) can be solved in less than $20s$ on our lab desktops).

Visualization of MVC iterations $(m = 30)$. Figure 2.2 visualizes successive iterations of the $d = 3$ dimensional MVC embedding of the $5-$puzzle problem. All edges are colored proportionally to their relative admissibility gap,

$$\xi_{ij} = \frac{d_{ij} - ||\mathbf{x}_i - \mathbf{x}_j||}{||\mathbf{x}_i - \mathbf{x}_j||}. \tag{2.15}$$

The plot in the top left shows the original Isomap initialization after re-scaling, as defined in (2.4). The plot in the bottom right shows the actual MVU embedding from (1.15)— which can be computed precisely because of the small problem size. Intermediate plots show the embeddings after several iterations of MVC. Two trends can be observed: 1. the admissibility gap decreases with MVC (all edges are blue in the final embedding) and 2. the variance $\sum_i \mathbf{x}_i^2$ of the embedding, *i.e.* the MVU objective, increases monotonically. The final embedding has the same variance as the actual MVU embedding. The figure also shows that the $5-$puzzle state space lies on a sphere, which is a beautiful example that visualization

36
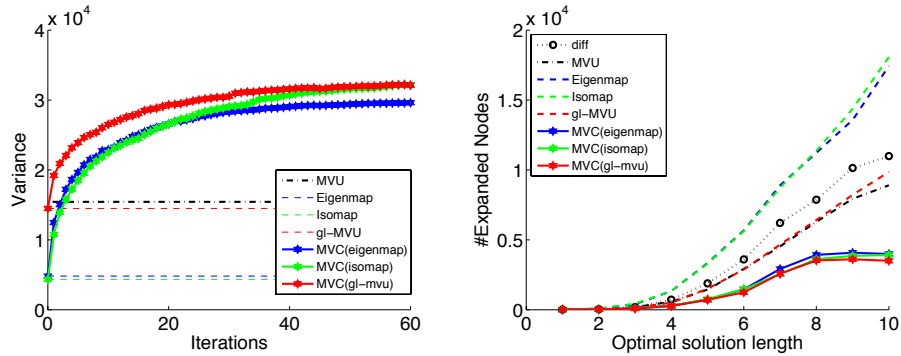
Figure 2.3: (*Left*) the embedding variance of 6-blocksworld plotted over 30 MVC iterations. The variance increases monotonically and even outperforms the actual MVU embedding [146] after only a few iterations. (*Right*) the number of expanded nodes in A^* search as a function of the optimal solution length. All MVC solutions strictly outperform the Differential Heuristic (*diff*) and even expand fewer nodes than MVU.

of states spaces in itself can be valuable. For example, the discovery of specific topological properties might lead to a better understanding of the state space structure and aid the development of problem specific heuristics.

Setup. As a baseline heuristic, we compare all results with a differential heuristic [102]. The differential heuristic pre-computes the exact distance from all states to a few pivot points in a (randomly chosen) set $S \subseteq V$. The graph distance between two states a, b is then approximated with $\max_{s \in S} |\delta(a, s) - \delta(b, s)| \leq \delta(a, b)$. In our experiments we set the number of pivots to 3 so that differential heuristics and embedding heuristics share the same memory limit. Figure 2.3 (*right*) shows the total expanded nodes as a function of the solution length, averaged over 100 start/goal pairs for each solution length. The figure compares MVC with various initializations, the differential heuristic and the MVU algorithm on the 6-blocksworld puzzle. Speedups (reported in Table 2.1) measure the reduction in expanded states during search, relative to the differential heuristic, averaged over 100 random (start, goal) pairs across all solution lengths.

Table 2.2: Training time for MVU [145] and MVC, reported after initialization, the first 10 iterations (MVC-10), and after convergence.

Method	game	6-block	7-puzz	7-block	8-puzz
$|V|$	3,155	4,051	20,160	37,633	181,440
MVU	3h	10h	N/A	N/A	N/A
Eigenmap	1s	1s	4s	2m	7m
Isomap	14s	57s	3m	4m	32m
gl-MVU	2m	1m	1m	8m	15m
MVC-10 (eig)	20m	2m	14m	9m	2h
MVC-10 (iso)	15m	3m	20m	11m	3h
MVC-10 (glm)	21m	3m	18m	14m	3h
MVC (eig)	36m	9m	72m	53m	6h
MVC (iso)	17m	8m	56m	51m	7h
MVC (glm)	34m	5m	26m	33m	7h

Comprehensive evaluation. Table 2.1 shows the A^* search performances of Euclidean heuristics obtained by the MVC initializations, MVC after only 10 iterations (MVC-10) and after convergence (bottom section). Table 2.1 also shows the MVU objective/variance, $\sum_{\mathbf{x} \in V} \mathbf{x}_i^2$, of each embedding. Several trends can be observed: 1. MVC performs best when initialized with gl-MVU—this is not surprising as gl-MVU has a similar objective and is likely to lead to better initializations; 2. all MVC embeddings lead to drastic speedups over the differential heuristics; 3. the variance is highly correlated with speedup—supporting Rayner et al. [110] that the MVU objective is well suited to learn Euclidean heuristics; 4. even MVC after only 10 iterations already outperforms the differential heuristic on almost all data sets. The consistency of the speedups and their unusually high factors (up to 2.22) show great promise for MVC as an embedding algorithm for Euclidean heuristics.

Exceeding MVU. On the 6-blocksworld data set in table 2.1, the variance of MVC actually exceeds that of MVU. In other words, the MVC algorithm finds a better solution for (1.14). This phenomenon can be explained by the fact that the convex MVU problem (1.15)

presented in Chapter 1 is rank-relaxed and the final embedding is obtained after projection into a $d = 3$ dimensional sub-space. As MVC performs its optimization directly in this d-dimensional sub-space, it can find a better *rank-constrained* solution. This effect is further illustrated in Figure 2.3 (*left*), which shows the monotonic increase of the embedding variance as a function of the MVC iterations (on 6-blocksworld). After only a few iterations, all three MVC runs exceeds the MVU solution. A similar effect is utilized by Shaw and Jebara [125], who optimize MVU in lower dimensional spaces directly (but cannot scale to large data sets). Figure 2.3 (*left*) also illustrates the importance of initialization: MVC initialized with Isomap and gl-mvu converge to the same (possibly globally optimal) solution, whereas the run with Laplacian Eigenmaps initialization is stuck in a sub-optimal solution. Our findings are highly encouraging and show that we might not only approximate MVU effectively on very large data sets, but actually *outperform it* if the intrinsic dimensionality of the data is higher than the desired embedding dimensionality d.

Embedding time. Table 2.2 shows the training time required for the convex MVU algorithm (1.15), three MVC initializations (Eigenmap, Isomap, gl-MVU), the time for 10 MVC iterations and the time until MVC converges, across all five data sets. Note that for real deployment, such as GPS systems, MVC only needs to be run once to obtain the embedding. The online calculations of Euclidean heuristics are very fast. All embeddings were computed on an off-the-shelve desktop with two 8-core Intel(R) Xeon(R) processors of 2.67 GHz and $128GB$ of RAM. Our MVC implementation is in MATLAB^{TM} and uses CSDP [9] as the SDP solver. We parallelize each run of MVC on eight cores. All three initializations require roughly similar time (although Laplacian Eigenmaps is the fastest on all data sets), which is only a small part of the overall optimization. Whereas MVU requires 10 hours for graphs with $|V| = 4051$ (and cannot be executed on larger problems), we can find a superior solution

to the same problem in 5 minutes and are able to run MVC on $45\times$ larger problems in only 7 hours.

2.1.5 Conclusion

In this chapter, we have presented MVC, an iterative algorithm to transform graph embeddings into MVU feasible solution. On several small-sized problems where MVU can finish, we show that MVC gives comparable or even better solutions than MVU. We apply MVU on data sets of unprecedented sizes ($n = 180,000$) and, because of *linear* scalability, expect future (parallel) implementations to scale to graphs with millions of nodes. By satisfying all MVU constraints, MVC embeddings are provably well-defined Euclidean heuristics for A^* search and unleash an exciting new area of applications to all of manifold learning. We hope it will fuel new research directions in both fields.

2.2 Goal-oriented Euclidean heuristics - a refined Euclidean heuristic

2.2.1 Introduction

With the development of MVC described in Section 2.1, EH becomes an attractive and scalable choice for computing heuristics. However, its potential is yet to be fully explored. The objective of MVU/MVC minimizes the sum of the distance gaps between all pairs of states, while A^* search is guided only by the heuristic distance to the goal state. In many applications, possible (or likely) goal states form a small subset of the overall state space.

For example, GPS driving assistants are mostly used to find directions to registered street addresses, which are a tiny fraction of all possible locations on a map. This suggests that the EH can be further improved by "tightening" the heuristic distances towards likely goal states.

Moreover, state graphs are typically not isometric to low dimensional Euclidean spaces, which leads to distance gaps between the EH heuristic and the true distances—in particular, for states that are far away from each other. We find that it is possible to compactly encode the information about distance gaps, using only a small amount of memory, and significantly improve the search performance by correcting heuristic estimates on-the-fly.

Our main contributions include, 1) a goal-oriented graph embedding framework that optimizes the heuristic distance to goals while preserving admissibility and consistency, and 2) an in-memory enhancement technique that can be used online to speed up search. Since the enhancement technique generates better heuristics that are admissible but no longer consistent, we employ the B′ search to make sure that the first solution found is an optimal one.

2.2.2 Goal-oriented Euclidean heuristic

We make several assumptions about our problem domain: The state-space is represented as an undirected graph with n nodes, which fits into memory. We are asked to solve search problems repeatedly, with different starting and goal states. We would like to minimize the time required for these search problems through better heuristics. The heuristics can be optimized offline, where computation time is of no particular importance, but the storage

required to encode the heuristic must be small (as it might need to be communicated to the consumers and loaded into memory).

In many A^* search applications, some states are much more likely to be considered goal states than others. For example, in video games, certain locations (*e.g.* treasure targets) are typical goals that a players might want to move to, whereas most arbitrary positions in the game space are moved to very infrequently. In the subsequent section we describe a robot planning domain, where robots can pick up objects from pre-specified source locations and move them to pre-specified target locations. Here, there exists a strict subset of states that could potentially become goal states—important information that ideally should be incorporated into the heuristic design. As a final example, GPS navigation assistants are typically exclusively used to direct users to registered home addresses—a tiny subset of all possible locations on the map. Further, a particular user might only traverse between no more than 100 locations on the world map. It is fair to assume that she might prefer accelerating the search for these frequent goals, even at the cost that the search for infrequent goals takes a little longer.

Let $G = (V, E)$ be the state-space graph. For convenience, we assume that there is a subset of possible goal states $V_G \subseteq V$. When we know a set of possible goals, we can improve EH by maximizing the distances to the goals. Note that during an A^* search, only those distances to the particular goal state will be used as the heuristic function (h), and heuristic distances between two non-goal states are never used during search. This motivates us to modify the objective function in the EH/MVU optimization so that it exclusively maximizes distances to goals. Note that we can still guarantee admissibility and consistency of EH, since we keep all local constraints.

The proposed *goal-oriented Euclidean heuristic* (GOEH) solves the following:

$$\underset{\mathbf{x}_1,\ldots,\mathbf{x}_n \in \mathcal{R}^d}{\text{maximize}} \quad \sum_{i=1..n, g \in V_G} \|\mathbf{x}_i - \mathbf{x}_g\|_2^2$$

$$\text{subject to} \quad \|\mathbf{x}_i - \mathbf{x}_j\|_2 \leq d_{ij}, \quad \forall(i,j) \in E \tag{2.16}$$

$$\sum_{i=1}^{n} \mathbf{x}_i = 0$$

Due to the centering constraint $\sum_{i=1}^{n} \mathbf{x}_i = 0$, the objective in (2.16) can be further reduced to

$$\underset{\mathbf{x}_1,\ldots,\mathbf{x}_n \in \mathcal{R}^d}{\text{maximize}} \quad n_g \sum_{i=1..n} \|\mathbf{x}_i\|_2^2 + n \sum_{g \in V_G} \|\mathbf{x}_j\|_2^2, \tag{2.17}$$

where $n_g = |V_G|$ is the number of goals.

Following the same rank relaxation as in MVU [146] and considering (2.17), (2.16) can be rephrased as a convex SDP by optimizing over the inner-product matrix $\mathbf{K}$, with $k_{ij} = \mathbf{x}_i^\top \mathbf{x}_j$:

$$\underset{\mathbf{K}}{\text{maximize}} \quad n_g \text{trace}(\mathbf{K}) + n \sum_{g \in V_G} k_{gg}$$

$$\text{subject to} \quad k_{ii} - 2k_{ij} + k_{jj} \leq d_{ij}^2, \quad \forall(i,j) \in E$$

$$\sum_{i,j} k_{ij} = 0 \tag{2.18}$$

$$\mathbf{K} \succeq 0.$$

The final embedding is projected onto $\mathcal{R}^d$ by composing the vectors $\mathbf{x}_i$ out of the d leading eigenvectors of $\mathbf{K}$.

Note that a general weighted EH model is already discussed in [110]. However, GOEH makes the goal-oriented cases explicit.
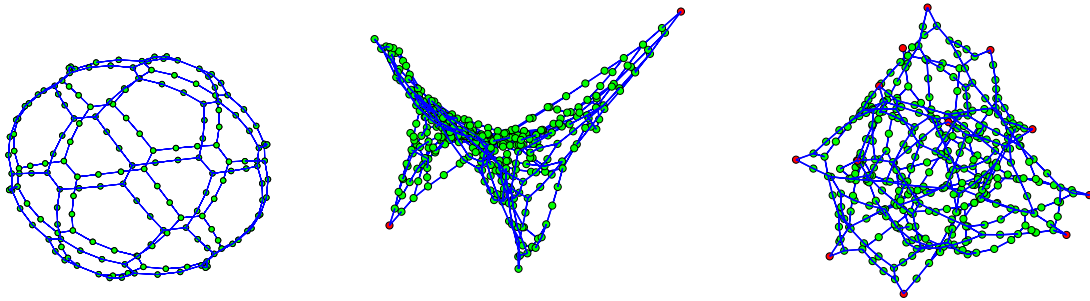
Figure 2.4: EH and GOEH embeddings ($d = 3$) illustrated on a 5-puzzle problem. Goal states are colored in red, others in green. In this spherical embedding in the left figure, the Euclidean distance is a bad approximation for distant states. GOEH deforms the embedding to better reflect the spherical distance from far away states to the goal states—at the cost of shrinkage between non-goal states.

Figure 2.4 illustrates the effects of GOEH. We can see that GOEH "stretches" the embedding so that the goal states are further away from other states, while the local distance constraints still ensure the admissibility and consistency.

The time complexity for solving the SDP in (2.18) is the same as the original MVU formulation, which makes it prohibitive for larger data sets. To improve its scalability, we propose a modified version of MVC for solving (2.16). We follow the same steps in MVC to generate the initial embedding and r patches. However, each subproblem in (2.6) for patch p is changed to:

$$
\begin{aligned}
\underset{\mathbf{x}_i \in V_p^x}{\text{maximize}} \quad & \sum_{i \in V_p, g \in V_G} \|\mathbf{x}_i - \mathbf{x}_g\|_2^2 \\
\underset{\mathbf{a}_k \in V_p^a}{\text{subject to}} \quad & \|\mathbf{x}_i - \mathbf{x}_j\|_2 \le d_{ij}, \quad \forall (i,j) \in E_p^{xx} \\
& \|\mathbf{x}_i - \mathbf{a}_k\|_2 \le d_{ik}, \quad \forall (i,k) \in E_p^{ax},
\end{aligned}
\tag{2.19}
$$

Intuitively, for the subproblem of each patch, we maximize the distances of its inner nodes to the goals, while still enforcing the local distance constraints involving inner nodes and anchor nodes.

Following a similar approach as in MVC described in Section 2.1, we reformulate (2.19) as a SDP. Given a patch $G_p = (V_p, E_P)$ with $n_p = |V_p|$, we define a design matrix $X = [\mathbf{x}_1, \ldots, \mathbf{x}_n] \in \mathcal{R}^{d \times n_p}$, where each column corresponds to one embedding coordinate of V_p^x. Define the matrix $K \in \mathcal{R}^{(d+n_p) \times (d+n_p)}$ as:

$$\mathbf{K} = \begin{pmatrix} \mathbf{I} & \mathbf{X} \\ \mathbf{X}^\top & \mathbf{H} \end{pmatrix} \quad \text{where } \mathbf{H} = \mathbf{X}^\top \mathbf{X}. \tag{2.20}$$

Let the vector $\mathbf{e}_{i,j} \in \mathcal{R}^{n_p}$ be all-zero except the ith element is 1 and the jth element is -1. Let the vector $\mathbf{e}_i$ be all-zero except the ith element is -1. With this notation, and the Schur Complement Lemma [11], we can relax (2.19) into a SDP:

$$\begin{aligned}
\max_{\mathbf{X}, \mathbf{H}} \quad & \sum_{i \in V_p^x} \left[n_g \mathbf{H}_{ii} - \sum_{g \in V_p^1} 2\bar{\mathbf{x}}_g^\top \mathbf{x}_i + \sum_{g \in V_p^2} (\mathbf{H}_{gg} - \mathbf{H}_{ig}) \right] \\
\text{s.t.} \quad & (\mathbf{0}; \mathbf{e}_{ij})^\top \mathbf{K}(\mathbf{0}; \mathbf{e}_{ij}) \leq d_{ij}^2 \quad \forall (i,j) \in E_p^{xx} \\
& (\mathbf{a}_k; \mathbf{e}_i)^\top \mathbf{K}(\mathbf{a}_k; \mathbf{e}_i) \leq d_{ik}^2 \quad \forall (i,k) \in E_p^{ax} \\
& \mathbf{K} = \begin{pmatrix} \mathbf{I} & \mathbf{X} \\ \mathbf{X}^\top & \mathbf{H} \end{pmatrix} \succeq 0
\end{aligned} \tag{2.21}$$

where $V_p^1 = V_G \backslash V_p^x$, $V_p^2 = V_G \cap V_p^x$, $\mathbf{H}_{ij}$ are elements in $\mathbf{H}$, $\mathbf{x}_i$ is the ith column of $\mathbf{X}$, and $\bar{\mathbf{x}}_g$ is the coordinate for node g. The optimization (2.21) is a convex SDP and can be solved very efficiently for medium sized n_p. The r sub-problems are completely independent and can be solved *in parallel*, leading to almost perfect parallel speed-up on multi-core computers or clusters. Like MVC, we reiterate solving the r subproblems until convergence.

Both the centralized solution in (2.18) and the partitioned solution in (2.21) maintain the admissibility and consistency of EH, because the constraints are kept the same as in (1.14), and the proof for admissibility and consistency of EH only relies on these constraints [110].

Proposition 1. *Any feasible solution to (2.18) or (2.21) gives admissible and consistent Euclidean heuristics.*

The memory requirement for storing the embedding results $\mathbf{x}_1, \ldots, \mathbf{x}_n \in \mathcal{R}^d$ is still $O(dn)$, which is reasonable since d is often a small constant such as 3 or 4.

2.2.3 State heuristic enhancement

We propose a *state heuristic enhancement* (SHE) technique to further improve the quality of GOEH. Since GOEH gives a lower bound of the true distance, we can calculate their gaps in a preprocessing phase and store the information in the memory to aid the search.

Suppose we are given a state-space graph $G = (V, E)$ and a goal set $V_G \subseteq V$. After we use GOEH to generate a d-dimensional embedding $\mathbf{x}_1, \ldots, \mathbf{x}_n \in \mathcal{R}^d$, for any $i = 1, \cdots, n$, we store a real number η_i defined as:

$$\eta_i = \min_{j \in V_G} \left\{ d_{ij} - \|\mathbf{x}_i - \mathbf{x}_j\|_2 \right\}. \tag{2.22}$$

During the search towards any goal g, for any state i, its enhanced heuristic value will be

$$h(i, g) = \|\mathbf{x}_i - \mathbf{x}_g\|_2 + \eta_i. \tag{2.23}$$

Intuitively, η_i stores the minimum gap between the EH and true distance from state i to any goal state in the goal set. During a search, we can add η_i to the Euclidean distance from i to g in the embedded space. Clearly, we have:

Proposition 2. *The heuristic function in (2.23) is* admissible.

However, the heuristic in (2.23) is no longer guaranteed to be consistent. A parent node i may receive a much larger η_i than the η_j received by a child node j, so that $h(i, g) > d_{ij} + h(j, g)$, leading to inconsistency.

As found in [156], inconsistent but admissible heuristics can often be preferable to consistent heuristics. To ensure optimality of the first solution found, we employ the B$'$ algorithm proposed in [93].

Suppose the current expanded node is i, the rules of the B$'$ algorithm to handle inconsistency are:

a) For each successor j of i, if $h(j, g) < h(i, g) - d_{ij}$, set $h(j, g) = h(i, g) - d_{ij}$

b) Let j be the successor of i with minimum $h(j, g) + d_{ij}$. If $h(i, g) < h(j, g) + d_{ij}$, set $h(i, g) = h(j, g) + d_{ij}$
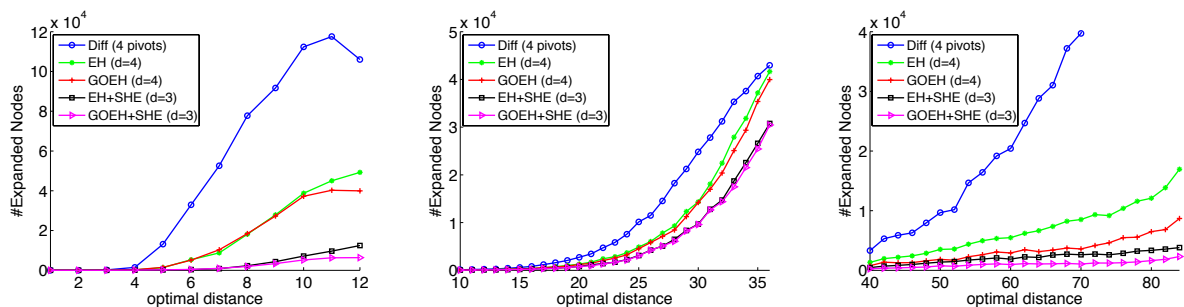
Figure 2.5: The number of expanded nodes in the optimal search as a function of the optimal solution length. For EH+SHE and GOEH+SHE, B′ search is used and the re-opened nodes are counted as new expansions.

It is shown in [93] that adding those rules to A^* search makes it optimal even when the heuristic is inconsistent. They can actually further improve the heuristic since it propagates improvements on the heuristic values based on consistency constraints. It is also shown that if the heuristic is consistent, then these rules will never be invoked and the B′ search is exactly the same as the A^* search [93]. Experimentally, we found that inconsistency does not occur often. For many problem instances we tested, the enhanced heuristics are consistent. For other instances, these B′ rules are invoked for some states to improve their GOEH values.

We note that there is a tradeoff between space complexity and heuristic accuracy. SHE uses $O(n)$ memory since it stores one real number per state, which adds only $1/d$ overhead to the $O(dn)$ space used by EH and GOEH. As we will see, this simple SHE technique can drastically improve the efficiency of optimal search on every domain we test. Note that EH cannot utilize dimensions that exceed the intrinsic dimensionality of the state space. This is in contrast to SHE, which does take advantage of such "extra" dimensions.

2.2.4 Experimental results

We evaluate our algorithms on two well-known benchmark AI problems and on a real world service robot application.

M**-Puzzle Problem** [67] is a popular benchmark problem for search algorithms. It consists of a frame of M tiles and one tile missing. All tiles are numbered and a state constitutes any order of the tiles. An action is to move a cardinal neighbor tile of the empty space into the empty space. The task is to find a shortest action sequence from a pre-defined start to a goal state. We evaluate our algorithm on 7- and 8-puzzle problems (4×2 and 3×3 frames), which contain 20160 and 181440 states, respectively.

Blocks World [55] is a NP-hard problem with the goal to build several given stacks out of a set of blocks. Blocks can be placed on the top of others or on the ground. Any block that is currently under another block cannot be moved. We test blocks world problems with 6 blocks (4,051 states) and 7 blocks (37,633 states), respectively.

Home Service Robot is designed to handle daily indoor activities and can interact with human. In the Home Service Robot Competition at the RoboCup (http://robocup.rwth-aachen.de/athomewiki/index.php/Main_Page), there are a service robot, human, small objects that can be picked up and moved by the robot, and some big objects that cannot be moved. A typical task is to ask the robot to pick up a small object and bring it to the human. In this problem, each state describes different variables, such as the locations of the robot, human and small objects. There are a lot of intermediate states that the robot never takes as the goal. The robot can store the precomputed GOEH and SHE information in memory and use it to solve various daily tasks online.

49

Goal sets. We design three kinds of goal settings for our datasets. For M-puzzles, we let the goal set include all the states where the first three tiles are blank, tile 1 and tile 2, respectively. In this case, all goal states are distributed uniformly on the surface of the embedded sphere (see the rightmost subfigure in Figure 2.4). For blocks world problems, we randomly pick a state and add more states in its vicinity to the goal set. For the home service robot application, the goal states are built-in goals for completing specific tasks from the competition. In this way, we evaluate our algorithms on the scenarios of distributed goals, clustered goals, and real-world goals, leading to a comprehensive assessment.

Experimental setup. We use MVC to learn GOEH and use Isomap [137] to initialize MVC. For datasets of a size greater than 8K, we set 8K landmarks for Isomap. For MVC we use a patch size of $m=500$ throughout (for which problem (2.21) can be solved in less than $20s$). Following [110, 20], we choose a small embedding dimensionality for saving memory space. We set the number of embedding dimensions $d = 4$ for all experiments, meaning that each heuristic stores $4n$ real numbers. Since SHE requires another array of n numbers, the embedding dimension is set to $d = 3$ when SHE is used. This gives a fair comparison since all algorithms use $4n$ space. In our experiments, all MVC or goal-oriented MVC algorithms are stopped after a maximum of 50 iterations.

We also test the differential heuristic [102, 134] as a baseline. The differential heuristic pre-computes the exact distance from all states to a few pivot nodes in a set $S \subseteq V$. We implemented the algorithm to select good pivot nodes in [134]. The differential heuristic between two states a, b is $\max_{s \in S} |\delta(a, s) - \delta(b, s)| \leq \delta(a, b)$. In our experiments, we set the number of pivot nodes to 4 so that both differential heuristics and Euclidean heuristics have the same space complexity of $4n$.

Problem	Diff	EH	GOEH	EH+SHE	GOEH+SHE
6-block	1.00	3.83	5.77	5.02	**6.26**
7-block	1.00	3.02	3.46	15.06	**23.30**
7-puzzle	1.00	1.40	1.53	2.01	**2.08**
8-puzzle	1.00	1.25	1.36	**3.20**	3.18
robot1	1.00	5.09	14.14	17.12	**26.83**
robot2	1.00	4.63	9.19	14.68	**29.28**

Table 2.3: Speedup of various methods as compared to the differential heuristic.

Comprehensive evaluation.   Figure 2.5 shows the total expanded nodes of three problems as a function of the optimal solution length, averaged over 500 start/goal pairs for each solution length. Each goal is randomly chosen from the goal set V_G. The figures compare the performance of the differential heuristic (Diff), EH, GOEH, EH combined with SHE (EH+SHE), and GOEH+SHE. To quantify the performance improvement, Table 1 shows the speedup of each method over the differential heuristic, defined as:

$$\text{Speedup(M)} = \frac{\sum_l \sum_{p=1}^{500} \text{NumExpand}(l,p,\text{Diff})}{\sum_l \sum_{p=1}^{500} \text{NumExpand}(l,p,\text{M})}$$

where $\text{NumExpand}(l,p,\text{M})$ is the number of states expanded by algorithm M to solve the pth start/goal pair under solution length l. From Figure 2 and Table 1, we can see that each of GOEH and SHE dramatically reduces the number of expanded states. Combining them gives the most reduction.

Embedding time. Table 2.4 shows the training time for each embedding algorithm. Note that for real deployment, such as GPS systems, MVC only needs to be run once to obtain the embedding. This offline computing cost is of no importance – it is the online search speed that matters to end users. Once such an embedding is loaded into memory, the online calculation of Euclidean heuristics is very fast. Since we set $d = 4$ when SHE is not used and $d = 3$ when SHE is used, the training times for the MVC optimization in EH and EH+SHE

Problem	n	n_g	EH	GOEH	EH+SHE	GOEH+SHE
6-block	$4K$	60	9m	10m	9m+1s	9m+1s
7-block	$37K$	100	56m	62m	51m+9s	60m+9s
7-puzzle	20K	120	40m	49m	40m+6s	45m+7s
8-puzzle	181K	720	7h	11h	6h+3m	10h+3m
robot1	50K	80	5h	6h	4h+15s	6h+15s
robot2	90K	100	7h	10h	7h+33s	9h+32s

Table 2.4: The total number of states (n), size of goal sets (n_g), and training time for various heuristics on different problems. For EH+SHE and GOEH+SHE, we also report the additional time for computing SHE.

are different. The same difference applies to GOEH and GOEH+SHE. All embeddings were computed on a desktop with two 8-core Intel(R) Xeon(R) processors at 2.67 GHz and 128GB of RAM. We implement MVC in MATLAB^{TM} and use CSDP [9] as the SDP solver. We parallelize each run of MVC on eight cores.

From the last two columns of Table 2, we can observe that the overhead for computing SHE is negligible compared to the training time for MVC optimization.

2.2.5   Conclusions

In this chapter, we have introduced several substantial improvements to the Euclidean Heuristic [110]. We narrow the gap between heuristic estimates and true distances through two different means: 1) we optimize the Euclidean embedding to yield especially accurate distance estimates for the relevant goal states, and 2) we store the remaining approximation gaps in a compact fashion for online correction during search. The combination of these two enhancements yields drastic reductions in search space expansion.

An interesting extension would be automatic EH re-optimization of problem domains with frequent A^* applications. If the solver keeps statistics of how often states are chosen as goals, it can periodically re-optimize the heuristics to best serve the users' demands. Another natural extension would be the generalization where we know a prior distribution of the goal state in the state space and design a new optimization objective to incorporate such probability distributions.

Chapter 3

Compressing Deep Learning Models

As described in Chapter 1, deep learning models are memory-consuming. However, more and more deep learning applications have shifted towards mobile and embedded devices which typically have limited memory and storage. This dilemma increases the need of compressing deep learning models. In this chapter, we present two methods, HashedNets [26] and FreshNets [27], to compress fully connected layers and convolutional layers in deep learning models, respectively.

3.1 Compressing neural networks with the hashing trick

3.1.1 Introduction

In the past decade deep neural networks have set new performance standards in many high-impact applications. These include object classification [72, 124], speech recognition [63], image caption generation [141, 68] and domain adaptation [52]. As data sets increase in

size, so do the number of parameters in these neural networks in order to absorb the enormous amount of supervision [32]. Increasingly, these networks are trained on industrial-sized clusters [76] or high-performance graphics processing units (GPUs) [32].

Simultaneously, there has been a second trend as applications of machine learning have shifted toward mobile and embedded devices. As examples, modern smart phones are increasingly operated through speech recognition [123], robots and self-driving cars perform object recognition in real time [98], and medical devices collect and analyze patient data [82]. In contrast to GPUs or computing clusters, these devices are designed for low power consumption and long battery life. Most importantly, they typically have small working memory. For example, even the top-of-the-line iPhone 6 only features a mere 1GB of RAM.[8]

The disjunction between these two trends creates a dilemma when state-of-the-art deep learning algorithms are designed for deployment on mobile devices. While it is possible to train deep nets offline on industrial-sized clusters (server-side), the sheer size of the most effective models would exceed the available memory, making it prohibitive to perform testing on-device. In speech recognition, one common cure is to transmit processed voice recordings to a computation center, where the voice recognition is performed server-side [29]. This approach is problematic, as it only works when sufficient bandwidth is available and incurs artificial delays through network traffic [70]. One solution is to train small models for the on-device classification; however, these tend to significantly impact accuracy [29], leading to customer frustration.

This dilemma motivates *neural network compression*. Recent work by Denil et al. [39] demonstrates that there is a surprisingly large amount of redundancy among the weights of neural networks. The authors show that a small subset of the weights are sufficient to reconstruct

---

[8]http://en.wikipedia.org/wiki/IPhone_6

the entire network. They exploit this by training low-rank decompositions of the weight matrices. Ba and Caruana [3] show that deep neural networks can be successfully compressed into "shallow" single-layer neural networks by training the small network on the (log-) outputs of the fully trained deep network [15]. Courbariaux et al. [34] train neural networks with reduced bit precision, and, long predating this work, LeCun et al. [78] investigated dropping unimportant weights in neural networks. In summary, the accumulated evidence suggests that much of the information stored within network weights may be redundant.

In this section we propose *HashedNets*, a novel network architecture to reduce and limit the memory overhead of neural networks. Our approach is compellingly simple: we use a hash function to group network connections into hash buckets uniformly at random such that all connections grouped to the ith hash bucket share the same weight value w_i. Our parameter hashing is akin to prior work in feature hashing [148, 127, 47] and is similarly fast and requires no additional memory overhead. The backpropagation algorithm [80] can naturally tune the hash bucket parameters and take into account the random weight sharing within the neural network architecture.

We demonstrate on several real world deep learning benchmark data sets that HashedNets can drastically reduce the model size of neural networks with little impact in prediction accuracy. Under the same memory constraint, HashedNets have more adjustable free parameters than the low-rank decomposition methods suggested by Denil et al. [39], leading to smaller drops in descriptive power.

Similarly, we also show that for a finite set of parameters it is beneficial to "inflate" the network architecture by re-using each parameter value multiple times. Best results are achieved when networks are inflated by a factor 8–16×. The "inflation" of neural networks

56

with HashedNets imposes no restrictions on other network architecture design choices, such as dropout regularization [133], activation functions [51, 80], or weight sparsity [31].

3.1.2 Feature Hashing

Learning under memory constraints has previously been explored in the context of large-scale learning for sparse data sets. *Feature hashing* (or the *hashing trick*) [148, 127] is a technique to map high-dimensional text documents directly into bag-of-word [120] vectors, which would otherwise require use of memory consuming dictionaries for storage of indices corresponding with specific input terms.

Formally, an input vector $\mathbf{x} \in \mathcal{R}^d$ is mapped into a feature space with a mapping function $\phi \colon \mathcal{R}^d \to \mathcal{R}^k$ where $k \ll d$. The mapping ϕ is based on two (approximately uniform) hash functions $h \colon \mathbb{N} \to \{1, \ldots, k\}$ and $\xi \colon \mathbb{N} \to \{-1, +1\}$ and the kth dimension of the hashed input $\mathbf{x}$ is defined as $\phi_k(\mathbf{x}) = \sum_{i : h(i) = k} x_i \xi(i)$.

The hashing trick leads to large memory savings for two reasons: it can operate directly on the input term strings and avoids the use of a dictionary to translate words into vectors; and the parameter vector of a learning model lives within the much smaller dimensional $\mathcal{R}^k$ instead of $\mathcal{R}^d$. The dimensionality reduction comes at the cost of collisions, where multiple words are mapped into the same dimension. This problem is less severe for sparse data sets and can be counteracted through multiple hashing [127] or larger hash tables [148].

In addition to memory savings, the hashing trick has the appealing property of being sparsity preserving, fast to compute and storage-free. The most important property of the hashing trick is, arguably, its (approximate) preservation of inner product operations. The second

hash function, ξ, guarantees that inner products are unbiased in expectation [148]; that is,

$$\mathbb{E}[\phi(\mathbf{x})^\top \phi(\mathbf{x}')]_\phi = \mathbf{x}^\top \mathbf{x}'. \tag{3.1}$$

Finally, Weinberger et al. [148] also show that the hashing trick can be used to learn multiple classifiers within the same hashed space. In particular, the authors use it for multi-task learning and define multiple hash functions $\phi_1, \ldots, \phi_T$, one for each task, that map inputs for their respective tasks into one joint space. Let $\mathbf{w}_1, \ldots, \mathbf{w}_T$ denote the weight vectors of the respective learning tasks, then if $t' \neq t$ a classifier for task t' does not interfere with a hashed input for task t; *i.e.* $\mathbf{w}_t^\top \phi_{t'}(\mathbf{x}) \approx 0$.

3.1.3   Notation

Throughout this chapter we type vectors in bold ($\mathbf{x}$), scalars in regular (C or b) and matrices in capital bold ($\mathbf{X}$). Specific entries in vectors or matrices are scalars and follow the corresponding convention, *i.e.* the ith dimension of vector $\mathbf{x}$ is x_i and the $(i,j)^{th}$ entry of matrix $\mathbf{V}$ is V_{ij}.

Feed Forward Neural Networks.   We define the forward propagation of the ℓth layer in a neural networks as,

$$a_i^{\ell+1} = f(z_i^{\ell+1}), \quad \text{where} \quad z_i^{\ell+1} = \sum_{j=0}^{n^\ell} V_{ij}^\ell a_j^\ell, \tag{3.2}$$

where $\mathbf{V}^\ell$ is the (virtual) weight matrix in the ℓth layer. The vectors $\mathbf{z}^\ell, \mathbf{a}^\ell \in \mathcal{R}^{n^\ell}$ denote the activation units before and after transformation through the transition function $f(\cdot)$. Typical activation functions are rectifier linear unit (ReLU) [100], sigmoid or tanh [80].

3.1.4 HashedNets

In this section we present HashedNets, a novel variation of neural networks with drastically reduced model sizes (and memory demands). We first introduce our approach as a method of random weight sharing across the network connections and then describe how to facilitate it with the hashing trick to avoid any additional memory overhead.

Random weight sharing

In a standard fully-connected neural network, there are $(n^\ell + 1) \times n^{\ell+1}$ weighted connections between a pair of layers, each with a corresponding free parameter in the weight matrix $\mathbf{V}^\ell$. We assume a finite memory budget per layer, $K^\ell \ll (n^\ell + 1) \times n^{\ell+1}$, that cannot be exceeded. The obvious solution is to fit the neural network within budget by reducing the number of nodes $n^\ell, n^{\ell+1}$ in layers $\ell, \ell + 1$ or by reducing the bit precision of the weight matrices [34]. However if K^ℓ is sufficiently small, both approaches significantly reduce the ability of the neural network to generalize (see Section 3.1.6). Instead, we propose an alternative: we keep the size of $\mathbf{V}^\ell$ untouched but reduce its *effective* memory footprint through *weight sharing*. We only allow exactly K^ℓ different weights to occur within $\mathbf{V}^\ell$, which we store in a weight vector $\mathbf{w}^\ell \in \mathcal{R}^{K^\ell}$. The weights within $\mathbf{w}^\ell$ are shared across multiple randomly chosen connections within $\mathbf{V}^\ell$. We refer to the resulting matrix $\mathbf{V}^\ell$ as *virtual*, as its size could be
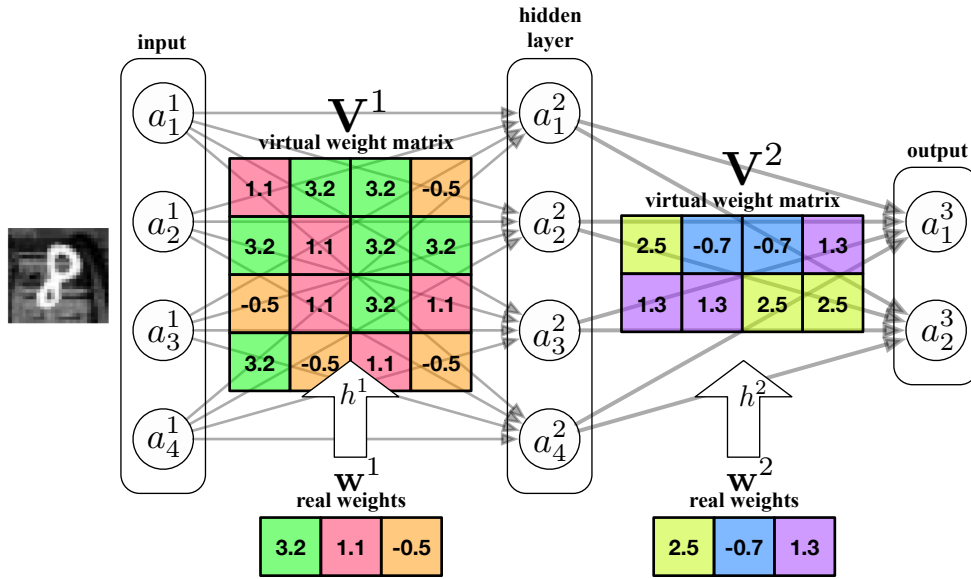
Figure 3.1: An illustration of a neural network with random weight sharing under compression factor $\frac{1}{4}$. The $16+9=25$ virtual weights are compressed into 6 real weights. The colors represent matrix elements that share the same weight value.

increased (*i.e.* nodes are added to hidden layer) without increasing the *actual* number of parameters of the neural network.

Figure 3.1 shows a neural network with one hidden layer, four input units and two output units. Connections are randomly grouped into three categories per layer and their weights are shown in the virtual weight matrices $\mathbf{V}^1$ and $\mathbf{V}^2$. Connections belonging to the same color share the same weight value, which are stored in $\mathbf{w}^1$ and $\mathbf{w}^2$, respectively. Overall, the entire network is compressed by a factor $1/4$, *i.e.* the 24 weights stored in the virtual matrices $\mathbf{V}^1$ and $\mathbf{V}^2$ are reduced to only six real values in $\mathbf{w}^1$ and $\mathbf{w}^2$. On data with four input dimensions and two output dimensions, a conventional neural network with six weights would be restricted to a single (trivial) hidden unit.

Hashed Neural Nets (HashedNets)

A naïve implementation of random weight sharing can be trivially achieved by maintaining a secondary matrix consisting of each connection's group assignment. Unfortunately, this explicit representation places an undesirable limit on potential memory savings.

We propose to implement the random weight sharing assignments using the hashing trick. In this way, the shared weight of each connection is determined by a hash function that requires no storage cost with the model. Specifically, we assign to V_{ij}^{ℓ} an element of $\mathbf{w}^{\ell}$ indexed by a hash function $h^{\ell}(i, j)$, as follows:

$$V_{ij}^{\ell} = w_{h^{\ell}(i,j)}^{\ell}, \tag{3.3}$$

where the (approximately uniform) hash function $h^{\ell}(\cdot, \cdot)$ maps a key (i, j) to a natural number within $\{1, \ldots, K^{\ell}\}$. In the example of Figure 3.1, $h^1(2, 1) = 1$ and therefore $V_{2,1}^1 = w^1 = 3.2$. For our experiments we use the open-source implementation *xxHash*.[9]

Feature hashing versus weight sharing

This section focuses on a single layer throughout and to simplify notation we will drop the super-scripts ℓ. We will denote the input activation as $\mathbf{a} = \mathbf{a}^{\ell} \in \mathcal{R}^m$ of dimensionality $m = n^{\ell}$. We denote the output as $\mathbf{z} = \mathbf{z}^{\ell+1} \in \mathcal{R}^n$ with dimensionality $n = n^{\ell+1}$.

To facilitate weight sharing within a feed forward neural network, we can simply substitute Eq. (3.3) into Eq. (3.2):

$$z_i = \sum_{j=1}^{m} V_{ij} a_j = \sum_{j=1}^{m} w_{h(i,j)} a_j. \tag{3.4}$$

---

[9]`https://code.google.com/p/xxhash/`

Alternatively and more in line with previous work [148], we may interpret HashedNets in terms of feature hashing. To compute z_i, we first hash the activations from the previous layer, $\mathbf{a}$, with the hash mapping function $\phi_i(\cdot): \mathcal{R}^m \to \mathcal{R}^K$. We then compute the inner product between the hashed representation $\phi_i(\mathbf{a})$ and the parameter vector $\mathbf{w}$,

$$z_i = \mathbf{w}^\top \phi_i(\mathbf{a}). \tag{3.5}$$

Both $\mathbf{w}$ and $\phi_i(\mathbf{a})$ are K-dimensional, where K is the number of hash buckets in this layer. The hash mapping function ϕ_i is defined as follows. The kth element of $\phi_i(\mathbf{a})$, $i.e.$ $[\phi_i(\mathbf{a})]_k$, is the sum of variables hashed into bucket k:

$$[\phi_i(\mathbf{a})]_k = \sum_{j:h(i,j)=k} a_j. \tag{3.6}$$

Starting from Eq. (3.5), we show that the two interpretations (Eq. (3.4) and (3.5)) are equivalent:

$$
\begin{aligned}
z_i &= \sum_{k=1}^{K} w_k \left[\phi_i(\mathbf{a})\right]_k = \sum_{k=1}^{K} w_k \sum_{j:h(i,j)=k} a_j \\
&= \sum_{j=1}^{m} \sum_{k=1}^{K} w_k a_j \delta_{[h(i,j)=k]} \\
&= \sum_{j=1}^{m} w_{h(i,j)} a_j.
\end{aligned}
$$

The final term is equivalent to Eq. (3.4).

Sign factor. With this equivalence between random weight sharing and feature hashing on input activations, HashedNets inherit several beneficial properties of the feature hashing.

Weinberger et al. [148] introduce an additional sign factor $\xi(i,j)$ to remove the bias of hashed inner-products due to collisions. For the same reasons we multiply (3.3) by the sign factor $\xi(i,j)$ for parameterizing $\mathbf{V}$ [148]:

$$V_{ij} = w_{h(i,j)}\xi(i,j), \tag{3.7}$$

where $\xi(i,j)\colon \mathbb{N} \to \pm 1$ is a second hash function independent of h. Incorporating $\xi(i,j)$ to feature hashing and weight sharing does not change the equivalence between them as the proof in the previous section still holds with the sign term (details omitted for improved readability).

Sparsity. As pointed out in Shi et al. [127] and Weinberger et al. [148], feature hashing is most effective on sparse feature vectors since the number of hash collisions is minimized. We can encourage this effect in the hidden layers with sparsity inducing transition functions, *e.g.* rectified linear units (ReLU) [51] or through specialized regularization [17, 10]. In our implementation, we use ReLU transition functions throughout, as they have also been shown to often result in superior generalization performance in addition to their sparsity inducing properties [51].

Alternative neural network architectures. While this work focuses on general, fully connected feed forward neural networks, the technique of HashedNets could naturally be extended to other kinds of neural networks, such as recurrent neural networks [107] or others [6]. It can also be used in conjunction with other approaches for neural network compression. All

weights can be stored with low bit precision [34, 56], edges could be removed [30] and Hashed-Nets can be trained on the outputs of larger networks [3] — yielding further reductions in memory requirements.

Training HashedNets

Training HashedNets is equivalent to training a standard neural network with equality constraints for weight sharing. Here, we show how to (a) compute the output of a hash layer during the feed-forward phase, (b) propagate gradients from the output layer back to input layer, and (c) compute the gradient over the shared weights $\mathbf{w}^\ell$ during the back propagation phase. We use dedicated hash functions between layers ℓ and $\ell + 1$, and denote them as h^ℓ and ξ^ℓ.

Output. Adding the hash functions $h^\ell(\cdot, \cdot)$ and $\xi^\ell(\cdot)$ and the weight vectors $\mathbf{w}^\ell$ into the feed forward update (3.2) results in the following forward propagation rule:

$$a_i^{\ell+1} = f\left(\sum_{j}^{n^\ell} w_{h^\ell(i,j)}^\ell \xi^\ell(i,j) a_j^\ell \right). \tag{3.8}$$

Error term. Let $\mathcal{L}$ denote the loss function for training the neural network, *e.g.* cross entropy or the quadratic loss [6]. Further, let δ_j^ℓ denote the gradient of $\mathcal{L}$ over activation j in layer ℓ, also known as the error term. Without shared weights, the error term can be expressed as $\delta_j^\ell = \left(\sum_{i=1}^{n^{\ell+1}} V_{ij}^\ell \delta_i^{\ell+1} \right) f'(z_j^\ell)$, where $f'(\cdot)$ represents the first derivative of the

64

transition function $f(\cdot)$. If we substitute Eq. (3.7) into the error term we obtain:

$$\delta_j^\ell = \left(\sum_{i=1}^{n^{\ell+1}} \xi^\ell(i,j) w_{h^\ell(i,j)}^\ell \delta_i^{\ell+1} \right) f'(z_j^\ell). \tag{3.9}$$

Gradient over parameters. To compute the gradient of $\mathcal{L}$ with respect to a weight w_k^ℓ we need the two gradients,

$$\frac{\partial \mathcal{L}}{\partial V_{ij}^\ell} = a_j^\ell \delta_i^{\ell+1} \text{ and } \frac{\partial V_{ij}^\ell}{\partial w_k^\ell} = \xi^\ell(i,j) \delta_{h^\ell(i,j)=k}. \tag{3.10}$$

Here, the first gradient is the standard gradient of a (virtual) weight with respect to an activation unit and the second gradient ties the virtual weight matrix to the actual weights through the hashed map. Combining these two, we obtain

$$\frac{\partial \mathcal{L}}{\partial w_k^\ell} = \sum_{i,j} \frac{\partial \mathcal{L}}{\partial V_{ij}^\ell} \frac{\partial V_{ij}^\ell}{\partial w_k^\ell} \tag{3.11}$$

$$= \sum_{i=1}^{n^{\ell+1}} \sum_j a_j^\ell \delta_i^{\ell+1} \xi^\ell(i,j) \delta_{h^\ell(i,j)=k}. \tag{3.12}$$

3.1.5 Related Work

Deep neural networks have achieved great progress on a wide variety of real-world applications, including image classification [72, 41, 124, 158], object detection [50, 141], image retrieval [111], speech recognition [63, 54, 97], and text representation [96].

There have been several previous attempts to reduce the complexity of neural networks under a variety of contexts. Arguably the most popular method is the widely used convolutional

neural network [130]. In the convolutional layers, the same filter is applied to every receptive field, both reducing model size and improving generalization performance. The incorporation of pooling layers [157] can reduce the number of connections between layers in domains exhibiting locality among input features, such as images. Autoencoders [52] share the notion of tied weights by using the same weights for the encoder and decoder (up to transpose).

Other methods have been proposed explicitly to reduce the number of free parameters in neural networks, but not necessarily for reducing memory overhead. Nowlan and Hinton [103] introduce soft weight sharing for regularization in which the distribution of weight values is modeled as a Gaussian mixture. The weights are clustered such that weights in the same group have similar values. Since weight values are unknown before training, weights are clustered during training. This approach is fundamentally different from HashedNets since it requires auxiliary parameters to record the group membership for every weight.

Instead of sharing weights, LeCun et al. [78] introduce "optimal brain damage" to directly drop unimportant weights. This approach requires auxiliary parameters for storing the sparse weights and needs retraining time to fine-tune the resulting architecture. Cireşan et al. [30] demonstrate in their experiments that randomly removing connections leads to superior empirical performance, which shares the same spirit of HashedNets.

Courbariaux et al. [34] and Gupta et al. [56] learn networks with reduced numerical precision for storing model parameters (*e.g.* 16-bit fixed-point representation [56] for a compression factor of $\frac{1}{4}$ over double-precision floating point). Experiments indicate little reduction in accuracy compared with models trained with double-precision floating point representation. These methods can be readily incorporated with HashedNets, potentially yielding further reduction in model storage size.

A recent study by Denil et al. [39] demonstrates significant redundancy in neural network parameters by directly learning a low-rank decomposition of the weight matrix within each layer. They demonstrate that networks composed of weights recovered from the learned decompositions are only slightly less accurate than networks with all weights as free parameters, indicating heavy over-parametrization in full weight matrices. A follow-up work by Denton et al. [40] uses a similar technique to speed up test-time evaluation of convolutional neural networks. The focus of this line of work is not on reducing storage and memory overhead, but evaluation speed during test time. HashedNets is complementary to this research, and the two approaches could be used in combination.

Following the line of model compression, Bucilua et al. [15], Hinton et al. [64] and Ba and Caruana [3] recently introduce approaches to learn a "distilled" model, training a more compact neural network to reproduce the output of a larger network. Specifically, Hinton et al. [64] and Ba and Caruana [3] train a large network on the original training labels, then learn a much smaller "distilled" model on a weighted combination of the original labels and the (softened) softmax output of the larger model. The authors show that the distilled model has better generalization ability than a model trained on just the labels. In our experimental results, we show that our approach is complementary by learning HashedNets with soft targets. Rippel et al. [117] propose a novel dropout method, nested dropout, to give an order of importance for hidden neurons. Hypothetically, less important hidden neurons could be removed after training, a method orthogonal to HashedNets.

Ganchev and Dredze [47] are among the first to recognize the need to reduce the size of natural language processing models to accommodate mobile platform with limited memory and computing power. They propose *random feature mixing* to group features at random based on a hash function, which dramatically reduces both the number of features and the
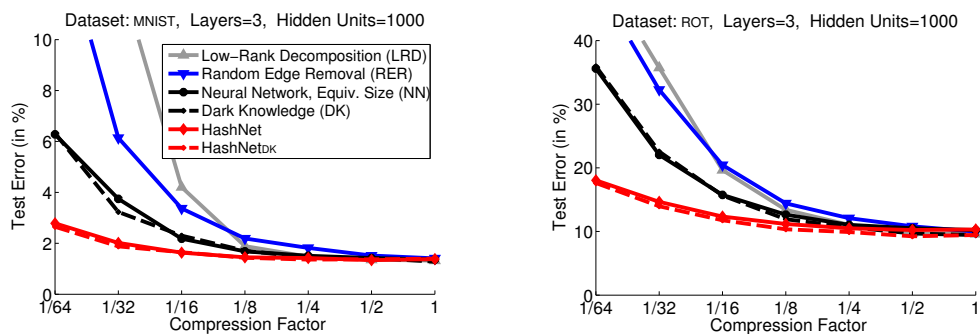
Figure 3.2: Test error rates under varying compression factors with 3-layer networks on MNIST (*left*) and ROT (*right*).
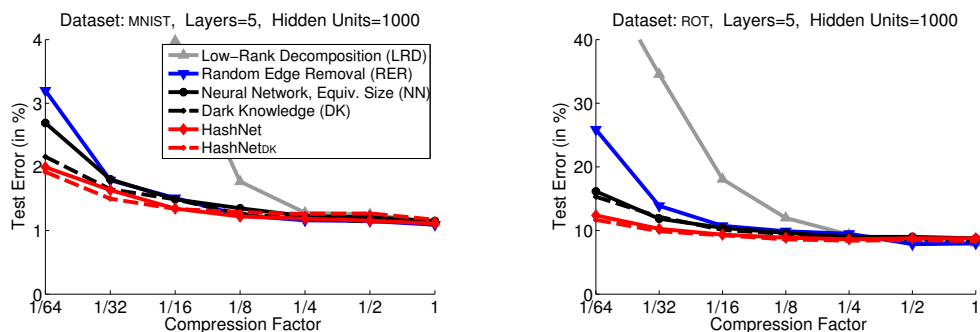
Figure 3.3: Test error rates under varying compression factors with 5-layer networks on MNIST (*left*) and ROT (*right*).

number of parameters. With the help of feature hashing [148], *Vowpal Wabbit*, a large-scale learning system, is able to scale to terafeature datasets [1].

3.1.6 Experimental Results

We conduct extensive experiments to evaluate HashedNets on eight benchmark datasets.

Datasets. Datasets consist of the original MNIST handwritten digit dataset, along with four challenging variants [75]. Each variation amends the original through digit rotation

	3 Layers						5 Layers					
	RER	LRD	NN	DK	HashNet	HashNet$_{DK}$	RER	LRD	NN	DK	HashNet	HashNet$_{DK}$
MNIST	2.19	1.89	1.69	1.71	1.45	**1.43**	1.24	1.77	1.35	1.26	**1.22**	1.29
BASIC	3.29	3.73	3.19	3.18	2.91	**2.89**	2.87	3.54	2.73	2.87	**2.62**	2.85
ROT	14.42	13.41	12.65	11.93	11.17	**10.34**	9.89	11.98	9.61	9.46	8.87	**8.61**
BG-RAND	18.16	45.12	13.00	12.41	13.38	**12.27**	11.31	45.02	11.19	10.91	**10.76**	10.96
BG-IMG	24.18	38.83	20.93	19.31	22.57	**18.92**	19.81	35.06	19.33	18.94	19.07	**18.49**
BG-IMG-ROT	59.29	67.00	52.90	53.01	51.96	**50.05**	45.67	64.28	48.47	48.22	46.67	46.78
CONVEX	27.32	32.73	23.91	24.74	27.06	**22.93**	27.13	35.79	24.58	**23.86**	29.58	25.99
RECT	3.69	4.56	4.24	3.07	3.23	**2.96**	3.92	7.09	3.43	2.37	3.92	**2.36**

Table 3.1: Test error rates (in %) with a compression factor of $\frac{1}{8}$ across all data sets. Best results are printed in **blue**.

	3 Layers						5 Layers					
	RER	LRD	NN	DK	HashNet	HashNet$_{DK}$	RER	LRD	NN	DK	HashNet	HashNet$_{DK}$
MNIST	15.03	28.99	6.28	6.32	2.79	**2.65**	3.20	28.11	2.69	2.16	1.99	**1.92**
BASIC	13.95	26.95	7.67	8.44	4.17	**3.79**	5.31	27.21	4.55	4.07	3.49	**3.19**
ROT	49.20	52.18	35.60	35.94	18.04	**17.62**	25.87	52.03	16.16	15.30	12.38	**11.67**
BG-RAND	44.90	76.21	43.04	53.05	21.50	**20.32**	90.28	76.21	16.60	14.57	16.37	**13.76**
BG-IMG	44.34	71.27	32.64	41.75	26.41	**26.17**	55.76	70.85	22.77	23.59	22.22	**20.01**
BG-IMG-ROT	73.17	80.63	79.03	77.40	59.20	**58.25**	88.88	80.93	53.18	53.19	**51.93**	54.51
CONVEX	37.22	39.93	34.37	31.85	31.77	**30.43**	50.00	39.65	29.76	**26.95**	29.70	32.04
RECT	18.23	23.67	5.68	5.78	3.67	**3.37**	50.03	23.95	4.28	3.10	5.67	**2.64**

Table 3.2: Test error rates (in %) with a compression factor of $\frac{1}{64}$ across all data sets. Best results are printed in **blue**.

(ROT), background superimposition (BG-RAND and BG-IMG), or a combination thereof (BG-IMG-ROT). In addition, we include two binary image classification datasets: CONVEX and RECT [75]. All data sets have pre-specified training and testing splits. Original MNIST has splits of sizes $n = 60000$ (training) and $n = 10000$ (testing). CONVEX and RECT have 8000 and 1200 training images, respectively. And they both have 50000 testing images. Each MNIST variation set has $n = 12000$ (training) and $n = 50000$ (testing).

Baselines and method. We compare HashedNets with several existing techniques for size-constrained, feed-forward neural networks. *Random Edge Removal* (RER) [30] reduces the total number of model parameters by randomly removing weights prior to training. *Low-Rank Decomposition* (LRD) [39] decomposes the weight matrix into two low-rank matrices. One of these component matrices is fixed while the other is learned. Elements of the fixed
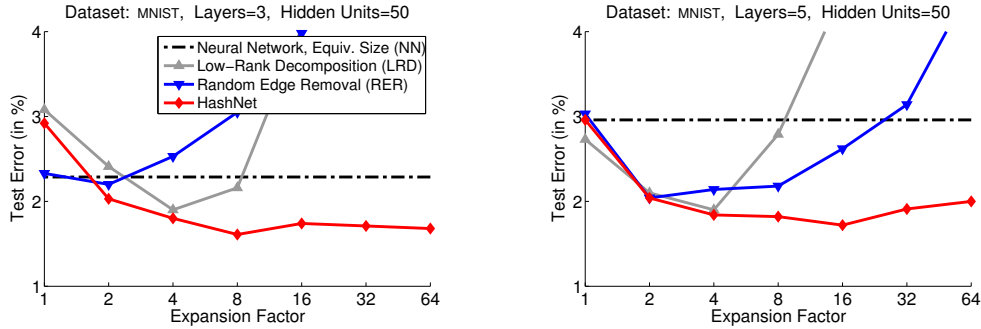
Figure 3.4: Test error rates with fixed storage but varying expansion factors on MNIST with 3 layers (*left*) and 5 layers (*right*).

matrix are generated according to a zero-mean Gaussian distribution with standard deviation $\frac{1}{\sqrt{n^\ell}}$ with n^ℓ inputs to the layer.

Each model is compared against a standard neural network with an equivalent number of stored parameters, *Neural Network (Equivalent-Size)* (NN). For example, for a network with a single hidden layer of 1000 units and a storage compression factor of $\frac{1}{10}$, we adopt a size-equivalent baseline with a single hidden layer of 100 units. For deeper networks, all hidden layers are shrunk at the same rate until the number of stored parameters equals the target size. In a similar manner, we examine *Dark Knowledge* (DK) [64, 3] by training a distilled model to optimize the cross entropy with both the original labels and soft targets generated by the corresponding full neural network (compression factor 1). The distilled model structure is chosen to be same as the "equivalent-sized" network (NN) at the corresponding compression rate.

Finally, we examine our method under two settings: learning hashed weights with the original training labels (HashNet) and with combined labels and DK soft targets (HashNet$_{\mathrm{DK}}$). In all cases, memory and storage consumption is defined strictly in terms of free parameters.

As such, we count the fixed low rank matrix in the Low-Rank Decomposition method as taking no memory or storage (providing this baseline a slight advantage).

Experimental setting. HashedNets and all accompanying baselines were implemented using Torch7 [33] and run on NVIDIA GTX TITAN graphics cards with 2688 cores and 6GB of global memory. We use 32 bit precision throughout but note that the compression rates of all methods may be improved with lower precision [34, 56]. We verify all implementations by numerical gradient checking. Models are trained via stochastic gradient descent (mini-batch size of 50) with dropout and momentum. ReLU is adopted as the activation function for all models. Hyperparameters are selected for all algorithms with Bayesian optimization [132] and hand tuning on 20% validation splits of the training sets. We use the open source Bayesian Optimization MATLAB implementation "bayesopt.m" from Gardner et al. [48].[10]

Results with varying compression. Figures 3.2 and 3.3 show the performance of all methods on MNIST and the ROT variant with different compression factors on 3-layer (1 hidden layer) and 5-layer (3 hidden layers) neural networks, respectively. Each hidden layer contains 1000 hidden units. The x-axis in each figure denotes the fractional compression factor. For HashedNets and the low rank decomposition and random edge removal compression baselines, this means we fix the number of hidden units (n^ℓ) and vary the storage budget (K^ℓ) for the weights ($\mathbf{w}^\ell$).

We make several observations: The accuracy of HashNet and HashNet$_{DK}$ outperforms all other baseline methods, especially in the most interesting case when the compression factor is

---

[10]http://tinyurl.com/bayesopt

small (*i.e.* very small models). Both compression baseline algorithms, low rank decomposition and random edge removal, tend to not outperform a standard neural network with fewer hidden nodes (black line), trained with dropout. For smaller compression factors, random edge removal likely suffers due to a significant number of nodes being entirely disconnected from neighboring layers. The size-matched NN is consistently the best performing baseline, however its test error is significantly higher than that of HashNet especially at small compression rates. The use of Dark Knowledge training improves the performance of HashedNets and the standard neural network. Of all methods, only HashNet and HashNet$_{\text{DK}}$ maintain performance for small compression factors.

For completeness, we show the performance of all methods on all eight datasets in Table 3.1 for compression factor $\frac{1}{8}$ and Table 3.2 for compression factor $\frac{1}{64}$. HashNet and HashNet$_{\text{DK}}$ outperform other baselines in most cases, especially when the compression factor is very small (Table 3.2). With a compression factor of $\frac{1}{64}$ on average only 0.5 *bits* of information are stored per (virtual) parameter. Also note that non-neural network classifiers [153, 24] with the same model size cannot compete with this result either.

Results with fixed storage. We also experiment with the setting where the model size is fixed and the virtual network architecture is "inflated". Essentially we are fixing K^ℓ (the number of "real" weights in $\mathbf{w}^\ell$), and vary the number of hidden nodes (n^ℓ). An expansion factor of 1 denotes the case where every virtual weight has a corresponding "real" weight, $(n^\ell + 1)n^{\ell+1} = K^\ell$. Figure 3.4 shows the test error rate under various expansion rates of a network with one hidden layer (*left*) and three hidden layers (*right*). In both scenarios we fix the number of real weights to the size of a standard fully-connected neural network with 50 hidden units in each hidden layer whose test error is shown by the black dashed line.

With no expansion (at expansion rate 1), different compression methods perform differently. At this point edge removal is identical to a standard neural network and matches its results. If no expansion is performed, the HashNet performance suffers from collisions at no benefit. Similarly the low-rank method still randomly projects each layer to a random feature space with same dimensionality.

For expansion rates greater 1, all methods improve over the fixed-sized neural network. There is a general trend that more expansion decreases the test error until a "sweet-spot" after which additional expansion tends to hurt. The test error of the HashNet neural network decreases substantially through the introduction of more "virtual" hidden nodes, despite that no additional parameters are added. In the case of the 5-layer neural network (right) this trend is maintained to an expansion factor of $16\times$. One could hypothetically increase n^{ℓ} arbitrarily for HashNet, however, in the limit, too many hash collisions would result in increasingly similar gradient updates for all weights in $\mathbf{w}$.

The benefit from expanding a network cannot continue forever. In the *random edge removal* the network will become very sparsely connected; the low-rank decomposition approach will eventually lead to a decomposition into rank-1 matrices. HashNet also respects this trend, but is much less sensitive when the expansion goes up. Best results are achieved when networks are inflated by a factor $8-16\times$.

3.1.7 Conclusion

Prior work shows that weights learned in neural networks can be highly redundant [39]. In this chapter, we have presented HashedNets to exploit this property to create neural networks with "virtual" connections that seemingly exceed the storage limits of the trained

73

model. This can have surprising effects. Figure 3.4 in Section 3.1.6 shows the test error of neural networks can drop nearly 50%, from 3% to 1.61%, through expanding the number of weights "virtually" by a factor $8\times$. Although the collisions (or weight-sharing) might serve as a form of regularization, we can probably safely ignore this effect as both networks (with and without expansion) were also regularized with dropout [133] and the hyper-parameters were carefully fine-tuned through Bayesian optimization.

So why should additional virtual layers help? One answer is that they probably truly increase the expressiveness of the neural network. As an example, imagine we are provided with a neural network with 100 hidden nodes. The internal weight matrix has 10000 weights. If we add another set of m hidden nodes, this increases the expressiveness of the network. If we require all weights of connections to these m additional nodes to be "re-used" from the set of existing weights, it is not a strong restriction given the large number of weights in existence. In addition, the backprop algorithm can adjust the shared weights carefully to have useful values for all their occurrences.

3.2 Compressing convolutional neural network in the frequency domain

3.2.1 Introduction

We have introduced using HashedNets to compress neural networks. In this section, we aim to compress convolutional neural networks (CNN). Although CNNs have been known for a quarter of a century [46], only recently have their superb generalization abilities been

accepted widely across the machine learning and computer vision communities. This broad acceptance coincides with the release of very large collections of labeled data [38]. Deep networks and CNNs are particularly well suited to learn from large quantities of data, in part because they can have arbitrarily many parameters. As data sets grow, so do model sizes. In 2012, the first winner of the ImageNet competition that used a CNN had already 240MB of parameters and the most recent winning model, in 2014, required 567MB [131].

Independently, same as described in Section 3.1, there has been another parallel shift of computing from servers and workstations to mobile platforms. As of January 2014 there have already been more web searches through smart phones than computers[11]. Today speech recognition is primarily used on cell phones with intelligent assistants such as Apple's Siri, Google Now or Microsoft's Cortana. As this trend continues, we are expecting applications of CNNs to also shift increasingly towards mobile devices which have tight memory and storage limitations.

Of course, HashedNets presented in Section 3.1 also applies to convolutional layers by random weight sharing with the hashing trick. However, it does not harness the distinct property of CNNs, which is the *local smoothness* of the parameters in the filters. Building on Hashed-Nets, in this section we propose a novel approach for neural network compression targeted especially for CNNs. Due to the nature of local pixel correlation in images (*i.e.* spatial locality), filters in CNNs tend to be smooth. We transform these filters into frequency domain with the discrete cosine transform (DCT) [109]. In frequency space, the filters are naturally dominated by low frequency components. Our compression takes this smoothness property into account and randomly hashes the frequency components of all CNN filters at a given layer into one common set of hash buckets. All components inside one hash bucket share the

---

[11]http://tinyurl.com/omd58sq

same value. As lower frequency components are more pronounced than higher frequencies, we allow collisions only between similar frequencies and allocate fewer hash buckets for the high frequencies (which are less important).

Our approach has several compelling properties: 1. The number of parameters in the CNN is *independent* of the number of convolutional filters; 2. During testing we only need to add a low-cost hash function and the inverse DCT transformation to any existing CNN code for filter reconstruction; 3. During training, the hashed weights can be learned with simple back-propagation [6]—the gradient of a hash bucket value is the sum of gradients of all hashed frequency components in that bucket.

We evaluate our compression scheme on eight deep learning image benchmark data sets and compare against four competitive baselines. Although all compression schemes lead to lower test accuracy as the compression increases, our FreshNets method is by far the most effective compression method and yields the lowest generalization error rates on almost all classification tasks.

3.2.2   Background

Discrete Cosine Transform (DCT) [109].   Methods built on the DCT are widely used for compressing images and movies, including forming the standard technique for JPEG [142]. DCT expresses a function as a weighted combination of sinusoids of different phases/frequencies where the weight of each sinusoid reflects the magnitude of the corresponding frequency in the input. When employed with sufficient numerical precision and without quantization or other compression operations, the DCT and inverse DCT (projecting frequency inputs back to the spatial domain) are lossless. Compression is made possible

in images by local smoothness of pixels (*e.g.* a blue sky) which can be well represented regionally by fewer non-zero frequency components. Though highly related to the discrete Fourier transformation (DFT), DCT is often preferable for compression tasks because of its *spectral compaction* property where weights for most images tend to be concentrated in a few low-frequency components of the DCT [109]. Further, the DCT transformation yields a real-valued representation, unlike the DFT whose representation has imaginary components. Given an input matrix $\boldsymbol{V} \in \mathbb{R}^{d \times d}$, the corresponding matrix $\boldsymbol{\mathcal{V}} \in \mathbb{R}^{d \times d}$ in frequency domain after DCT is defined as:

$$\mathcal{V}_{j_1 j_2} = s_{j_1} s_{j_2} \sum_{i_1=0}^{d-1} \sum_{i_2=0}^{d-1} c(i_1, i_2, j_1, j_2) \, V_{i_1 i_2}, \tag{3.13}$$

$$\text{where} \quad c(i_1, i_2, j_1, j_2) = \cos\left[\frac{\pi}{d}\left(i_1 + \frac{1}{2}\right) j_1\right] \cos\left[\frac{\pi}{d}\left(i_2 + \frac{1}{2}\right) j_2\right]$$

is the cosine basis function, and $s_j = \sqrt{\frac{1}{d}}$ when $j = 0$ and $s_j = \sqrt{\frac{2}{d}}$ otherwise. We use the shorthand f_{dct} to denote the DCT operation in Eq. (3.13), *i.e.* $\boldsymbol{\mathcal{V}} = f_{dct}(\boldsymbol{V})$. The inverse DCT converts $\boldsymbol{\mathcal{V}}$ from the frequency domain back to the spatial domain, reconstructing $\boldsymbol{V}$ without loss:

$$V_{i_1 i_2} = \sum_{j_1=0}^{d-1} \sum_{j_2=0}^{d-1} s_{j_1} s_{j_2} \, c(i_1, i_2, j_1, j_2) \, \mathcal{V}_{j_1 j_2}. \tag{3.14}$$

We denote the inverse DCT function in Eq. (3.14) as f_{dct}^{-1}, *i.e.* $\boldsymbol{V} = f_{dct}^{-1}(\boldsymbol{\mathcal{V}})$.

3.2.3   Frequency-Sensitive Hashed Nets

Here we present FreshNets, a method for using weight sharing to reduce the model size (and memory demands) of convolutional neural networks. Similar to HashedNets, we achieve smaller models by randomly forcing weights throughout the network to share identical values.
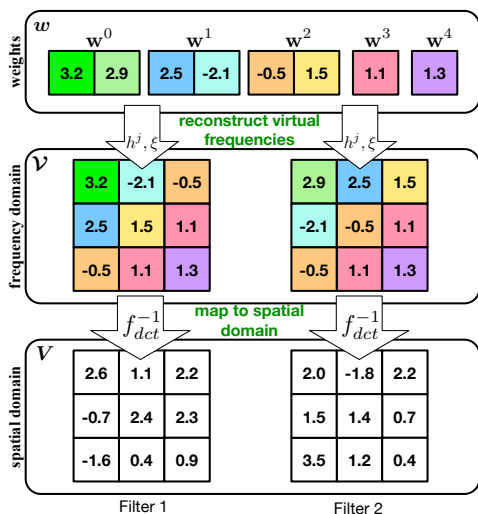
Figure 3.5: A schematic illustration of FreshNets. Two spatial filters are re-constructed from the frequency weights in vector $\boldsymbol{w}$. The frequency weights are accessed with two hash functions and then transformed to the spatial domain. The vector $\boldsymbol{w}$ is partitioned into sub-vectors $\boldsymbol{w}^j$ shared by all entries with similar frequency (corresponding to index sum $j = j_1 + j_2$). Colors indicate which hash bucket was accessed.

Unlike previous work, we implement the weight sharing and gradient updates of convolutional filters in the *frequency domain*. These sharing constraints are made prior to training, and we learn frequency weights under the sharing assignments. Since the assignments are made with a hash function, they incur no additional storage.

Filters in spatial and frequency domain. Let the matrix $\boldsymbol{V}^{k\ell} \in \mathbb{R}^{d \times d}$ denote the weight matrix of the $d \times d$ convolutional filter that connects the kth input plane to the ℓth output plane. (For notational convenience we assume square filters and only consider the filters in a single layer of the network.) The weights of all filters in a convolutional layer can be denoted by a 4-dimensional tensor $\boldsymbol{V} \in \mathbb{R}^{m \times n \times d \times d}$ where m and n are the number of input planes and output planes, respectively, resulting in a total of $m \times n \times d^2$ parameters. Convolutional filters can be represented equivalently in either the spatial or frequency domain, mapping between the two via the DCT and its inverse. We denote the filter in frequency domain

as $\boldsymbol{\mathcal{V}}^{k\ell} = f_{dct}(\boldsymbol{V}^{k\ell}) \in \mathbb{R}^{d \times d}$ and recover the original spatial representation through $\boldsymbol{V}^{k\ell} = f_{dct}^{-1}(\boldsymbol{\mathcal{V}}^{k\ell})$, as defined in Eq. (3.13) and (3.14), respectively. The tensor of all filters is denoted $\boldsymbol{\mathcal{V}} \in \mathbb{R}^{m \times n \times d \times d}$.

Random Weight Sharing by Hashing. We would like to reduce the number of model parameters to exactly K values stored in a weight vector $\boldsymbol{w} \in \mathbb{R}^K$, where $K \ll m \times n \times d^2$. To achieve this, we randomly assign a value from $\boldsymbol{w}$ to each filter frequency weight in $\boldsymbol{\mathcal{V}}$. A naïve implementation of this random weight sharing would introduce an auxiliary matrix for $\boldsymbol{\mathcal{V}}$ to track the weight assignments, using to significant additional memory. To address this problem, FreshNets adopts the hashing trick used in HashedNets (See Section 3.1) to (pseudo-)randomly assign shared parameters. Using the hashing trick, we tie each filter weight $\mathcal{V}_{j_1 j_2}^{k\ell}$ to an element of $\boldsymbol{w}$ indexed by the output of a hash function $h(\cdot)$:

$$\mathcal{V}_{j_1, j_2}^{k\ell} = \xi(k, \ell, j_1, j_2) \, w_{h(k, \ell, j_1, j_2)}, \tag{3.15}$$

where $h(k, \ell, j_1, j_2) \in \{1, \cdots, K\}$, and $\xi(k, \ell, j_1, j_2) \in \{\pm 1\}$ is a sign factor computed by a second hash function $\xi(\cdot)$ to preserve inner-products in expectation as described in Section 3.1.2. With the mapping in Eq. (3.15), we can implement shared parameter assignments with no additional storage cost. (For a schematic illustration, see Figure 3.5. The figure also incorporates a frequency sensitive hashing scheme discussed later in this section.)

Gradients over Shared Frequency Weights. Typical convolutional neural networks learn filters in the spatial domain. As our shared weights are stored in the frequency domain, we derive the gradient with respect to filter parameters in frequency space. Following Eq. (3.14), we express the gradient of parameters in the spatial domain *w.r.t.* their counterparts

in the frequency domain:

$$\frac{\partial V_{i_1 i_2}^{k\ell}}{\partial \mathcal{V}_{j_1 j_2}^{k\ell}} = s_{j_1} s_{j_2} \; c(i_1, i_2, j_1, j_2). \tag{3.16}$$

Let $\mathcal{L}$ be the loss function adopted for training. Using standard back-propagation, we can derive the gradient *w.r.t.* filter parameters in the spatial domain, $\frac{\partial \mathcal{L}}{\partial V_{i_1 i_2}^{k\ell}}$. By the chain rule with Eq. (3.16), we express the gradient of $\mathcal{L}$ in the frequency domain:

$$\frac{\partial \mathcal{L}}{\partial \mathcal{V}_{j_1 j_2}^{k\ell}} = \sum_{i_1=0}^{d-1} \sum_{i_2=0}^{d-1} \frac{\partial \mathcal{L}}{\partial V_{i_1 i_2}^{k\ell}} \frac{\partial V_{i_1 i_2}^{k\ell}}{\partial \mathcal{V}_{j_1 j_2}^{k\ell}} = s_{j_1} s_{j_2} \sum_{i_1=0}^{d-1} \sum_{i_2=0}^{d-1} c(i_1, i_2, j_1, j_2) \; \frac{\partial \mathcal{L}}{\partial V_{i_1 i_2}^{k\ell}}. \tag{3.17}$$

Comparing with Eq. (3.13), we see that the gradient in the frequency domain is merely the DCT of the gradient in the spatial domain:

$$\frac{\partial \mathcal{L}}{\partial \boldsymbol{\mathcal{V}}^{k\ell}} = f_{dct} \left(\frac{\partial \mathcal{L}}{\partial \boldsymbol{V}^{k\ell}} \right). \tag{3.18}$$

We compute gradient for each shared weight w_h by simply summing over the gradient at each filter parameter where the weight is assigned, *i.e.* all $\mathcal{V}_{j_1 j_2}^{k\ell}$ where $h = h(k, \ell, j_1, j_2)$:

$$\frac{\partial \mathcal{L}}{\partial w_h} = \sum_{k=0}^{m} \sum_{\ell=0}^{n} \sum_{j_1=0}^{d-1} \sum_{j_2=0}^{d-1} \frac{\partial \mathcal{L}}{\partial \mathcal{V}_{j_1 j_2}^{k\ell}} \frac{\partial \mathcal{V}_{j_1 j_2}^{k\ell}}{\partial w_h} = \sum_{\substack{k,\ell,j_1,j_2: \\ h=h(k,\ell,j_1,j_2)}} \xi(k, \ell, j_1, j_2) \left[f_{dct} \left(\frac{\partial \mathcal{L}}{\partial \boldsymbol{V}^{k\ell}} \right) \right]_{j_1 j_2} \tag{3.19}$$

where $[\boldsymbol{A}]_{j_1 j_2}$ denotes the (j_1, j_2) entry in matrix $\boldsymbol{A}$.

Frequency Sensitive Hashing. Figure 3.6 shows a filter in spatial (left) and frequency (right) domains. In the spatial domain CNN filters are smooth [72] due to the local pixel smoothness in natural images. In the frequency domain this corresponds to components with large magnitudes in the low frequencies, depicted in the upper left half of $\boldsymbol{\mathcal{V}}^{k\ell}$ in Figure 3.6.
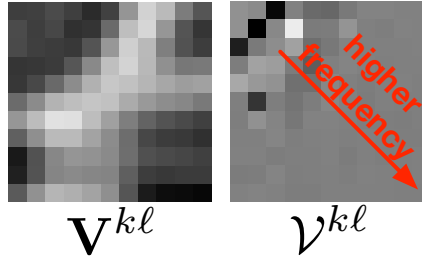
Figure 3.6: An example of a filter in spatial (left) and frequency domain (right).

Correspondingly, the high frequencies, in the bottom right half of $\boldsymbol{\mathcal{V}}^{k\ell}$, have magnitudes near zero.

As components of different frequency groups tend to be of different magnitudes (and thereby varying importance to the spatial structure of the filter), we want to avoid collisions between high and low frequency components. Therefore, we assign separate hash spaces to different frequency groups. In particular, we partition the K values of $\boldsymbol{w}$ into sub-vectors $\boldsymbol{w}^0, \ldots, \boldsymbol{w}^{2d-2}$ of sizes $K_0, \ldots, K_{2d-2}$, where $\sum_j K_j = K$. This partitioning allows parameters with the same frequency, corresponding to their index sum $j = j_1 + j_2$, to be hashed into a corresponding dedicated hash space $\boldsymbol{w}^j$. We rewrite Eq. (3.15) with the new frequency sensitive shared weight assignments:

$$\mathcal{V}^{k\ell}_{j_1, j_2} = \xi(k, \ell, j_1, j_2) \; w^j_{h^j(k, \ell, j_1, j_2)}$$

where $h^j(\cdot)$ maps an input key to a natural number in $\{1, \cdots, K_j\}$ and $j = j_1 + j_2$.

We define a compression rate $r_j \in (0, 1]$ for each frequency region j and assign $K_j = r_j N_j$. A smaller r_j induces more collisions during hashing, leading to increased weight sharing. Since lower frequency components tend to be of higher importance, making collisions more hurtful, we commonly assign larger r_j (fewer collisions) to low-frequency regions. Intuitively, given

a size budget for the whole convolutional layer, we want to squeeze the hash space of high frequency region to save space for low frequency regions. These compression rates can either be assigned by hand or determined programmatically by cross-validation, as demonstrated in Section 3.2.5.

3.2.4 Related Work

Several recent studies have confirmed that there is significant redundancy in the parameters learned in deep neural networks. Recent work by Denil et al. [39] learns parameters in fully-connected layers after decomposition into two low-rank matrices, *i.e.* $\boldsymbol{W} = \boldsymbol{AB}$ where $\boldsymbol{W} \in \mathbb{R}^{m \times n}$, $\boldsymbol{A} \in \mathbb{R}^{m \times k}$ and $\boldsymbol{B} \in \mathbb{R}^{k \times n}$. In this way, the original $O(mn)$ parameters could be stored with $O(k(m + n))$ storage, where $k \ll \min(m, n)$. Several works apply related approaches to speed up the evaluation time with convolutional neural networks. Two works propose to approximate convolutional filters by a weighted linear combination of basis filters [116, 66]. In this setting, the convolution operation only needs to be performed with the small set of basis filters. The desired output feature maps are computed by matrix multiplication as the weighted sum of these basis convolutions. Further speedup can be achieved by learning rank-one basis filters so that the convolution operations are very cheap to compute [40, 77]. Based on this idea, Denton *et al.* [40] advocate decomposing the four-dimensional tensor of the filter weights into a sum of different rank-one, four-dimensional tensors. In addition, they adopt bi-clustering to group filters such that each subgroup can be better approximated by rank-one tensors.

In each of these works, evaluation time is the main focus, with any resulting storage reduction achieved merely as a side effect. Other works focus entirely on compressing the

fully-connected layers of CNNs [53, 155]. However, with the trend toward architectures with fewer fully connected layers and additional convolutional layers [135], compression of filters is of increased importance. Another technique for speeding up convolutional neural network evaluation is computing convolutions in the Fourier frequency domain, as convolution in the spatial domain is equivalent to (comparatively lower-cost) element-wise multiplication in the frequency domain [91, 139]. Unlike FreshNets, for a filter of size $d \times d$ and an image of size $n \times n$ where $n > d$, Mathieu et al. [91] convert the filter to its frequency domain of size $n \times n$ by oversampling the frequencies, which is necessary for doing element-wise multiplication with a larger image but also increases the memory overhead at test time. Training in the Fourier frequency domain may be advantageous for similar reasons, particularly when convolutions are being performed over large 3-D volumes [14].

3.2.5 Experimental Results

In this section, we conduct several comprehensive experiments on benchmark datasets to evaluate the performance of FreshNets.

Datasets. We experiment with eight benchmark datasets: CIFAR10, CIFAR100, SVHN and five challenging variants of MNIST. The CIFAR10 dataset contains 60000 images of 32×32 pixels with three color channels. Images are selected from ten classes with each class consisting of 6000 unique instances. The CIFAR100 dataset also contains 60000 32×32 images, but is more challenging since the images are selected from 100 classes (each class has 600 images). For both CIFAR datasets, 50000 images are designated for training and the remaining 10000 images for testing. To improve accuracy on CIFAR100, we augment by horizontal reflection and cropping [72], resulting in 0.8M training images. The SVHN

dataset is a large collection of digits (10 classes) cropped from real-world scenes, consisting of 73257 training images, 26032 testing images and 531131 less difficult images for additional training. In our experiments, we use all available training images, for a total of 604388 training samples. For the MNIST variants [75], each variation either reduces the training size (MNIST-07) or amends the original digits by rotation (ROT), background superimposition (BG-RAND and BG-IMG), or a combination thereof (BG-ROT). We preprocess all datasets with whitening (except CIFAR100 and SVHN which were prohibitively large).

Baselines. We compare the proposed FreshNets with four baseline methods: Hashed-Nets [26], low-rank decomposition (LRD) [39], filter dropping (DropFilt) and frequency dropping (DropFreq). HashedNets was first proposed to compress fully-connected layers in deep neural networks via the hashing trick. In this baseline, we apply the hashing trick directly to the convolutional layer by hashing filter weights in the spatial domain. This induces random weight sharing across all filters in a single convolutional layer. Additionally, we compare against low-rank decomposition of the convolutional filters [39]. Following the method in [40], we unfold the four-dimensional filter tensor to form a two dimensional matrix on which we apply the low-rank decomposition. The parameters of the decomposition are fine-tuned via back-propagation. DropFreq learns parameters in the DCT frequency domain but sets high frequency components to 0 to meet the compression requirement. DropFilt compresses simply by reducing the number of filters in each convolutional layer.

All methods were implemented using Torch7 [33] and run on NVIDIA GTX TITAN graphics cards with 2688 cores and 6GB of global memory. Model parameters are stored and updated as 32 bit floating-point values.[12]

---

[12]The compression rates of all methods could be further improved by learning and storing parameters in lower precision [34, 56].

Layer	Operation	Input dim.	Inputs	Outputs	C size	MP size	Parameters
1	C,RL	32×32	3	32	5×5		$2K$
2	C,MP,DO,RL	32×32	32	64	5×5	$2\times2(2)$	$51K$
3	C,RL	16×16	64	64	5×5		$102K$
4	C,MP,DO,RL	16×16	64	128	5×5	$2\times2(2)$	$205K$
5	C,MP,DO,RL	8×8	128	256	5×5	$2\times2(2)$	$819K$
6	FC,Softmax	$-$	4096	10/100			$40/400K$

Table 3.3: Network architecture. C: Convolution. RL: ReLu. MP: Max-pooling. DO: Dropout. FC: Fully-connected. The number of parameters in the fully-connected layer is specific to 32×32 input images and varies with the number of classes, either 10 or 100 depending on the dataset.

	(a) Compression $=1/16$						(b) Compression $=1/64$			
	CNN	DropFilt	DropFreq	LRD	HashedNets	FreshNets	CNN	LRD	HashedNets	FreshNets
CIFAR10	14.91	54.87	30.45	23.23	24.70	**21.42**	14.37	34.35	43.08	**30.79**
CIFAR100	33.66	81.17	55.93	51.88	48.64	**47.49**	33.76	66.44	67.06	**62.33**
SVHN	3.71	30.93	14.96	10.67	9.00	**8.01**	3.69	22.32	23.31	**18.37**
MNIST-07	0.80	4.90	2.20	1.18	1.10	**0.94**	0.85	1.95	1.77	**1.24**
ROT	3.42	29.74	8.39	4.79	5.53	**3.87**	3.32	9.90	10.10	**6.60**
BG-ROT	11.42	88.88	56.63	20.19	**16.15**	18.43	11.28	35.64	32.40	**27.91**
BG-RAND	2.17	90.10	8.83	2.94	2.80	**2.63**	1.77	4.57	5.10	**3.62**
BG-IMG	2.61	89.41	27.89	4.35	**3.26**	3.97	2.38	7.23	**6.68**	8.04

Table 3.4: Test error rates (in %) with compression factors 1/16 and 1/64. Convolutional layers were compressed by the indicated methods (DropFilt, DropFreq, LRD, HashedNets, and FreshNets), with no *convolutional layer* compression applied to CNN. The *fully connected* layer is compressed by HashNets for *all methods*, including CNN.

Comprehensive evaluation. We adopt the network network architecture shown in Table 3.3 for all datasets. The architecture is a deep convolutional neural network consisting of five convolutional layers (with 5×5 filters) and one fully-connected layer. Before convolution, input feature maps are zero-padded such that output maps remain the same size as the (un-padded) input maps after convolution. Max-pooling is performed after convolutions in layers 2, 4 and 5 with filter size 2×2 and stride 2, reducing both input map dimensions by half. Rectified linear units are adopted as the activation function throughout. The output of the network is a softmax function over labels.
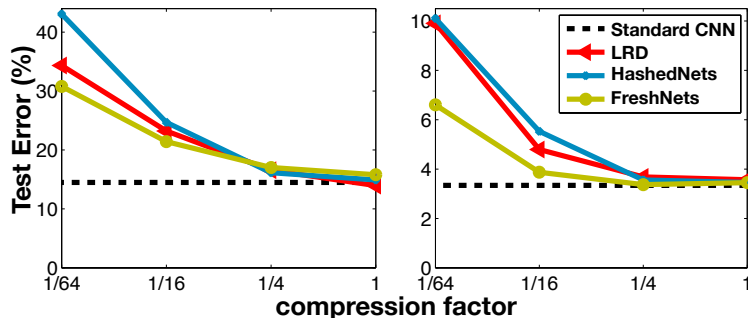
Figure 3.7: Test error rates at varying compression levels for datasets CIFAR10 (left) and ROT (right).

In this architecture, the convolutional layers hold the majority of parameters (1.2 million in convolutional layer *v.s.* 40 thousand in the fully connected layer with 10 output classes). During training, we optimize parameters using mini-batch gradient descent with batch size 64 and momentum 0.9. We use 20 percent of the training set as a validation set for early stopping. For FreshNets, we use a frequency-sensitive compression scheme which increases weight sharing among higher frequency components.[13] For all baselines, we apply Hashed-Nets [26] to the fully connected layer at the corresponding level of compression. All error results are reported on the test set.

Table 3.4(a) and (b) show the comprehensive evaluation of all methods under compression ratios 1/16 and 1/64, respectively. We exclude DropFilt and DropFreq in Table 3.4(b) because neither supports 1/64 compression in this architecture for all layers. For all methods, the fully connected layer (top layer) is compressed by HashedNets [26] at the corresponding compression rate. In this way, the final size of the entire network respects the specified compression ratio. For reference, we also show the error rate of a standard convolutional neural network (CNN, columns 2 and 8) with the fully-connected layer compressed by HashedNets

---

[13]We evaluate several frequency-sensitive schemes later in this section, but for this comprehensive evaluation we set frequency compression rates by a rescaled beta distribution with $\alpha = 0.25$ and $\beta = 2.5$ for all layers.
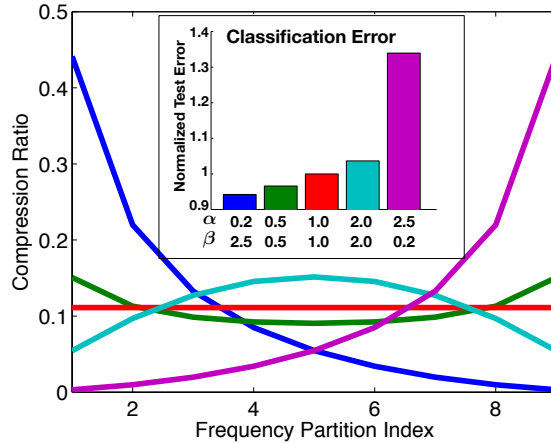
Figure 3.8: Results with different frequency sensitive compression schemes, each adopting a different beta distribution as the compression rate for each frequency. The inner figure shows normalized test error of each scheme on CIFAR10 with the beta distribution hyperparameters. The outer figure depicts the corresponding beta distributions. The setting $\alpha = 0.2, \beta = 2.5$ (blue line), which compresses low frequencies the least and high frequencies the most, yields lowest error.

and *no compression* in the convolutional layers. Excluding this reference, we highlight the method with best test error on each dataset in **bold**.

We discern several general trends. In Table 3.4(a), we observe the performance of the DropFilt and DropFreq at 1/16 compression. At this compression rate, DropFilt corresponds to a network 1/16 filters at each layer: 2, 4, 4, 8, 16 at layers $1 - 5$ respectively. This architecture yields particularly poor test accuracy, including essentially random predictions on three datasets. DropFreq, which at 1/16 compression parameterizes each filter in the original network by only 1 or 2 low-frequency values in the DCT frequency space, performs with similarly poor accuracy. Low rank decomposition (LRD) and HashedNets each yield similar performance at both 1/16 and 1/64 compression. Neither explicitly considers the smoothness inherent in learned convolutional filters, instead compressing the filters in the spatial domain. Our method, FreshNets, consistently outperforms all baselines, particularly

at the higher compression rate as shown in Table 3.4(b). Using the same model in Table 3.3, Figure 3.7 shows more complete curves of test errors with multiple compression factors on the CIFAR10 and ROT datasets.

Varying compression by frequency. As mentioned in Section 3.2.3, we allow a higher collision rate in the high frequency components than in the low frequency components for each filter. To demonstrate the utility of this scheme, we evaluate several hash compression schemes. Systematically, we set the compression rate of the jth frequency band r_j with a parameterized function, *i.e.* $r_j = f(j)$. In this experiment, we use the beta distribution: $f(j; \alpha, \beta) = Zx^{\alpha-1}(1-x)^{\beta-1}$, where $x = \frac{j+1}{2k-1}$ is a real number between 0 and 1, k is the filter size, and Z is a normalizing factor such that the resulting distribution of parameters meets the target parameter budget K, *i.e.* $\sum_{j=0}^{2k-2} r_j N_j = K$. We adjust α and β to control the compression rate for each frequency region. As shown in Figure 3.8, we have multiple pairs of α and β, each of which results in a different compression scheme. For example, if $\alpha = 0.25$ and $\beta = 2.5$, the compression rate monotonically decreases as a function of component frequency, meaning more parameter sharing among high frequency components (blue curve in Figure 3.8).

To quickly evaluate the performance of each scheme, we use a simple four-layer FreshNets where the first two layers are DCT-hashed convolutional layers (with 5×5 filters) containing 32 and 64 feature maps respectively, and the last two layers are fully connected layers. We test FreshNets on CIFAR10 with each of the compression schemes shown in Figure 3.8. In each, weight sharing is limited to be within groups of similar frequencies, as described in Section 3.2.3, however number of unique weights shared within each group is varied. We denote the compression scheme with $\alpha, \beta = 1$ (red curve) as a *frequency-oblivious scheme*

(a) Standard CNN	(b) FreshNets	(c) HashedNets
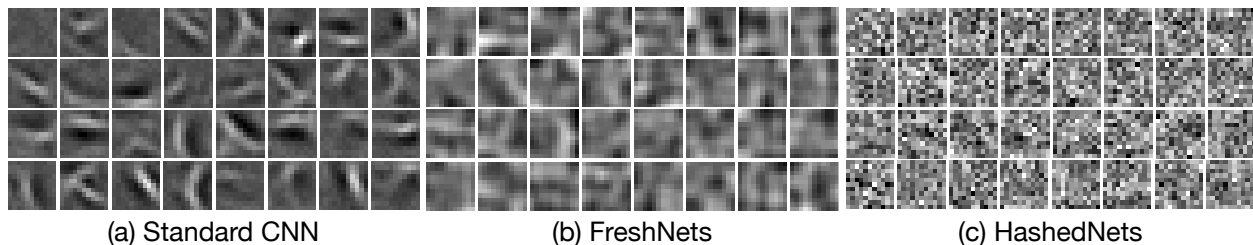
Figure 3.9: Visualization of filters learning on MNIST in (a) an uncompressed CNN, (b) a CNN compressed with FreshNets, and (c) a CNN compressed with HashedNets (compression rate 1/16 in both (b) and (c)). FreshNets preserves the smoothness of the filters, whereas HashedNets does not.

since it produces a uniform compression independent of frequency. In the inset bar plot in Figure 3.8, we report test error normalized by the test error of the frequency-oblivious scheme and averaged over compression rates 1, 1/2, 1/4, 1/16, 1/64, and 1/256. We can see that the proposed scheme with fewer shared weights allocated to high frequency components (represented by the blue curve) outperforms all other compression schemes. An inverse scheme where the high frequency regions have the lowest collision rate (purple curve) performs the worst. These empirical results fit our assumption that the low frequency components of a filter are more important than the high frequency components.

Filter visualization.   We investigate the smoothness of the learned convolutional filters in Figure 3.9 by visualizing the filter weights (first layer) of (a) a standard, uncompressed CNN, (b) FreshNets, and (c) HashedNets (with weight sharing in the spatial domain). For this experiment, we again apply a four layer network with two convolutional layers but adopt larger filters (11×11) for better visualization. All three networks are trained on MNIST, and both FreshNets and HashedNets have 1/16 compression on the first convolutional layer. When plotting, we scale the values in each filter matrix to the range $[0, 255]$. Hence, white and black pixels stand for large positive and negative weights, respectively. We observe that,

although more blurry due to the compression, the filter weights of FreshNets are still smooth while weights in HashedNets appear more chaotic.

3.2.6   Conclusion

In this chapter we have presented FreshNets, a method for learning convolutional neural networks with dramatically compressed model storage. Harnessing the hashing trick for parameter-free random weight sharing and leveraging the smoothness inherent in convolutional filters, FreshNets compresses parameters in a frequency-sensitive fashion such that significant model parameters (*e.g.* low-frequency components) are better preserved. As such, FreshNets preserves prediction accuracy significantly better than competing baselines at high compression rates.

Chapter 4

Deep learning Meets Embedding: An Application to Model Compression

In previous chapters, we have discussed model compression for deep learning models as well as the embedding method for compressing heuristics. In this chapter, we combine the topics of deep learning and embedding, and introduce neural networks with category embedding tailored for traditional data mining tasks in which the one-hot encoding is widely used for converting categorical features to numerical features. We show that a naïve use of one-hot encoding might result in great memory consumption, as the weight matrix in the first layer can be gigantic when many categories are present. We demonstrate that, similar to the technique of low-rank decomposition described in Chapter 3, the category embedding is equivalent to factorizing the weight matrix induced by the classic one-hot encoding, leading to great memory savings. We further compress the embedding matrix with the hashing trick discussed in Chapter 3. Our method is highly inspired by word embedding [5] and the CBOW model [95]. The novelty is that we demonstrate the visualization of the embeddings

91

of categories provides certain degree of interpretability, which is critical for data mining tasks. In particular, similar categories are mapped to nearby regions in the embedding space. At the beginning of this chapter, we first switch our attention to the pros and cons of using neural network in traditional data mining task to motivate category embedding. We discuss its compression property in Section 4.3.1. At the end, we provide surprisingly good visualization and clustering for categorical features.

4.1 Introduction

Deep neural networks and their variants have become the gold standard for a broad range of applications as we can see in Chapter 3. There are many reasons contributing to the recent success of neural networks in machine learning communities. The most important reason, arguably, is that neural network itself has superior expressive power. According to the *universal approximation theorem* [65], a multi-layer feed-forward neural neural network is capable of approximating any measurable functions to any desired degree of accuracy. However, can we get to that "perfect" neural net? There have been a longstanding conventional wisdom that the function surfaces of neural networks contain a large amount of local minima until Dauphin *et al.* [37] argue that they are in fact just critical points most of which are actually saddle points. With proper training such as stochastic gradient descent, we can escape from those saddle points [49]. Also, the emergence of training techniques such as Adagrad [43] and dropout [133] further improve the practical performance of neural networks. Another key reason is the increasing availability of big datasets which enable neural networks to absorb sufficient amount of data for parameter learning. Meanwhile, the use of GPU dramatically speeds up the computation within neural networks by several orders

of magnitude compared with traditional multi-thread CPU computing, allowing neural networks to take in more data inputs given the same amount of training time and consequently leading to better generalization performance.

However, compared to its success in AI applications such as computer vision and speech recognition, neural networks seem not graining as much popularity as it should be in traditional data mining tasks. As opposed to computer vision where the input data are all "raw" features of same type (*e.g.* pixels), traditional data mining tasks typically contain many features generated from multiple sources (*e.g.* gender, country, height, education background, and etc). For these problems, traditional algorithms such as logistic regression, SVM or tree emsembles are still in favor. However, they all have their downsides. Logistic regression is a linear model which limits the expressive power. SVM with kernel is non-parametric and thus the number of support vectors might grow fast for large-scale datasets. Its online training is also a big hassle. Tree ensembles like random forest and gradient boosting trees are not good at handling sparse data, and their generalization ability is unstable when the test instance goes beyond the region of training set. In contrast, neural networks do not have those problems and offer much better expressive power. In fact, SVM and tree emsembles may need an exponentially large number of training examples to get the same generalization error as some deep neural networks [99].

Although neural networks have the above advantages, there are some special needs in traditional data mining tasks that standard neural networks have not addressed well. First, hand-crafted features are usually a mix of numerical and categorical features, which poses a challenge for directly applying neural networks as they can only deal with numerical inputs by design. Second, the amount of categorical features keeps increasing in lots of applications.

In fact, in order to gain more nonlinearity, a trend is to make numerical features categorical by binning or tree partition. Binning is a method to partition each numerical feature with independent equal-size bins where each bin stands for a category. Third, to capture high-order relationship between features, cross features are often used, which is a Cartesian product of the category sets of all involved features, leading to exponentially growing number of categories. Another need by a data mining task is interpretability [35], the ability to extract human-readable knowledge from the model. There have been some early attempts trying to extract rules from trained neural networks [2, 85]. However, those rules are just a proxy for neural networks rather than knowledge directly extracted from neural networks.

To address these problems, we advocate an end-to-end neural network architecture with categorical feature embeddings. The model not only naturally handles both categorical and numerical features, but also (and more importantly) visualizes feature similarity, which provides certain degree of interpretability. Our model is inspired by word embedding [5] and the CBOW model [95], and therefore is by no means a brand-new method. For ease of presentation, we use the name "CENN" to denote this architecture throughout this chapter. In particular, CENN has two branches to deal with numerical and categorical inputs, respectively. Inspired by word embedding, the categorical branch is responsible for converting each categorical feature to a numerical one by learning an embedding for each category of each feature. These two branches are joined in the hidden layer and fed into the remaining feedforward neural network. Both the embeddings and the weights of CENN are jointly learned through backpropagation. We further discuss the relationship between one-hot encoding and CENN and how we can extend CENN to incorporate feature hashing [148]. With embeddings in place, we can directly plot the embeddings, which visualizes the feature similarity found by CENN. Moreover, clustering of the embeddings yields unprecedented visualization
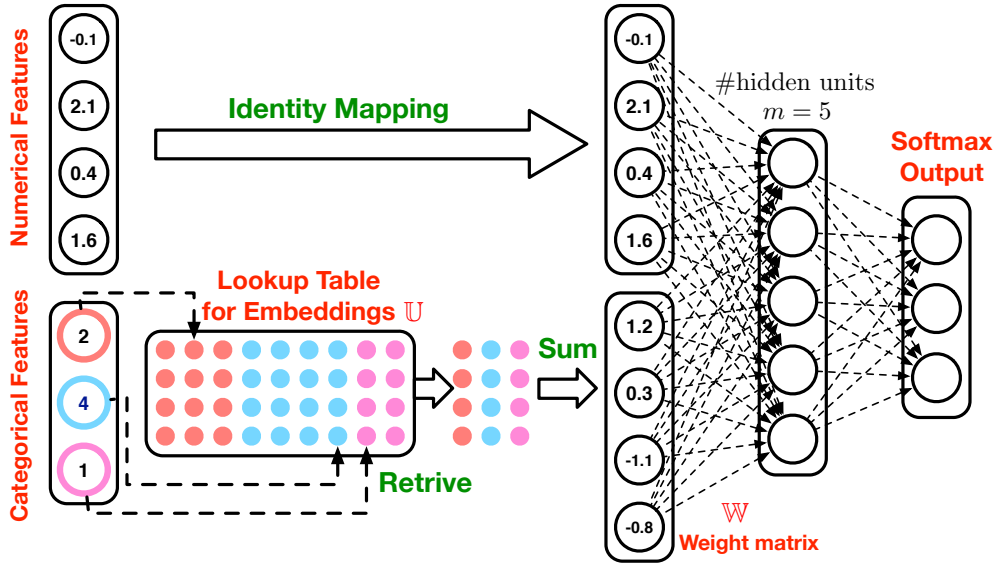
Figure 4.1: The architecture of CENN for classification.

of feature categories. As in the case of word embedding, CENN maps similar categories to nearby regions in the embedding space.

4.2 Method

Suppose we have a dataset $\{\mathbf{x}_i, y_i\}_{i=1}^N$ containing N instances, where $\mathbf{x}_i$ and y_i are the feature vector and label of instance i, respectively. Each feature vector is a concatenation of two parts, numerical features $\mathbf{x}_i^R$ and categorical features $\mathbf{x}_i^C$. Each element in $\mathbf{x}_i^R$ is numerical and each element of $\mathbf{x}_i^C$ is ordinal. CENN first converts the categorical part to a numerical hidden representation which is then concatenated with the original numerical part. This new representation will be fed into the remaining neural network and generate the final output. Figure 4.1 shows the general architecture of CENN for classification purpose. Next, we discuss the detail of each part in the architecture.

95

4.2.1 Categorical feature embedding

Suppose the categorical part $\mathbf{x}^C$ has P features, $\mathbf{x}^C = \left[[\mathbf{x}^C]_1, \cdots, [\mathbf{x}^C]_P\right]$. And the pth categorical feature has K_p categories, $[\mathbf{x}^C]_p \in \{1, 2, \cdots, K_p\}$. Let $K = \sum_{p=1}^{P} K_p$ be the total number of all categories. For example, in Figure 4.1, $P = 3, K_1 = 3, K_2 = 2, K_3 = 4$, and $K = 9$.

The first component of the categorical part is a lookup table that contains a numerical embedding for each category as shown in Figure 4.1. The lookup table is divided into a number of independent zones (with different colors as depicted in Figure 4.1). Categories from the same feature reside in the same zone. The number of embeddings in each zone is equal to the number of categories of the corresponding categorical feature. At its core, the lookup table is a matrix $\mathbb{U} \in \mathcal{R}^{d \times K}$ where each column vector represents a d dimensional embedding for a corresponding category. $d > 0$ is a user defined integer. For example, in Figure 4.1 we have $d = 4$. Each categorical feature would retrieve its corresponding embedding in the lookup table as its new feature representation.

Mathematically, let $\mathbf{u}_i$ be the ith column vector in lookup table $\mathbb{U}$, and $q(j)$ be the index that the jth categorical feature would use as index for retrieving. Let $A_j = \sum_{p=1}^{j} K_p$ be the total number of previous categories up to categorical feature j. $[\mathbf{x}^C]_j$, the value of jth categorical feature, would retrive embedding by index

$$q(j) = A_{j-1} + [\mathbf{x}^C]_j \tag{4.1}$$

Take Figure 4.1 as an example. There are 3 categorical features and totally 9 categories. The value of the second categorical feature $[\mathbf{x}^C]_2 = 4$, and therefore we have $q(1) = A_1 + [\mathbf{x}^C]_2 = 7$, meaning that the second categorical feature will retrieve the 7th embedding

in the lookup table $\mathbb{U}$ as shown in Figure 4.1. After embedding retrieval, we obtain P number of d dimensional embeddings. Similar to the summation in CBOW [95], we do an element-wise summation to get the representation of all categorical features. Suppose the new representation for categorical features is $g(\mathbf{x}^C)$. Then we have

$$g(\mathbf{x}^C) = \sum_{j=1}^{P} \mathbf{u}_{q(j)} \tag{4.2}$$

This new representation would then be fed into the next layer in the neural networks, and all the embeddings are learned through back propagation.

4.2.2 Remaining layers

After obtaining the embedding for categorical features $g(\mathbf{x}^C)$, CENN concatenates $g(\mathbf{x}^C)$ and the original numerical features $\mathbf{x}^R$ to form a new representation for the original input $\mathbf{x}$. Suppose $\mathbf{h}^\ell$ is the vector of hidden units in the layer ℓ. The first hidden layer $\mathbf{h}^1 = \big(g(\mathbf{x}^C), \mathbf{x}^R\big)$. For the following layers, we have

$$\mathbf{h}^{\ell+1} = \sigma(\mathbb{W}^\ell \mathbf{h}^\ell + \mathbf{b}^\ell) \tag{4.3}$$

where $\mathbb{W}^\ell$ and $\mathbf{b}^\ell$ are the weight matrix and the bias vector for layer ℓ, respectively. σ is an activation function to make each layer a non-linear transformation. Possible activation functions include rectifier linear units (ReLU) [51], sigmoid or tanh function. Note that Figure 4.1 only shows two hidden layers for ease of illustration. However, one can use as many hidden layers as necessary. For classification tasks, the final output layer is a softmax function which estimates the probability of the given input belonging to each class. Thus,

we have that

$$o_k = \frac{e^{\langle \mathbf{w}_k^L, \mathbf{h}^L \rangle + b_k^L}}{\sum_j e^{\langle \mathbf{w}_j^L, \mathbf{h}^L \rangle + b_j^L}} \tag{4.4}$$

where o_k is the probability of class k and L is the number of hidden layers.

4.2.3 Training

The objective is to maximize the log likelihood of the dataset as follows:

$$\underset{\mathbb{W}^\ell, \mathbf{b}^\ell, \mathbb{U}}{\text{maximize}} \sum_{i=1}^{N} \log o_{y_i}^{(i)} \tag{4.5}$$

where $o_{y_i}^{(i)}$ denotes the y_i^{th} output of instance i through the neural network, which is the probability of its true label. All the parameters including the categorical embedding matrix $\mathbb{U}$ as well as the weights and biases of each hidden layer are *learned jointly* by back-propagation [118, 95, 96]. For efficient update, mini-batch gradient descent with momentum is adopted. Regularization techniques including dropout [133] and L2 regularization are also applied to improve the generalization ability of the network.

4.2.4 Visualization

Once CENN is trained, we are able to visualize the embedding of each category of each categorical feature, which allows us to visually observe the relation between categories. For example, if the task is to predict the income of a person based on his/her gender, country and degree, we can plot the embeddings stored in the lookup table. If country A is close to country B in the embedding space, these two countries might have similar characteristic

with respect to income. This visual information is important to interpret the model and provides valuable insights. In addition, it is different from traditional visualization scenarios where the visualized objects are instances rather than features in our case.

A naïve way to visualize the embeddings in the lookup table is to set the dimensionality of embeddings to two or three. Once the training is done, we can directly plot the embedding in a 2-D or 3-D space. Another way is to keep the dimensionality as is, which may be high-dimensional. Then we can use off-the-shelf visualization methods such as *t-SNE* [138] for the plot.

4.3 Discussion

We discuss some appealing properties of CENN in this section.

4.3.1 Compressing one-hot encoding

One-hot encoding is the most popular way to convert a categorical feature to a numerical one. The new representation is a vector with one element being one and all others being zero. For example, a feature with three categories (*e.g.* red, blue and green) would be encoded as $(1, 0, 0)$, $(0, 1, 0)$ and $(0, 0, 1)$. We show that the embeddings in CENN is a matrix factorization of the weight matrix associated with one-hot encoding. For ease of explanation, let's assume there is no numerical features. The proof and conclusion still apply in the presence of numerical features.

Let $\mathbf{h}$ be the vector of units in the hidden layer right after the lookup table and before the activation function, and there are m hidden units in that layer. We use *NN-onehot* to denote the neural network applying one-hot encoding to transform categorical features, where the first hidden layer still contains m hidden units. In NN-onehot, Let $\mathbb{V} \in \mathcal{R}^{m \times K}$ be the weight matrix of the first layer where K is the total number of categories of all features. Note that K is also the length of the feature vector after one-hot encoding. In CENN, let $\mathbb{U} \in \mathcal{R}^{d \times K}$ and $\mathbb{W} \in \mathcal{R}^{m \times d}$ be the embedding matrix and weight matrix as shown in Figure 4.1 (assuming there is no numerical feature). Similar to [39], CENN is a direct application of matrix decomposition on the first layer of NN-onehot.

Theorem 1 *The category embeddings and their associated weight matrix in CENN is a low-rank matrix decomposition of the weight matrix in NN-onehot,* i.e. $\mathbb{V} = \mathbb{W}\mathbb{U}$.

The proof is quite straightforward. Suppose $\mathbf{r} \in \mathcal{R}^{K}$ is the numerical vector converted from $\mathbf{x}^{C}$ with one-hot encoding scheme. Note that the indexing scheme in Eq. (4.1) is consistent with the one-hot encoding. Hence, $r_{j} = 1$ when $j \in \{q(p)|p = 1, \cdots, P\}$, and $r_{j} = 0$ otherwise. In NN-onehot, the hidden layer before activation is a linear transformation of $\mathbf{r}$ as $\mathbf{h} = \mathbb{V}\mathbf{r}$. If we decompose $\mathbb{V}$ into $\mathbb{W}$ and $\mathbb{U}$, we have $\mathbf{h} = \mathbb{W}\mathbb{U}\mathbf{r}$. For CENN, $\mathbb{U}$ is the embedding matrix, and we can see that the representation for categorical features in CENN is $g(\mathbf{x}^{C}) = \sum_{j=1}^{P} \mathbf{u}_{q(j)} = \mathbb{U}\mathbf{r}$ according to Eq. (4.2). We illustrate this equation in Figure 4.2 which is consistent with the example in Figure 4.1. Therefore, in CENN we have $\mathbf{h} = \mathbb{W}g(\mathbf{x}^{C}) = \mathbb{W}\mathbb{U}\mathbf{r}$, which is equivalent to NN-onehot.

With Theorem 1, one can always convert NN-onehot to CENN by having an intermediate hidden layer (between the input layer and the first hidden layer) that contains d number of hidden units without activation function, where the weight matrix between the input and

100
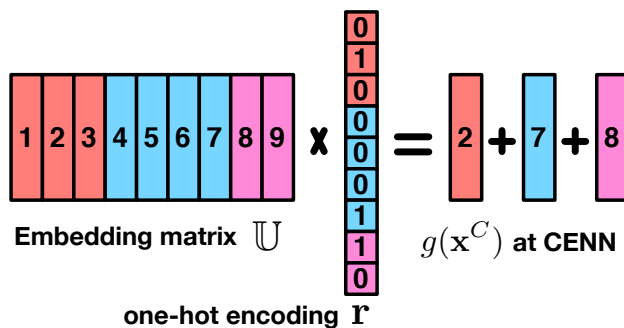
Figure 4.2: One-hot encoding, mathematically $\mathbb{U}\mathbf{r}$, is equivalent to the transformation performed in CENN that retrieves embeddings and does element-wise sum.

intermediate layer is $\mathbb{U}$, and the weight matrix between the intermediate and the first hidden layer is $\mathbb{W}$ [39].

Moreover, we have the following remarks about the comparison between CENN and one-hot encoding:

- CENN is compact and exploits the low-rank structure of one-hot encoding in neural networks thanks to matrix decomposition [39]. The memory footprint of the weight matrix in one-hot encoding is mK, while CENN takes Kd for the lookup table and md for the weight matrix, leading to $d(K+m)$ footprint in total. Depending on tasks, both K and m could be extremely large. For example, for industrial advertisement prediction, the total number of categories could be at the scale of millions [92, 60]. With CENN, one can smoothly control the memory footprint by adjusting d, the dimensionality of embeddings.

- With a more compact model, CENN does not necessarily lose generalization ability compared with one-hot encoding. As demonstrated in Chapter 3, there has been a general consensus that neural networks have certain degree of redundancy [26, 39, 64, 57, 27]. Denil *et al.* [39] show that matrix decomposition, which is what categorical

101

embedding in CENN is reduced to according to Theorem 1, can effectively preserve the accuracy performance while reducing the size of a neural network.

From the discussion above, we can see that CENN can achieve superior tradeoff between model size, efficiency and generalization ability, and adjust it by simply adjusting the dimensionality of embeddings.

4.3.2   Feature hashing for CENN

Typically, one-hot encoding results in high-dimensional sparse vectors, and thus is often followed by feature hashing [148, 128, 36] as discussed in Chapter 3. Feature hashing has been previously studied as a technique for reducing model size and speeding up learning, and has been widely deployed in modern machine learning systems, such as *vowpal wabbit* [1]. In general, it can be regarded as a dimensionality reduction method which maps an input vector $\mathbf{x} \in \mathcal{R}^K$ to a much smaller feature space via a mapping $\phi \colon \mathcal{R}^K \to \mathcal{R}^D$ where $D \ll K$. The mapping function ϕ consists of two approximately uniform auxiliary hash functions $h \colon \mathcal{N} \to \{1, \ldots, D\}$ and $\xi \colon \mathcal{N} \to \{-1, +1\}$. The jth element of the D-dimensional hashed input is defined as

$$\phi_j(\mathbf{x}) = \sum_{i:h(i)=j} \xi(i)\ x_i. \tag{4.6}$$

The dimensionality reduction comes at a price of collisions incurred by hashing, where multiple features are mapped into the same dimension. This problem is less severe for sparse data sets, which is why feature hashing is a good fit for one-hot encoding.

We now show CENN can readily incorporate feature hashing. Let $\mathbf{r}$ still be the one-hot encoded feature vector. After feature hashing, the ith element of the hashed vectors is

$$\phi_i(\mathbf{r}) = \sum_{j:h(j)=i}^{K} \xi(j)r_j = \sum_{p:h(q(p))=i}^{P} \xi(j) \tag{4.7}$$

where the first equality is a rewrite of Eq. (4.6), and the second equality holds because $r_j = 1$ only when $j \in \{q(p)|p = 1, \cdots, P\}$ and $r_j = 0$ otherwise. The hidden layer is still a linear transformation of hashed input:

$$\mathbf{h} = \mathbb{V}_h\phi(\mathbf{r}) \tag{4.8}$$

where $\mathbb{V}_h \in \mathcal{R}^{m \times D}$ is the weight matrix.

CENN can be extended to incorporate feature hashing by simply making the indexing function in Eq. (4.1) a hash function. To avoid confusion, we use q_h as the new indexing function, and q still keeps its definition in Eq. (4.1). As stated in Theorem 1, we can decompose $\mathbb{V}_h = \mathbb{W}\mathbb{U}_h$ where $\mathbb{W} \in \mathcal{R}^{m \times d}$ is still the weight matrix in CENN and $\mathbb{U}_h \in \mathcal{R}^{d \times D}$ is the new lookup table with D number of d-dimensional embeddings. Following Eq. (4.8), we have that $\mathbf{h} = \mathbb{W}\mathbb{U}_h\phi(\mathbf{r})$. Let the new representation after lookup table be $g_h(\mathbf{x}^C) = \mathbb{U}_h\phi(\mathbf{r})$, we have that

$$g_h(\mathbf{x}^C) = \mathbb{U}_h\phi(\mathbf{r}) = \sum_{p=1}^{P} \xi(q(p))\mathbf{u}_{h(q(p))} \tag{4.9}$$

$$= \sum_{p=1}^{P} \xi_h(p)\mathbf{u}_{q_h(p)} \tag{4.10}$$

where $q_h(\cdot) = h(q(\cdot))$ and $\xi_h(\cdot) = \xi(q(\cdot))$ are the hash functions for CENN.

In summary, CENN can seamlessly incorporate feature hashing by the following three steps:

103

- Change the number of embeddings in lookup table from K to D.

- Change the indexing function of lookup table from q to q_h.

- After the embeddings are retrieved, do element-wise summation up to a sign factor ξ_h according to Eq. (4.10).

With feature hashing, different categories share the same embedding when they are mapped to the same bucket by the hash function, which further reduces the size of the lookup table.

4.3.3 Dimensionality of embeddings

The dimensionality of the embeddings d in the lookup table is an important factor in CENN. As discussed in Section 4.3.1, d is a tradeoff between model size, efficiency and the representation power of CENN. Here, one reluctant assumption CENN makes is that all embeddings share the same dimensionality, which may not be realistic for some tasks and does not accurately reflect each category's representation complexity. For example, a feature with 100 categories may need a larger d to capture all information than one with only 3 categories. One way to address this problem is to group features of similar number of categories and have a separate lookup table for each group. Then we can independently adjust the dimensionality of each lookup table. However, this might introduce a lot of ad-hoc work for each task as well as overhead of keeping multiple lookup tables. Besides, for some tasks, the vast majority of categories are rarely used [92]. A feature with many categories may not deserve a higher dimensional lookup table. Feature hashing described in Section 4.3.2 may alleviate this problem by sharing embedding between frequent categories and rare categories. Another interesting idea is to have variable-length embedding for each category, which was recently

introduced by [101]. It introduces a latent variable z for each embedding that represents the dimensionality which is learned jointly with the embedding. This would allow the data to speak for themselves and automatically determine the dimensionality of the embedding of each category.

4.3.4   Relation to factorization machines

Factorization machine (FM) [112, 113] is a general approach to model the interaction between categorical features, and has been used in many applications such as recommender systems [115]. The model prediction, given a feature vector, is defined as

$$\hat{y}(\mathbf{r}) = w_0 + \sum_{i=1}^{n} w_i r_i + \sum_{i=1}^{n} \sum_{j=i+1}^{n} \langle \mathbf{v}_i, \mathbf{v}_j \rangle r_i r_j \tag{4.11}$$

where $\mathbf{r}$ is a sparse high-dimensional feature vector generated by one-hot encoding, feature engineering or discretization of numerica features. Usually, the value of each element of $\mathbf{r}$ is either 0 or 1. Like CENN, FM also learns an embedding for each category (v_i in Eq. (4.11)) and captures the interaction between two categories by the inner product of their embeddings.

CENN and FM are fundamentally different in the following three aspects.

- FM is a second-order function over the input $\mathbf{r}$ while CENN is a highly nonlinear function with respect to $\mathbf{r}$ depending on the activation functions and the number of layers in the neural network.

- FM models interaction by the inner product of embeddings. In contrast, CENN models the interaction leveraging the nonlinearity of neural networks. Further, CENN can also directly model the interaction by learning embeddings for *cross features*. Suppose two

features have category sets A and B, respectively. We can create a new feature whose value is the Cartesian product of these two features, *i.e.* $A \times B$. The embedding learned for categories in the cross feature directly models the interaction between these two features.

- FM cannot naturally handle multi-label classification as it only learns a single score function. Current off-the-shelf packages [113] do not support multi-label classification either. In contrast, CENN can naturally do multi-class classification with a softmax output. Moreover, CENN does not require ad-hoc implementation because all of its building blocks have been implemented by current deep learning packages, such as *Torch*, *Theano* and etc. With these packages, it is also very easy to incorporate state-of-the-art training techniques such as dropout [133] and Adagrad [43] in CENN with only a few lines of code.

4.4   Related work

The CENN architecture is inspired by embedding-based modeling, especially the distributed word representation for natural language processing (NLP) [5, 95, 96, 94, 21]. The goal of language modeling is to estimate the probability of generating a particular sentence. With the Markovian assumption, the probability of a word only hinges on its context, which can be computed by the *n-gram* counting-based model [18]. However, its model complexity increases dramatically as n gets large. To overcome this problem, Bengio *et al.* [5] proposed to learn a representation for each word. The neural network can take the embedding of each word in the context as input and make the prediction. Its biggest difference compared with CENN is that it enforces different positions of the context to have exactly the same word

set, meaning that the same word embedding coud appear everywhere associated with the input. In contrast, in CENN, different features possess different category sets which is more suitable for traditional data mining tasks.

In addition to NLP, embedding-based methods also widely exist in recommender systems to model pair-wise relationship. Lots of recommender systems are based on the classic user-item patterns (*e.g.* user-movie, user-ads and image-tag) where the task is to estimate the similarity score between users and items. It can be regarded as a classification/regression problem with two categorical features: user ID and item ID. Each category of user ID and item ID would be assigned an embedding, and their similarity is mostly modeled by the inner product of their embeddings. A majority of collaborative filtering models fall into this category, such as *Wsabie* [149] and *SVD++* [69]. Further, tensor decomposition [114] and factorization machines [112] are able to model the pair-wise interactions between more categorical variables, and take side information into account with careful feature design.

CENN handles numerical and categorical features naturally which is vital to a wide range of data mining tasks. In order to do this, CENN has two input branches dealing with numerical and categorical features, respectively, each of which is independent from the other. This is different than the *siamese network* [13, 28] where two branches share the same parameters. In the literature, lots of traditional machine learning models require the input to be numerical, such as SVM, logistic regression and vanilla neural networks, which all require a preprocessing step to convert categorical features to numerical features, such as one-hot encoding [144]. Besides one-hot encoding, another transformation approach is mapping a category to the conditional probability of a particular label given the category [24, 22, 62, 61].

Like CENN, tree-based methods are also able to handle both numerical and categorical features. In particular, tree ensembles such as random forest [12], gradient boosting trees [45]

and adaboost [44] are usually preferred to alleviate potential issues of high bias or high variance [58] introduced by a single tree. Recently He *et al.* introduces a machine learning model [60] used by ads prediction at Facebook which combines a tree ensemble model with the one-hot encoding. The basic idea is to first convert the input to a new categorical feature vector using gradient boosting trees, and then use one-hot encoding to convert the categorical feature vector back to a numerical feature vector and use logistic regression as the final predictor. In contrast to the typical feature binning methods which partition the space into equal-size grid, boosting trees are able to take the supervised label information into account when partitioning the space, leading to better categorical features. This category generating technique could be well suited for CENN as CENN is good at handling categorical features.

As discussed in Section 4.3.1, CENN is essentially a compressed version of one-hot encoding, leading to a more compact model with less overfitting. In Chapter 3, we have surveyed several methods that try to attack the redundancy issue of neural nets. Denil *et al.* [39] re-parameterize the weight matrix as the product of two smaller matrices, resulting in less parameters as well as faster training and testing. CENN enjoys all its advantages since CENN also utilizes the same matrix decomposition technique. Similar observation have been made in the context of word embedding with the skip-gram model with negative-sampling (SGNS). Specifically, SGNS is implicitly factorizing a word-context matrix where each element is the point-wise mutual information of corresponding word and context [83]. Li *et al.* [84] further strengthen the statement that SGNS is an explicit matrix factorization of the word co-occurrence matrix.

Table 4.1: Test errors of various methods on various UCI datasets (in %).

Dataset	N	P	C	Linear	SVM-rbf	RF	GBT	CENN
Agaricus	8,124	22	2	0.00	0.00	0.00	0.00	0.00
Nursery	12,960	8	5	7.18	**0.05**	1.05	**0.05**	**0.05**
Bank	45,211	16	2	10.30	10.77	9.81	9.53	**9.07**
Adult	45,222	14	2	15.98	16.95	15.01	14.87	**14.48**
Connect-4	67,557	42	3	24.12	14.55	17.30	15.20	**14.33**
Census-income	299,285	41	2	5.00	5.18	**4.45**	4.60	4.51
Poker-hand	1,025,010	10	10	50.63	3.84	8.95	6.72	**0.86**

4.5 Experimental results

We conduct extensive experiments to evaluate CENN on several benchmark datasets. We first test CENN on categorical and mixed-type UCI datasets[14] to show CENN is capable of achieving state-of-the-art performance. Then we demonstrate the superior performance and convenience of classifying a large-scale dataset with a huge amount of categories in which one-hot encoding results in gigantic feature vectors and weight matrices making it prohibitively expensive. All the tested datasets are publicly available.

4.5.1 Experimental settings

We compare CENN with several mainstream classifiers [58]. The followings are the implementation details:

- Linear classifiers. In particular, we use logistic regression and softmax regression for binary and multinomial classification, respectively, which are both implemented with the *scikit-learn* package [106]. $\ell 2$ regularization is applied to prevent overfitting.

---

[14]https://archive.ics.uci.edu/ml/datasets.html

- Support vector machines with RBF kernels (SVM-rbf) implemented by *libSVM* [16]. Its hyperparameters include kernel bandwidth and $\ell 2$ regularization. In order for SVM-rbf to run as fast as possible, we set the cache size of LibSVM to $10GB$ which is sufficiently large for all the tested datasets.

- Random forest (RF). We adopt the implementation in the *scikit-learn* package [106]. The number of trees and the maximum depth of each tree are tuned via the validation set.

- Gradient boosting trees (GBT). We adopt the *xgboost* package [19] which is currently the state-of-the-art software for GBT. Early stopping is applied to prevent overfitting. In particular, if the validation error does not get reduced for 100 rounds, GBT would stop and the number of boosted trees would be the one that achieves the best validation error. The maximum number of trees is set to 3000. The shrinkage factor and the maximum depth of its tree is tuned via the validation set.

- CENN is implemented based on the *Torch7* package [33] and runs on GPUs (NVIDA GTX TITAN graphics cards). Models are trained via stochastic gradient descent. For UCI datasets, a small batch size such as 5 is used for computing the gradient. Momentum is always fixed at 0.5. The number of hidden units is 1000 for each hidden layer. All other hyperparameters are tuned including the initial learning rate, decay factor of learning rate, number of hidden layers, embedding size for CENN, dropout and $\ell 2$ regularization. Like GBT, early stopping is used to prevent overfitting. We use rectifier linear units for all activation functions. In the experiments, we do not show the result of standard neural network with one-hot encoding (NN-onehot), because CENN is equivalent to NN-onehot with an intermediate layer that contains d number

of hidden units where d is the dimensionality of the embeddings, as discussed in the Section 4.3.

The experiments are run on an off-the-shelve desktop with two 8-core Intel(R) Xeon(R) processors of 2.67 GHz and $128GB$ RAM. For datasets in which the test set is not specified, we split the dataset and use 2/3 for training and 1/3 for testing. We further hold out 1/3 from the training set as the validation set. All algorithms are trained on the training set, choosing hyperparameters based on the validation set and evaluated on the test set. All our reported results are based on the test error performance. Hyperparameters are selected for all algorithms with Bayesian optimization [132], implemented in the *spearmint*[15] package.

4.5.2   Evaluation on UCI datasets

We evaluate the performance of CENN on several UCI benchmark datasets as shown in Table 4.1. We show the dataset statistics on the left part of the table and the test error performance on the right part. Here, N, P and C stands for the number of instances, the number of features and the number of classes in each dataset, respectively. The datasets are ordered by N. We try to include datasets of different types, ranging from "easy" datasets that can be perfectly classified such as Agaricus to "hard" ones for which linear models are merely as good as random guess such as Poker-hand. Among all these datasets, Bank, Adult and Census datasets contain both categorical feature and numerical features, while the other datasets are all categorical datasets. We choose datasets with many categorical features since they are the focus of CENN. From Table 4.1, we make the following observations. First, linear classifiers perform the worst in most cases, especially on categorical datasets. Second,

---

[15]`https://github.com/JasperSnoek/spearmint`

Table 4.2: An description of the triptype dataset

Feature Name	#categories
VisitNumber	95,674
Weekday	7
UPC	97,715
ScanCount	39
Department Description	68
FinelineNumber	5,196

CENN is always the best or second best performer on all datasets, which demonstrates its effectiveness. In particular, on the Poker-hand dataset, CENN outperforms all other classifiers by a large margin.

4.5.3 Classification with many categories

We evaluate CENN on triptype[16], a large-scale real-world dataset with many categories, to showcase the distinctive advantages of CENN. This dataset is a transactional dataset of items purchased at Walmart. The goal of the task is to predict the type of each customer trip, which would help Walmart's decision making in business and improve customers' shopping experiences. There are in total 38 types/labels. For example, a customer may make a small daily dinner trip, a weekly large grocery trip, and so on. This dataset contains $647,054$ instances, each of which contains 6 categorical features[17].

The difficulty of mining this dataset lies in the huge amount of categories as shown in Table 4.2. There are in total $198,700$ distinct categories, leading to a $198,700$-dimensional

---

[16]https://www.kaggle.com/c/walmart-recruiting-trip-type
-classification

[17]Note that only the training set is available online. Therefore we randomly choose 1/3 of the dataset as the test set and the remaining 1/3 as the training set.

Table 4.3: Test error performance on the triptype dataset (in %).

Dataset	SFT	GBT	CENN
Triptype	28.39	24.97	**4.91**
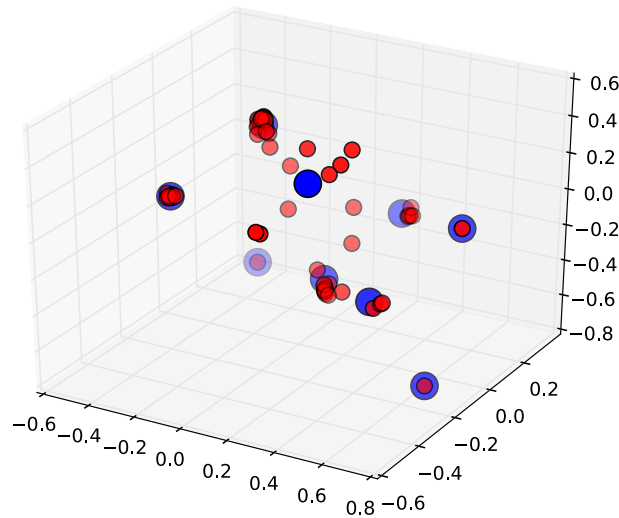
Figure 4.3: The embeddings for the "Department Description" feature

feature vector if one-hot encoding is used. For standard neural networks with one-hot encoding, there are two dilemmas. First, most existing deep learning softwares including Torch7 and Theano have no support for sparse matrix multiplication on GPUs. Second, even if GPU implementations for sparse matrices become available, the one-hot encoding still results in a large weight matrix in the first hidden layer. For example, suppose there are 1000 hidden units in the first hidden layer, the size of the weight matrix would be $198,700 \times 1000$, which is prohibitively expensive for GPU memory. Factorization machines (FM) is a good fit for such highly sparse data. However, FM is not capable of handling multinomial classification [113], and therefore cannot be easily applied to this dataset.

Table 4.4: Results of k-means clustering on the learned embeddings in CENN.

Cluster	Names of the categories
1	shoes, boys wear, jewelry and sunglasses, mens wear, accessories, infant consumable hardlines, ladieswear, sheer hosiery, wireless, infant apparel, ladies socks, plus and maternity, electronics, girls wear, 4-6x and 7-14, bras & shapewear, sleepwear/foundations, cameras and supplies, players and electronics, menswear, swimwear/outerwear, media and gaming, 1-hr photo, health and beauty aids
2	paint and accessories, impulse merchandise, candy, tobacco, cookies, home management, cook and dine, hardware, bedding, bath and shower, home decor, liquor,wine,beer, other departments, furniture, seasonal, large household goods
3	meat - fresh & frozen, dairy, pets and supplies, produce, grocery dry goods, frozen foods, service deli, pre packed deli, comm bread, bakery, seafood
4	fabrics and crafts, celebration, books and magazines, office supplies, toys, sporting goods, concept stores
5	household chemicals/supp, pharmacy otc, household paper goods, pharmacy rx, optical - frames, optical - lenses
6	automotive, lawn and garden, horticulture and access
7	personal care, beauty
8	dsd grocery
9	financial services

We only show the results of softmax regression, GBT[18] and CENN, since RF, SVM-rbf are too slow to achieve any meaningful results on this dataset even with state-of-the-art packages. For CENN, we adopt a deep structure with four hidden layers each of which contains 1000 hidden units. We intentionally use the raw feature without any complicated feature engineering, as that would introduce a number of additional factors which we want to disambiguate as alternative factors for success. We show the test error performance of each method on Table 4.3. We can clearly see that CENN outperforms other classifiers by

---

[18]We found GBT tends to underfit this dataset due to the huge amount of categories. In order for GBT to perform well, we use $10,000$ boosted trees and set the depth of each tree to 15, whose entire training process costs around 22 hours with 12 CPU cores. The early stop is triggered at the 9092nd tree.

a huge margin, which with no doubt demonstrates the great advantage of using CENN on datasets with many categories.

Regarding the good performance on this dataset, should we give credits to features with many categories, including VisitNumber, UPC and FinelineNumber? As a sanity check, we apply softmax regression on this dataset without these three features and get 64.95% test error. The presence of FinelineNumber help softmax regression reduce the test error to 63.72%. Likewise, CENN gets 63.22% test error with these three features removed. However, softmax and $CENN$ obtain 28.39% and 4.91% test errors, respectively, with the full dataset as we can see from Table 4.3. This analysis strongly indicates the importance of VisitNumber and UPC.

4.5.4 Visualization

We demonstrate the visualization ability of CENN on the triptype dataset and show that the learned embeddings are surprisingly appealing according to the clustering result. We set the embedding dimensionality to 3 and train CENN from scratch, which obtains 7.99% test error at the end. Next, we plot the categories using their embeddings as coordinates. Due to space limit and the fact that the "Department Description" is the only feature whose semantic meaning of each category is released, we only present the visualization of this feature which contains 68 categories as shown in Figure 4.3. From this figure in which each red point corresponds to a category, we can observe that there are some clustering structures. Therefore, we use *kmeans* to cluster all these 68 categories into 9 clusters where the similarity is measured by the Euclidean distance between their three-dimensional embeddings. The clustering centers are visualized as blue points in Figure 4.3. In addition, we

show the clustering results along with the semantic meaning of categories in each cluster in Table 4.4 ordered by cluster size. The clustering structure is surprisingly meaningful. For example, most categories in the 1st cluster are related to apparel; the 2nd cluster is related to household goods; the 3rd cluster is all about food; the 5th cluster is about family healthcare; the 6th cluster is related to horticulture. These results strongly indicate that CENN learns meaningful embeddings, which helps extract knowledge from data and improve interpretability of the model.

Importantly, this cannot be done with other classifiers as well as traditional visualization or clustering techniques. In CENN, each visualized point is a category of a categorical feature rather than a data instance. These cannot be visualized by unsupervised embedding models such as *tSNE* since similarity between categories is not well defined without supervision. Even with supervision information, traditional embedding models such as metric learning algorithms are only capable of learning a metric on data instances rather than categories. In contrast, CENN learns an embedding for each category from which we can get a clear picture of category similarities as shown in Table 4.4.

4.6 Conclusions

Neural networks are very powerful, beating other classifiers when trained properly. But they are not widely used for many data mining tasks due to its difficulty in handling categorical features with many categories as well as lack of interpretability. We have advocated the use of category embedding for data mining tasks. It offers enormous advantages for jointly handling large-scale mixed-type data as well as providing supervised visualization and knowledge extraction, which most mainstream classifiers do not offer. The category embeddings can

be regarded as a matrix decomposition of the weight matrix of a standard neural network with the classic one-hot encoding. We have also discussed the extension for incorporating feature hashing, which promotes embedding sharing among different categories. We have conducted comprehensive experiments to evaluate the empirical performance. Neural nets with category embedding not only achieves state-of-the-art performance on UCI datasets, but also beats all other classifiers by a large margin on a large-scale real-world dataset that contains a huge amount of categories. More importantly, the visualization and clustering of the learned embeddings uncover clear and reliable semantic meanings, as similar categories are mapped to nearby regions in the embedding space. In the future, we will explore these semantic clustering for enhancing the interpretability of data mining.

Chapter 5

Conclusions

Machine learning keeps setting new records in various applications, accompanied by ever-increasing model size. We identify that models with large memory consumption lie in two areas: memory-based learning and deep learning.

For memory-based learning, we have focused on one of its most promising applications—learning Euclidean heuristic with graph embedding, which is an effective method for compressing pair-wise distance matrix. However, training the underlying MVU embeddings are slow, dramatically limiting its usage. To address this efficiency issue, we have proposed maximum variance correction (MVC) that scales up MVU training by several order of magnitude, from 4000 states to $200,000$ states. Different than other large-scale graph embedding algorithms ($e.g$ gl-MVU [147, 150]), MVC preserves the local distance constraints without which the resulting heuristics are not able to find the optimal search path in the graph. Moreover, We propose the goal-oriented Euclidean heuristic (GOEH) to improve the search quality by better exploiting the prior knowledge of the goal sets.

For deep learning, we have proposed HashedNets, an approach to randomly grouping parameters within neural network using a low-cost hashing function. In particular, parameters

within the same group share the same magnitude up to a sign factor. Plus, HashedNets are general and modular, complementary to other compressing techniques such as Dark Knowledge [64]. We have demonstrated HashedNets achieve much better accuracy performance than other baselines such as low-rank decomposition [39]. Though the hashing trick could also be directly applied to convolutional layers, it does not leverage the distinct feature of the convolutional filters—local smoothness. To address this problem, we further propose Frequency-Sensitive HashedNets (FreshNets) that compresses parameters in the frequency domain of the convolutional filters. In particular, we compress more on high-frequency domain, which are less important due to the property of local smoothness. Our empirical results show that FreshNets obtains superior performance and outperforms a number of baseline methods such as HashedNets, especially when the compression rate is large.

Combining deep learning and embedding, we further propose neural networks with categorical feature embedding (CENN) with focus on traditional data mining tasks. We show that the traditional one-hot encoding results into great memory consumption in the presence of a huge amount of categories. For example, if there are 10 categorical features each of which contains $100,000$ categories, the converted feature vector after one-hot encoding would be a $1,000,000$-dimensional sparse vector. If there are $1,000$ hidden neurons in the first layer, the one-hot encoding would lead to a weight matrix of size $1,000,000 \times 1,000$ in the first layer, which is prohibitively expensive for the GPU memory. CENN addresses this problem by learning a d-dimensional embedding for each category to form a new numerical representation for the neural network where d is a hyper-parameter. In the previous example, the memory cost of CENN is $1,000,000 \times d + 1,000 \times d$, which is a great memory saving. We further demonstrate that CENN is equivalent to a low-rank decomposition [39] of the one-hot encoding. CENN not only achieves state-of-the-art performance on several benchmark datasets, but also provides visualization and interpretability on the category similarity.

119

We believe the scalability and compactness of machine learning models will become increasingly important in the future, in part because of the trend of applications shifting towards mobile and embedded devices. As future work we plan to further investigate model compression for neural networks. One particular direction of interest is to optimize HashedNets for GPUs. GPUs are very fast (through parallel processing) but usually feature small on-board memory [87]. We plan to investigate how to use HashedNets to fit larger networks onto the finite memory of GPUs. A specific challenge in this scenario is to avoid non-coalesced memory accesses due to the pseudo-random hash functions—a sensitive issue for GPU architectures.

References

[1] Alekh Agarwal, Olivier Chapelle, Miroslav Dudík, and John Langford. A reliable effective terascale linear learning system. *The Journal of Machine Learning Research*, 15(1):1111–1133, 2014.

[2] Robert Andrews, Joachim Diederich, and Alan B Tickle. Survey and critique of techniques for extracting rules from trained artificial neural networks. *Knowledge-based systems*, 8(6):373–389, 1995.

[3] Jimmy Ba and Rich Caruana. Do deep nets really need to be deep? In *NIPS*, pages 2654–2662, 2014.

[4] M. Belkin and P. Niyogi. Laplacian eigenmaps for dimensionality reduction and data representation. *Neural Computation*, 15:1373–1396, 2002.

[5] Yoshua Bengio, Réjean Ducharme, Pascal Vincent, and Christian Janvin. A neural probabilistic language model. *The Journal of Machine Learning Research*, 3:1137–1155, 2003.

[6] Christopher M. Bishop. *Neural Networks for Pattern Recognition*. Oxford University Press, Inc., 1995.

[7] P. Biswas and Y. Ye. Semidefinite programming for ad hoc wireless sensor network localization. In *Proceedings of the 3rd international symposium on Information processing in sensor networks*, IPSN '04, pages 46–54, New York, NY, USA, 2004. ACM. ISBN 1-58113-846-6.

[8] J. Blitzer, K.Q. Weinberger, L. K. Saul, and F. C. N. Pereira. Hierarchical distributed representations for statistical language modeling. In *Advances in Neural and Information Processing Systems*, volume 17, Cambridge, MA, 2005. MIT Press.

[9] B. Borchers. Csdp, ac library for semidefinite programming. *Optimization Methods and Software*, 11(1-4):613–623, 1999.

[10] Y-lan Boureau, Yann L Cun, et al. Sparse feature learning for deep belief networks. In *NIPS*, pages 1185–1192, 2008.

[11] S. Boyd and L. Vandenberghe. *Convex Optimization*. Cambridge University Press, New York, NY, USA, 2004. ISBN 0521833787.

[12] L. Breiman. Random forests. *Machine Learning*, 45(1):5–32, 2001.

[13] Jane Bromley, James W Bentz, Léon Bottou, Isabelle Guyon, Yann LeCun, Cliff Moore, Eduard Säckinger, and Roopak Shah. Signature verification using a siamese time delay neural network. *International Journal of Pattern Recognition and Artificial Intelligence*, 7(04):669–688, 1993.

[14] T Brosch and R Tam. Efficient training of convolutional deep belief networks in the frequency domain for application to high-resolution 2d and 3d images. *Neural Computation*, 27(1):211–227, 2015.

[15] Cristian Bucilua, Rich Caruana, and Alexandru Niculescu-Mizil. Model compression. In *KDD*, 2006.

[16] Chih-Chung Chang and Chih-Jen Lin. LIBSVM: A library for support vector machines. *ACM Transactions on Intelligent Systems and Technology*, 2:27:1–27:27, 2011.

[17] Minmin Chen, Kilian Q. Weinberger, Fei Sha, and Yoshua Bengio. Marginalized denoising auto-encoders for nonlinear representations. In *ICML*, pages 1476–1484, 2014.

[18] Stanley F Chen and Joshua Goodman. An empirical study of smoothing techniques for language modeling. *Computer Speech & Language*, 13(4):359–393, 1999.

[19] Tianqi Chen and Carlos Guestrin. Xgboost: Reliable large-scale tree boosting system.

[20] W. Chen, K. Weinberger, and Y. Chen. Maximum variance correction with application to A^* search. In *Proc. ICML*, 2013.

[21] Welin Chen, David Grangier, and Michael Auli. Strategies for training large vocabulary neural language models. *arXiv preprint arXiv:1512.04906*, 2015.

[22] Wenlin Chen, Yixin Chen, Yi Mao, and Baolong Guo. Density-based logistic regression. In *KDD*, 2013.

[23] Wenlin Chen, Yixin Chen, Kilian Q Weinberger, Qiang Lu, and Xiaoping Chen. Goal-oriented euclidean heuristics with manifold learning. In *AAAI*, 2013.

[24] Wenlin Chen, Yixin Chen, and Kilian Q Weinberger. Fast flux discriminant for large-scale sparse nonlinear classification. In *KDD*, 2014.

[25] Wenlin Chen, Yixin Chen, and Kilian Q Weinberger. Filtered search for submodular maximization with controllable approximation bounds. In *AISTATS*, 2015.

[26] Wenlin Chen, James T Wilson, Stephen Tyree, Kilian Q Weinberger, and Yixin Chen. Compressing neural networks with the hashing trick. In *ICML*, 2015.

[27] Wenlin Chen, James T Wilson, Stephen Tyree, Kilian Q Weinberger, and Yixin Chen. Compressing convolutional neural networks. *arXiv preprint arXiv:1506.04449*, 2015.

[28] Sumit Chopra, Raia Hadsell, and Yann LeCun. Learning a similarity metric discriminatively, with application to face verification. In *CVPR*, 2005.

[29] Byung-Gon Chun and Petros Maniatis. Augmented smartphone applications through clone cloud execution. In *HotOS*, 2009.

[30] Dan C Cireşan, Ueli Meier, Jonathan Masci, Luca M Gambardella, and Jürgen Schmidhuber. High-performance neural networks for visual object classification. *arXiv preprint arXiv:1102.0183*, 2011.

[31] Adam Coates, Andrew Y Ng, and Honglak Lee. An analysis of single-layer networks in unsupervised feature learning. In *AISTATS*, 2011.

[32] Adam Coates, Brody Huval, Tao Wang, David Wu, Bryan Catanzaro, and Ng Andrew. Deep learning with cots hpc systems. In *Proceedings of The 30th International Conference on Machine Learning*, pages 1337–1345, 2013.

[33] Ronan Collobert, Koray Kavukcuoglu, and Clément Farabet. Torch7: A matlab-like environment for machine learning. In *BigLearn, NIPS Workshop*, 2011.

[34] M. Courbariaux, Y. Bengio, and J.-P. David. Low precision storage for deep learning. *arXiv preprint arXiv:1412.7024*, 2014.

[35] Zhicheng Cui, Wenlin Chen, Yujie He, and Yixin Chen. Optimal action extraction for random forests and boosted trees. In *Proceedings of the 21th ACM SIGKDD International Conference on Knowledge Discovery and Data Mining*, pages 179–188. ACM, 2015.

[36] Anirban Dasgupta, Ravi Kumar, and Tamás Sarlós. A sparse johnson: Lindenstrauss transform. In *Proceedings of the forty-second ACM symposium on Theory of computing*, pages 341–350. ACM, 2010.

[37] Yann N Dauphin, Razvan Pascanu, Caglar Gulcehre, Kyunghyun Cho, Surya Ganguli, and Yoshua Bengio. Identifying and attacking the saddle point problem in high-dimensional non-convex optimization. In *NIPS*, 2014.

[38] Jia Deng, Wei Dong, Richard Socher, Li-Jia Li, Kai Li, and Li Fei-Fei. Imagenet: A large-scale hierarchical image database. In *Computer Vision and Pattern Recognition, 2009. CVPR 2009. IEEE Conference on*, pages 248–255. IEEE, 2009.

[39] Misha Denil, Babak Shakibi, Laurent Dinh, Nando de Freitas, et al. Predicting parameters in deep learning. In *NIPS*, 2013.

[40] Emily L Denton, Wojciech Zaremba, Joan Bruna, Yann LeCun, and Rob Fergus. Exploiting linear structure within convolutional networks for efficient evaluation. In *Advances in Neural Information Processing Systems*, pages 1269–1277, 2014.

[41] Jeff Donahue, Yangqing Jia, Oriol Vinyals, Judy Hoffman, Ning Zhang, Eric Tzeng, and Trevor Darrell. Decaf: A deep convolutional activation feature for generic visual recognition. *arXiv preprint arXiv:1310.1531*, 2013.

[42] D.L. Donoho and C. Grimes. *When does isomap recover the natural parameterization of families of articulated images?* Department of Statistics, Stanford University, 2002.

[43] John Duchi, Elad Hazan, and Yoram Singer. Adaptive subgradient methods for online learning and stochastic optimization. *The Journal of Machine Learning Research*, 12: 2121–2159, 2011.

[44] Yoav Freund and Robert E Schapire. A decision-theoretic generalization of on-line learning and an application to boosting. *Journal of computer and system sciences*, 55 (1):119–139, 1997.

[45] Jerome H Friedman. Greedy function approximation: a gradient boosting machine. *Annals of statistics*, pages 1189–1232, 2001.

[46] Kunihiko Fukushima. Neocognitron: A self-organizing neural network model for a mechanism of pattern recognition unaffected by shift in position. *Biological cybernetics*, 36(4):193–202, 1980.

[47] Kuzman Ganchev and Mark Dredze. Small statistical models by random feature mixing. In *Workshop on Mobile NLP at ACL*, 2008.

[48] Jacob Gardner, Matt Kusner, Kilian Weinberger, John Cunningham, et al. Bayesian optimization with inequality constraints. In *ICML*, 2014.

[49] Rong Ge, Furong Huang, Chi Jin, and Yang Yuan. Escaping from saddle points—online stochastic gradient for tensor decomposition. *arXiv preprint arXiv:1503.02101*, 2015.

[50] Ross Girshick, Jeff Donahue, Trevor Darrell, and Jitendra Malik. Rich feature hierarchies for accurate object detection and semantic segmentation. In *CVPR*, 2014.

[51] Xavier Glorot, Antoine Bordes, and Yoshua Bengio. Deep sparse rectifier networks. In *AISTATS*, 2011.

[52] Xavier Glorot, Antoine Bordes, and Yoshua Bengio. Domain adaptation for large-scale sentiment classification: A deep learning approach. In *ICML*, pages 513–520, 2011.

[53] Yunchao Gong, Liu Liu, Ming Yang, and Lubomir Bourdev. Compressing deep convolutional networks using vector quantization. *arXiv preprint arXiv:1412.6115*, 2014.

[54] Alex Graves, A-R Mohamed, and Geoffrey Hinton. Speech recognition with deep recurrent neural networks. In *ICASSP*, 2013.

[55] N. Gupta and D.S. Nau. On the complexity of blocks-world planning. *Artificial Intelligence*, 56(2):223–254, 1992.

[56] Suyog Gupta, Ankur Agrawal, Kailash Gopalakrishnan, and Pritish Narayanan. Deep learning with limited numerical precision. *arXiv preprint arXiv:1502.02551*, 2015.

[57] Song Han, Jeff Pool, John Tran, and William Dally. Learning both weights and connections for efficient neural network. In *NIPS*, 2015.

[58] Trevor. Hastie, Robert. Tibshirani, and JH (Jerome H.) Friedman. *The elements of statistical learning*. Springer, 2009.

[59] Kaiming He, Xiangyu Zhang, Shaoqing Ren, and Jian Sun. Delving deep into rectifiers: Surpassing human-level performance on imagenet classification. In *Proceedings of the IEEE International Conference on Computer Vision*, pages 1026–1034, 2015.

[60] Xinran He, Junfeng Pan, Ou Jin, Tianbing Xu, Bo Liu, Tao Xu, Yanxin Shi, Antoine Atallah, Ralf Herbrich, Stuart Bowers, et al. Practical lessons from predicting clicks on ads at facebook. In *KDD*, 2014.

[61] Yujie He, Wenlin Chen, Yixin Chen, and Yi Mao. Kernel density metric learning. In *ICDM*, pages 271–280. IEEE, 2013.

[62] Yujie He, Yi Mao, Wenlin Chen, and Yixin Chen. Nonlinear metric learning with kernel density estimation. *Knowledge and Data Engineering, IEEE Transactions on*, 27(6):1602–1614, 2015.

[63] Geoffrey Hinton, Li Deng, Dong Yu, George E Dahl, Abdel-rahman Mohamed, Navdeep Jaitly, Andrew Senior, Vincent Vanhoucke, Patrick Nguyen, Tara N Sainath, et al. Deep neural networks for acoustic modeling in speech recognition: The shared views of four research groups. *Signal Processing Magazine, IEEE*, 29(6):82–97, 2012.

[64] Geoffrey Hinton, Oriol Vinyals, and Jeff Dean. Distilling the knowledge in a neural network. *NIPS workshop*, 2014.

[65] Kurt Hornik. Approximation capabilities of multilayer feedforward networks. *Neural networks*, 4(2):251–257, 1991.

[66] Max Jaderberg, Andrea Vedaldi, and Andrew Zisserman. Speeding up convolutional neural networks with low rank expansions. *arXiv preprint arXiv:1405.3866*, 2014.

[67] M.T. Jones. *Artificial Intelligence: A Systems Approach: A Systems Approach.* Jones & Bartlett Learning, 2008.

[68] Andrej Karpathy and Li Fei-Fei. Deep visual-semantic alignments for generating image descriptions. *arXiv preprint arXiv:1412.2306*, 2014.

[69] Yehuda Koren. Factorization meets the neighborhood: a multifaceted collaborative filtering model. In *KDD*, 2008.

[70] A.W. Kosner. Client vs. server architecture: Why google voice search is also much faster than siri @ONLINE, October 2012. URL `http://tinyurl.com/c2d2otr`.

[71] Alex Krizhevsky and Geoffrey Hinton. Learning multiple layers of features from tiny images, 2009.

[72] Alex Krizhevsky, Ilya Sutskever, and Geoffrey E Hinton. Imagenet classification with deep convolutional neural networks. In *NIPS*, 2012.

[73] J.B. Kruskal. Multidimensional scaling by optimizing goodness of fit to a nonmetric hypothesis. *Psychometrika*, 29(1):1–27, 1964.

[74] Matt J Kusner, Wenlin Chen, Quan Zhou, Zhixiang Eddie Xu, Kilian Q Weinberger, and Yixin Chen. Feature-cost sensitive learning with submodular trees of classifiers. In *AAAI*, pages 1939–1945, 2014.

[75] Hugo Larochelle, Dumitru Erhan, Aaron C Courville, James Bergstra, and Yoshua Bengio. An empirical evaluation of deep architectures on problems with many factors of variation. In *ICML*, pages 473–480, 2007.

[76] Quoc V Le. Building high-level features using large scale unsupervised learning. In *ICASSP*, pages 8595–8598. IEEE, 2013.

[77] Vadim Lebedev, Yaroslav Ganin, Maksim Rakhuba, Ivan Oseledets, and Victor Lempitsky. Speeding-up convolutional neural networks using fine-tuned cp-decomposition. *arXiv preprint arXiv:1412.6553*, 2014.

[78] Yann LeCun, John S Denker, Sara A Solla, Richard E Howard, and Lawrence D Jackel. Optimal brain damage. In *NIPS*, 1989.

[79] Yann LeCun, Léon Bottou, Yoshua Bengio, and Patrick Haffner. Gradient-based learning applied to document recognition. *Proceedings of the IEEE*, 86(11):2278–2324, 1998.

[80] Yann A LeCun, Léon Bottou, Genevieve B Orr, and Klaus-Robert Müller. Efficient backprop. In *Neural networks: Tricks of the trade*, pages 9–48. Springer, 2012.

[81] J.A. Lee and M. Verleysen. *Nonlinear dimensionality reduction.* Springer, 2007.

[82] Kyong Ho Lee and Naveen Verma. A low-power processor with configurable embedded machine-learning accelerators for high-order and adaptive analysis of medical-sensor signals. *Solid-State Circuits, IEEE Journal of*, 48(7):1625–1637, 2013.

[83] Omer Levy and Yoav Goldberg. Neural word embedding as implicit matrix factorization. In *NIPS*, 2014.

[84] Yitan Li, Linli Xu, Fei Tian, Liang Jiang, Xiaowei Zhong, and Enhong Chen. Word embedding revisited: A new representation learning and explicit matrix factorization perspective. In *IJCAI*, 2015.

[85] Hongjun Lu, Rudy Setiono, and Huan Liu. Effective data mining using neural networks. *Knowledge and Data Engineering, IEEE Transactions on*, 8(6):957–961, 1996.

[86] Qiang Lu, Wenlin Chen, Yixin Chen, Kilian Q Weinberger, and Xiaoping Chen. Utilizing landmarks in euclidean heuristics for optimal planning. In *AAAI (Late-Breaking Developments)*, 2013.

[87] Lin Ma and Roger D. Chamberlain. A performance model for memory bandwidth constrained applications on graphics engines. In *Proc. of Int'l Conf. on Application-specific Systems, Architectures and Processors*, 2012.

[88] Lin Ma, Kunal Agrawal, and Roger D. Chamberlain. A memory access model for highly-threaded many-core architectures. *Future Generation Computer Systems*, 30: 202–215, January 2014.

[89] Lin Ma, Kunal Agrawal, and Roger D. Chamberlain. Analysis of classic algorithms on GPUs. In *Proc. of the 12th ACM/IEEE Int'l Conf. on High Performance Computing and Simulation (HPCS)*, 2014.

[90] Yi Mao, Wenlin Chen, Yixin Chen, Chenyang Lu, Marin Kollef, and Thomas Bailey. An integrated data mining approach to real-time clinical monitoring and deterioration warning. In *Proceedings of the 18th ACM SIGKDD international conference on Knowledge discovery and data mining*, pages 1140–1148. ACM, 2012.

[91] Michael Mathieu, Mikael Henaff, and Yann LeCun. Fast training of convolutional networks through ffts. *arXiv preprint arXiv:1312.5851*, 2013.

[92] H Brendan McMahan, Gary Holt, David Sculley, Michael Young, Dietmar Ebner, Julian Grady, Lan Nie, Todd Phillips, Eugene Davydov, Daniel Golovin, et al. Ad click prediction: a view from the trenches. In *KDD*, 2013.

[93] L. Mero. A heuristic search algorithm with modifiable estimate. *JAIR*, 23:13–27, 1984.

[94] Tomas Mikolov, Martin Karafiát, Lukas Burget, Jan Cernockỳ, and Sanjeev Khudanpur. Recurrent neural network based language model. In *INTERSPEECH*, 2010.

[95] Tomas Mikolov, Kai Chen, Greg Corrado, and Jeffrey Dean. Efficient estimation of word representations in vector space. *arXiv preprint arXiv:1301.3781*, 2013.

[96] Tomas Mikolov, Ilya Sutskever, Kai Chen, Greg S Corrado, and Jeff Dean. Distributed representations of words and phrases and their compositionality. In *NIPS*, 2013.

[97] Abdel-rahman Mohamed, Tara N Sainath, George Dahl, Bhuvana Ramabhadran, Geoffrey E Hinton, and Michael A Picheny. Deep belief networks using discriminative features for phone recognition. In *ICASSP*, 2011.

[98] Michael Montemerlo, Jan Becker, Suhrid Bhat, Hendrik Dahlkamp, Dmitri Dolgov, Scott Ettinger, Dirk Haehnel, Tim Hilden, Gabe Hoffmann, Burkhard Huhnke, et al. Junior: The stanford entry in the urban challenge. *Journal of field Robotics*, 25(9): 569–597, 2008.

[99] Guido F Montufar, Razvan Pascanu, Kyunghyun Cho, and Yoshua Bengio. On the number of linear regions of deep neural networks. In *NIPS*, 2014.

[100] Vinod Nair and Geoffrey E Hinton. Rectified linear units improve restricted boltzmann machines. In *ICML*, pages 807–814, 2010.

[101] Eric Nalisnick and Sachin Ravi. Infinite dimensional word embeddings. *arXiv preprint arXiv:1511.05392*, 2015.

[102] T.S.E. Ng and H. Zhang. Predicting internet network distance with coordinates-based approaches. In *Proc. INFOCOM*, pages 170–179, 2002.

[103] Steven J Nowlan and Geoffrey E Hinton. Simplifying neural networks by soft weight-sharing. *Neural computation*, 4(4):473–493, 1992.

[104] A. Paprotny, J. Garcke, and S. Fraunhofer. On a connection between maximum variance unfolding, shortest path problems and isomap. In *Proceedings of the Fifteenth International Conference on Artificial Intelligence and Statistics*. MIT Press, 2012.

[105] Razvan Pascanu, Tomas Mikolov, and Yoshua Bengio. On the difficulty of training recurrent neural networks. *arXiv preprint arXiv:1211.5063*, 2012.

[106] F. Pedregosa, G. Varoquaux, A. Gramfort, V. Michel, B. Thirion, O. Grisel, M. Blondel, P. Prettenhofer, R. Weiss, V. Dubourg, J. Vanderplas, A. Passos, D. Cournapeau, M. Brucher, M. Perrot, and E. Duchesnay. Scikit-learn: Machine learning in Python. *Journal of Machine Learning Research*, 12:2825–2830, 2011.

[107] Fernando J Pineda. Generalization of back-propagation to recurrent neural networks. *Physical review letters*, 59(19):2229, 1987.

[108] J.C. Platt. Fast embedding of sparse music similarity graphs. *Advances in Neural Information Processing Systems*, 16:571578, 2004.

[109] K Ramamohan Rao and Ping Yip. *Discrete cosine transform: algorithms, advantages, applications.* Academic press, 2014.

[110] C. Rayner, M. Bowling, and N. Sturtevant. Euclidean Heuristic Optimization. In *Proc. AAAI*, pages 81–86, 2011.

[111] Ali Sharif Razavian, Hossein Azizpour, Josephine Sullivan, and Stefan Carlsson. Cnn features off-the-shelf: an astounding baseline for recognition. In *CVPR Workshop*, 2014.

[112] Steffen Rendle. Factorization machines. In *ICDM*, 2010.

[113] Steffen Rendle. Factorization machines with libfm. *ACM Transactions on Intelligent Systems and Technology*, 3(3):57, 2012.

[114] Steffen Rendle and Lars Schmidt-Thieme. Pairwise interaction tensor factorization for personalized tag recommendation. In *WSDM*, 2010.

[115] Steffen Rendle, Zeno Gantner, Christoph Freudenthaler, and Lars Schmidt-Thieme. Fast context-aware recommendations with factorization machines. In *SIGIR*, 2011.

[116] Roberto Rigamonti, Amos Sironi, Vincent Lepetit, and Pascal Fua. Learning separable filters. In *CVPR*, 2013.

[117] Oren Rippel, Michael A Gelbart, and Ryan P Adams. Learning ordered representations with nested dropout. *arXiv preprint arXiv:1402.0915*, 2014.

[118] David E Rumelhart, Geoffrey E Hinton, and Ronald J Williams. Learning representations by back-propagating errors. *Nature*, 323:533–536, 1986.

[119] S. J. Russell and Peter Norvig. *Artificial Intelligence: A Modern Approach.* Pearson Education, 2 edition, 2003. ISBN 0137903952.

[120] Gerard Salton and Christopher Buckley. Term-weighting approaches in automatic text retrieval. *Information processing & management*, 24(5):513–523, 1988.

[121] L.K. Saul, K.Q. Weinberger, J. H. Ham, F. Sha, and D. D. Lee. *Spectral methods for dimensionality reduction*, chapter 16, pages 293–30. 2006.

[122] Bernhard Scholkopf and Alexander J Smola. *Learning with kernels: support vector machines, regularization, optimization, and beyond.* MIT press, 2001.

[123] Mike Schuster. Speech recognition for mobile devices at google. In *PRICAI 2010: Trends in Artificial Intelligence*, pages 8–10. Springer, 2010.

[124] Pierre Sermanet, David Eigen, Xiang Zhang, Michaël Mathieu, Rob Fergus, and Yann LeCun. Overfeat: Integrated recognition, localization and detection using convolutional networks. *arXiv preprint arXiv:1312.6229*, 2013.

[125] B. Shaw and T. Jebara. Minimum volume embedding. In *Proceedings of the 2007 Conference on Artificial Intelligence and Statistics*. MIT press, 2007.

[126] B. Shaw and T. Jebara. Structure preserving embedding. In *Proc. ICML*, pages 937–944, 2009.

[127] Qinfeng Shi, James Petterson, Gideon Dror, John Langford, Alex Smola, and S.V.N. Vishwanathan. Hash kernels for structured data. *Journal of Machine Learning Research*, 10:2615–2637, December 2009.

[128] Qinfeng Shi, James Petterson, Gideon Dror, John Langford, Alexander L Strehl, Alex J Smola, and SVN Vishwanathan. Hash kernels. In *AISTATS*, 2009.

[129] V. Silva and J.B. Tenenbaum. Global versus local methods in nonlinear dimensionality reduction. *Advances in neural information processing systems*, 15:705–712, 2002.

[130] Patrice Y Simard, Dave Steinkraus, and John C Platt. Best practices for convolutional neural networks applied to visual document analysis. In *2013 12th International Conference on Document Analysis and Recognition*, volume 2, pages 958–958. IEEE Computer Society, 2003.

[131] Karen Simonyan and Andrew Zisserman. Very deep convolutional networks for large-scale image recognition. *CoRR*, abs/1409.1556, 2014. URL `http://arxiv.org/abs/1409.1556`.

[132] Jasper Snoek, Hugo Larochelle, and Ryan P Adams. Practical bayesian optimization of machine learning algorithms. In *NIPS*, 2012.

[133] Nitish Srivastava, Geoffrey Hinton, Alex Krizhevsky, Ilya Sutskever, and Ruslan Salakhutdinov. Dropout: A simple way to prevent neural networks from overfitting. *The Journal of Machine Learning Research*, 15(1):1929–1958, 2014.

[134] Nathan R. Sturtevant, Ariel Felner, Max Barrer, Jonathan Schaeffer, and Neil Burch. Memory-based heuristics for explicit state spaces. In *Proc. IJCAI*, pages 609–614, 2009.

[135] Christian Szegedy, Wei Liu, Yangqing Jia, Pierre Sermanet, Scott Reed, Dragomir Anguelov, Dumitru Erhan, Vincent Vanhoucke, and Andrew Rabinovich. Going deeper with convolutions. *arXiv preprint arXiv:1409.4842*, 2014.

[136] A. Talwalkar, S. Kumar, and H. Rowley. Large-scale manifold learning. In *Computer Vision and Pattern Recognition, 2008. CVPR 2008. IEEE Conference on*, pages 1–8. IEEE, 2008.

[137] J. B. Tenenbaum, V. Silva, and J. C. Langford. A Global Geometric Framework for Nonlinear Dimensionality Reduction. *Science*, 290(5500):2319–2323, 2000.

[138] Laurens Van der Maaten and Geoffrey Hinton. Visualizing data using t-sne. *Journal of Machine Learning Research*, 9(2579-2605):85, 2008.

[139] Nicolas Vasilache, Jeff Johnson, Michael Mathieu, Soumith Chintala, Serkan Piantino, and Yann LeCun. Fast convolutional nets with fbfft: A gpu performance evaluation. *arXiv preprint arXiv:1412.7580*, 2014.

[140] N. Vasiloglou, A.G. Gray, and D.V. Anderson. Scalable semidefinite manifold learning. In *Machine Learning for Signal Processing, 2008. MLSP 2008. IEEE Workshop on*, pages 368–373. IEEE, 2008.

[141] Oriol Vinyals, Alexander Toshev, Samy Bengio, and Dumitru Erhan. Show and tell: A neural image caption generator. *arXiv preprint arXiv:1411.4555*, 2014.

[142] Gregory K Wallace. The jpeg still picture compression standard. *Communications of the ACM*, 34(4):30–44, 1991.

[143] Y. Wang, W. Chen, K. Heard, M. Kollef, T. Bailey, Z. Cui, Y. He, C. Lu, and Y. Chen. Mortality prediction in icus using a novel time-slicing cox regression method. *Proc. American Medical Informatics Annual Fall Symposium*, 2015.

[144] Chih wei Hsu, Chih chung Chang, and Chih jen Lin. A practical guide to support vector classification, 2010.

[145] K. Weinberger, B. Packer, and L. Saul. Nonlinear dimensionality reduction by semidefinite programming and kernel matrix factorization. In *Proc. Int'l Workshop on Artificial Intelligence and Statistics*, 2005.

[146] K.Q. Weinberger and L.K. Saul. Unsupervised learning of image manifolds by semidefinite programming. *International Journal of Computer Vision*, 70:77–90, 2006. ISSN 0920-5691.

[147] K.Q. Weinberger, F. Sha, Q. Zhu, and L. Saul. Graph laplacian regularization for large-scale semidefinite programming. In *Proc. NIPS*. 2007.

[148] K.Q. Weinberger, A. Dasgupta, J. Langford, A. Smola, and J. Attenberg. Feature hashing for large scale multitask learning. In *ICML*, 2009.

[149] Jason Weston, Samy Bengio, and Nicolas Usunier. Wsabie: Scaling up to large vocabulary image annotation. In *IJCAI*, 2011.

[150] X. Wu, A. Man-Cho So, Z. Li, and S.R. Li. Fast graph laplacian regularized kernel learning via semidefinite quadratic linear programming. In Y. Bengio, D. Schuurmans, J. Lafferty, C. K. I. Williams, and A. Culotta, editors, *Advances in Neural Information Processing Systems 22*, pages 1964–1972. 2009.

[151] Zhixiang Xu, Olivier Chapelle, and Kilian Q. Weinberger. The greedy miser: Learning under test-time budgets. In *ICML*, pages 1175–1182, 2012.

[152] Zhixiang Xu, Matt Kusner, Kilian Q. Weinberger, and Minmin Chen. Cost-sensitive tree of classifiers. In *ICML*, pages 133–141, 2013.

[153] Zhixiang Xu, Jacob R Gardner, Stephen Tyree, and Kilian Q Weinberger. Compressed support vector machines. *arXiv preprint arXiv:1501.06478*, 2015.

[154] Zhixiang Eddie Xu, Matt J Kusner, Kilian Q. Weinberger, Minmin Chen, and Olivier Chapelle. Classifier cascades and trees for minimizing feature evaluation cost. *Journal of Machine Learning Research*, 15:2113–2144, 2014.

[155] Zichao Yang, Marcin Moczulski, Misha Denil, Nando de Freitas, Alex Smola, Le Song, and Ziyu Wang. Deep fried convnets. *arXiv preprint arXiv:1412.7149*, 2014.

[156] Uzi Zahavi, Ariel Felner, Jonathan Schaeffer, and Nathan Sturtevant. Inconsistent heuristics. In *Proc. AAAI*, pages 1211–1216, 2007.

[157] Matthew D Zeiler and Rob Fergus. Stochastic pooling for regularization of deep convolutional neural networks. *arXiv preprint arXiv:1301.3557*, 2013.

[158] Matthew D Zeiler and Rob Fergus. Visualizing and understanding convolutional networks. In *ECCV*, 2014.

[159] T. Zhang, D. Tao, X. Li, and J. Yang. Patch alignment for dimensionality reduction. *Knowledge and Data Engineering, IEEE Transactions on*, 21(9):1299–1313, 2009.

[160] Quan Zhou, Wenlin Chen, Shiji Song, Jacob Gardner, Kilian Weinberger, and Yixin Chen. A reduction of the elastic net to support vector machines with an application to gpu computing, 2015.

[161] Yixin Zhuang, Ming Zou, Nathan Carr, and Tao Ju. A general and efficient method for finding cycles in 3d curve networks. *ACM Transactions on Graphics (TOG)*, 32 (6):180, 2013.

[162] Yixin Zhuang, Ming Zou, Nathan Carr, and Tao Ju. Anisotropic geodesics for live-wire mesh segmentation. In *Proc. of the 22nd Pacific Conference on Computer Graphics and Applications*, 2014.

[163] Ming Zou, Tao Ju, and Nathan Carr. An algorithm for triangulating multiple 3d polygons. *Computer Graphics Forum*, 32(5):157–166, 2013.

[164] Ming Zou, Michelle Holloway, Nathan Carr, and Tao Ju. Topology-constrained surface reconstruction from cross-sections. *ACM Transactions on Graphics (TOG)*, 34(4):128, 2015.